

UNIVERSITÀ DEGLI STUDI DI NAPOLI “FEDERICO II”

SCUOLA POLITECNICA E DELLE SCIENZE DI BASE
AREA DIDATTICA DI SCIENZE MATEMATICHE FISICHE E NATURALI

Corso di Laurea in Fisica

ANNO ACCADEMICO 2018/2019



Tesi di Laurea Specialistica

Kinematical substructures in the Fornax cluster

Relatore: Prof. Giuseppe Longo
Dott. Nicola R. Napolitano
Prof. Maurizio Paolillo

Candidato: Massimiliano Gatto
Matricola: N94/344

Contents

Introduction	1
1 Galaxy evolution	5
1.1 Galaxy cluster as extreme environment of galaxy evolution	9
1.2 Evolution of the BCG	13
1.3 Intracluster population	16
1.3.1 GCs as tracers of the intracluster population	18
1.3.2 PNe as tracers of the intracluster population	22
1.4 Galaxy phase-space properties of discrete kinematical tracers	23
2 The Fornax cluster	27
2.1 Introduction	27
2.2 Galaxies	28
2.3 Extragalactic globular clusters (EGCs)	30
2.4 Relevance	33
3 Data	35
3.1 Fornax Deep Survey	35
3.1.1 Photometry	36
3.1.2 Spectroscopy of GCs	37
3.1.3 Selection of PNe	40
3.2 The catalog of GCs	42
3.3 The catalog of PNe	44
3.4 The dwarf galaxies	45

4	Data analysis	49
4.1	Introduction	49
4.2	Datasets	51
4.2.1	Kolmogorov-Smirnov test	56
4.3	An algorithm to find cold substructures	59
4.3.1	Simulation of the Fornax cluster	60
4.3.2	Selection of the parameters	66
4.3.3	Setting-up the best parameter range of the stream finding algorithm	67
4.3.4	Validation of selected parameters	68
4.3.5	Results on real data	70
4.4	An a posteriori test: recovering simulated substructures	76
4.5	Statistical analysis of the substructures	78
4.6	Cold substructures vs dwarf galaxies	83
4.7	Galmer simulations	86
	Conclusions	93
	A Theory of the merger	99
	Bibliography	103

Introduction

If we could observe the night sky and its changes over billion of years, we would see a faint object -nowadays barely visible to the naked eye- the *Andromeda galaxy*, to become increasingly larger and luminous, until it would dominate the whole sky. The future encounter between our galaxy, the *Milky Way* and the Andromeda galaxy, most likely will end up with the collision of the two galaxies, leading to the formation of a unique galaxy with completely different properties from those of the parent galaxies. This is an example of the most violent type of galaxy interaction: the **merging**. Merger events play a fundamental role in the formation and evolution of massive galaxies, because they have a huge impact on the properties of the galaxies involved, triggering the star formation activity and hence changing their color and luminosity, and often even changing their morphology.

According to the current cosmological model, the Λ CDM¹, the growth of the structures occurs through the assembly of many smaller systems, in a hierarchical scenario, called *merger tree*, where at the top we find the massive structures represented by the galaxy clusters, which are composed by hundreds or thousand of galaxies, all moving together in the deep gravitational potential of their dark matter dominated halo.

Near the center of the clusters there is a particular population of galaxies, called bright central galaxy (BCG) or central dominant (cD), which are elliptical-like galaxy with remarkable luminosity and mass and very extended haloes; there are some hints that their evolution were somewhat different from a typical elliptical, probably because the denser environment in the inner regions of the clusters lead to different evolution histories.

The accepted scenario is that cD built-up the bulk of their mass and their extended halo, in the last few Gyr, through tidal stripping accreting the smaller galaxies of the cluster (*minor*

¹The Λ CDM model is the standard cosmological model in which according to which the 95% of the mass-energy of the universe resides in the *dark energy* represented by the cosmological constant Λ , and in the *Cold Dark Matter*.

mergers events: namely the collision between two galaxies they have a significant different mass, for example the cD and a dwarf). This mass assembly is still ongoing, hence it is possible to observe such events in the cD while in the making and use them to test theories of galaxy evolution.

Thus the study of mergers is extremely interesting for several reasons:

- They play a fundamental role in the evolution of galaxies, especially in denser environments like galaxy cluster where the rate of the encounters is enhanced. Indeed the evolution history of the cD seems to be dominated by mergers.
- It is possible to test the paradigm of hierarchical assembly in the Λ CDM model by quantitatively testing the predictions for the formation of substructures.
- From the study of their debris it is possible to obtain informations about the parent galaxies.

Although these encounters are not so rare in galaxy clusters, the probability to observe directly such event is fairly low, hence the research of substructures as debris of these interactions becomes an important tool to obtain informations about the recent history of mass assembly of a galaxy. Unfortunately most of these substructures have a very low surface brightness,² hence it is very hard to reveal them through purely photometric observations beyond the closest galaxies to the Milky Way.

My thesis is focused on the research of candidate cold substructures which can be interpreted as signatures of recent or past interaction with dwarf galaxies of the larger members of the Fornax cluster, one of the nearest and massive clusters. To do so I made use of spectroscopic measures of the radial velocities of globular clusters (GCs) and planetary nebulae (PNe) in the intracluster region of the Fornax core. As It will become clearer in the following, since in these regions the dynamical time is longer, substructures should preserve their kinematic signature for a longer time, so that kinematic tracers may reveal as coherent substructures with a lower velocity dispersion than the local velocity dispersion which, in the intracluster region is determined mainly by the cluster potential. I used a *friend of friend* procedure in the right ascension (RA), declination (DEC) and radial velocity, in order to search for groups of tracers (particles) correlated both in position and in velocity.

The thesis is structured as it follows. In chapter 1 I summarize the theory of the galaxy evolution, focusing on the evolution of galaxies in clusters and on the evolution of the cD, and

²The surface brightness measures the flux density per unit solid angle of a spatially extended object such as a galaxy.

describing the kind of patterns that we expect from the debris of merger events. In chapter 2 I expose briefly the properties of the Fornax cluster. In chapter 3 I describe the sample of GCs and PNe and provide a description of the procedure used to detect them. In chapter 4 I describe the procedure used to reveal the cold substructures and the analysis performed on them, discussing what is the probability that these candidate structures are real ones. Finally I outline my conclusions. If the reader is not familiar with the theory of the merger can refer to the App. A

Chapter 1

Galaxy evolution

The galaxies that we have been observing for more than 150 years show a great variety of properties: morphology, luminosity, dimension, shape, color, kinematics and dynamics (figure 1.1). There are galaxies with a spiral pattern rotating around a central bulge, rich in gas and dust and there are elliptical galaxies, which are ruled by the random motion of the stars they are mainly made of. Some galaxies have an ill defined shape and are called 'irregular'. Galaxies have mass and luminosity ranging of several orders of magnitude. Our galaxy, the Milky Way, has about $10^{11}L_{\odot}$, but there are galaxies which have a luminosity thousand times greater than the Milky Way, others are composed of a small number of stars and are very small: *the dwarfs*. Galaxies are also different with respect their colours: there are galaxies with a blue color and with an extreme degree of star formation, others are red and made mainly of old and evolved stars. There are galaxy with a compact region at their center which emit so much energy, that this part alone is more luminous than the galaxy itself (the so called AGN or Active Galactic Nuclei). We can ask if these properties remain unchanged in time or if them vary. In other words: do galaxies evolve?

It is sufficient just a simple reasoning to realize that galaxies must evolve. Galaxies, indeed, are made mainly, but not only, of stars. Stars are born from the interstellar medium, evolve and die, expelling some of the elements produced in their inner parts by nuclear reactions, thus enriching the interstellar medium that supplies material for a new generation of stars. Therefore also galaxies, must evolve.

The first who built a model of galaxy evolution was Edwin P. Hubble, in the '920s, when he realized that most of the objects which at that time were called '*nebulae*' were just stellar



Figure 1.1: The Hubble Ultra Deep Field, imaged in 2004 by the Advanced Camera for Surveys. This is the deepest visible light image ever made of the Universe. The only way to see further is to look in infrared.

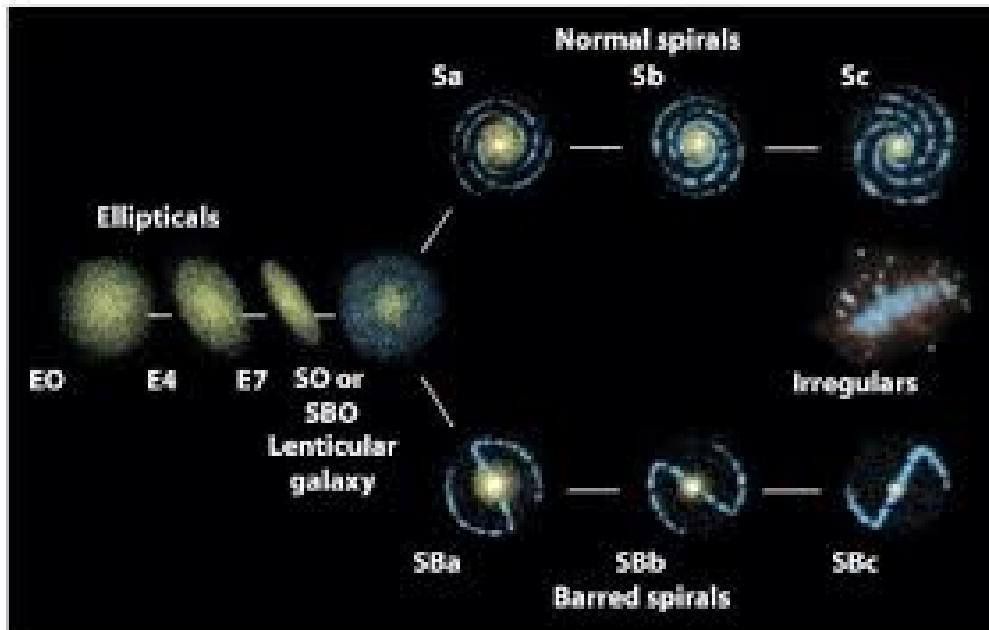


Figure 1.2: Hubble sequence: ellipticals are in the left side, while spirals lie in the right; between them, at the center, there are the lenticulars.

systems beyond the Milky Way.¹

He also found that these galaxies, in addition to recede from us, following the experimental law that himself found and which bears his name², also evolve. He in fact erroneously believed that his classification scheme reflected also a sort of temporal evolution of stellar systems. His morphological scheme sees galaxies ordered along a fork diagram, called now *Hubble sequence* (figure 1.2). He divided galaxies in three broad categories, ellipticals and lenticulars (also called early type galaxies, ETG), and spirals (late type galaxies, LTG). Spirals, in turn, were separated in normal spirals and barred spirals, which are galaxies with a bar-like structure, protruding from the bulge to the inner edge of the spiral arms.

Hubble simplistic explanation was that galaxies which appear of different morphological type are different evolutionary states of the same galaxy, moving along the diagram from the left (the so called Early Type Galaxies or ETG) to the right (Late Type Galaxies or LTG). Hubble, however did not succeed in placing on his diagram some types of galaxies (such as the irregulars).

¹Hubble measured in 1922-1923 the distance of several spirals *nebulae* using cepheid variables as standard candles.

²Hubble's law relates the velocity of a galaxy with its distance according the formula: $v = Hd$ where H is a universal constant named Hubble constant

Nowadays we know that this interpretation is completely wrong and that the physics behind galaxy evolution is much more complex than Hubble originally proposed, but nevertheless it was the first attempt to explain galaxy morphologies through an evolutionary theory³.

Surely the most important evidence of galaxy evolution are **mergers**, or the collision between two galaxies, which have a huge impact on them, changing their internal structures and overall morphology; hence these events may give some hints on the mechanisms that drive the evolution of the galaxies.

A powerful tool to obtain informations about galactic evolution is to study how average properties of galaxies change as a function of redshift; higher redshift means larger distances and therefore also longer look back time.

Study of the evolution of the luminosity function, which gives the number of galaxies per luminosity interval, revealed an overall brightening of galaxies at higher redshift, thus implying that star formation activity was substantially higher at $z \sim 1$ than what it is today (Hagen et al. 2015^[106]), reaching a peak at $z \sim 2.5 - 3$, i.e. when the universe was only ~ 2.5 Gyr old (Parsa et al. 2016^[182]). Also, there is a size evolution, with the effective radius growing up to a factor five between $z = 3$ and galaxies with the same mass in the local universe (e.g., Buitrago et al. 2008^[37]; Cassata et al. 2013^[43], Roy et al. 2018^[195]); probably, this is due to minor merger events (e.g., Bluck et al. 2012^[30]; McLure et al. 2013^[156]). There are good evidences also for the evolution of the merger fraction, defined as the ratio between the number of the merger events observed in a sample and the total number of objects in the same sample, increasing at higher z (Le Fevre et al. 2000^[142]); this is correlated to the number of the mergers that occur at some z , hence in the past mergers were more frequent. These, however, are only some aspects of galaxy evolution and in this chapter I will delve into this matter focusing in first section on the role of dense environments such as cluster of galaxies. Then, in section 2, I will describe the evolution of a particular population of galaxies, the brightest central galaxies. In section 3 I will introduce the intracluster medium and its mainly components, globular clusters (GCs) and planetary nebulae (PNe). Finally, I will illustrate the use of the phase-space as a tool to constraint galaxy evolution in a cluster.

³This is not completely true. Already in the late XVIII century, the german born astronomer Frederick William Herschel proposed an evolutionary classification of nebulae based on their degree of compactness. Herschel however did not separate galactic nebulae from extragalactic ones and therefore his theory did not go very far.

1.1 Galaxy cluster as extreme environment of galaxy evolution

Galaxies are not distributed uniformly in the universe, but they tend to be gathered in groups and clusters. The former are small agglomerates of tens of galaxies and typical total masses of $10^{14}M_{\odot}$, with a low enough density that encounters between galaxies are rare. The latter are the most massive objects gravitationally bound and very likely virialised in the universe⁴, with a number of galaxies ranging from hundreds to thousands, all moving in a common deep gravitational well defined by a very massive dark matter halo with a mass of about $10^{14}-10^{15}M_{\odot}$. Furthermore, clusters are often permeated by a hot plasma at very high temperature (about 10^6 degrees)⁵, with a pressure higher than that of the interstellar gas.

Dark halos plays a fundamental role in the galaxy evolution. According to the currently accepted hierarchical scenario, called *merger tree*, massive dark matter halos form through the accretion of smaller structures (subhalos), then through merger events these subhalos form a larger halo. In this scenario, at higher redshift, overdense regions of dark matter undergo a gravitational collapse once they overcome a critical value, thus forming the first subhalos, within which the gas bound in the potential well of these dark matter halos begin to cool and condense, forming the stars and hence the galaxies (White & Rees, 1978^[239]). The subhalos so formed will merge and grow with time forming larger and larger halos. At the top of this pyramidal growth we find galaxy clusters, which are the largest virialized structures in the universe. Hence, within dark matter halos (which contain most mass in the Universe), galaxies and clusters form and evolve, thus their properties depends on the formation history of the dark matter halos.

It is easy to imagine that in this hierarchical scheme galaxy clusters represent the densest environment where galaxies evolve in a substantially different manner with respect to those which live in less crowded regions. Here galaxies experience various encounters and interactions among them, considerably influencing their morphology, star formation rate and other properties such as luminosity and color. For this purpose surveys focusing on the study of the galaxies in clusters are very useful to understand galaxy evolution.

With a sample of about 6000 galaxies in 55 different clusters, Dressler et al. (1980)^[79] found a tight correlation between morphology and local galaxy density. As it is shown in the figure 1.3,

⁴Actually, superclusters are the largest known structures in the universe. They are made by several galaxy clusters or galaxy groups held together (even though not virialised) by the gravitational force.

⁵This component, discovered in the 70's from observations in the X-rays, accounts for about 25% of the total mass of the cluster

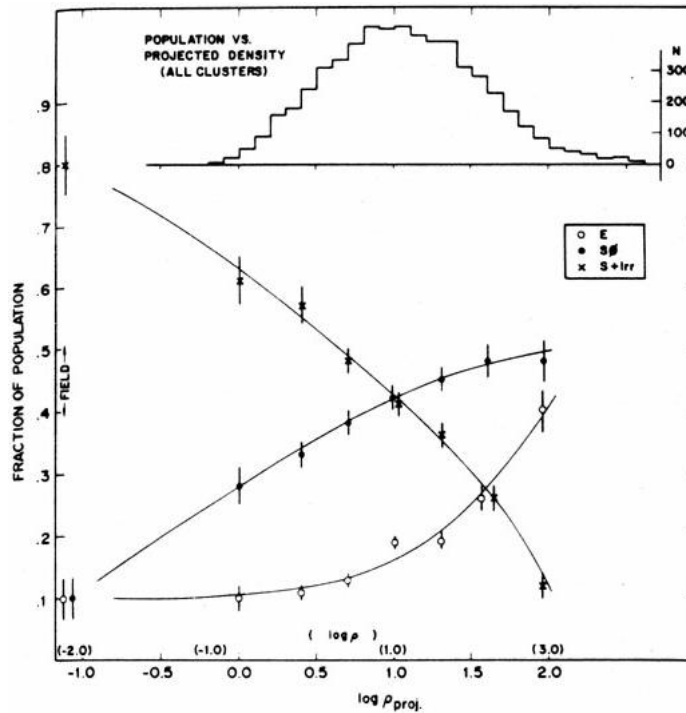


Figure 1.3: Dressler's plot: the fraction of E (open circles), S0 (black circles), and S+I galaxies (cross) as a function of the log of the local projected galaxy density, in galaxies Mpc^{-2} for 55 clusters. The upper histogram shows the number distribution. It is clear the tendency of the LTG to decrease in dense environments

despite the fact that 70% of the galaxy of the local universe are spirals, their fraction decreases for increasing local galaxy density, in favour of a growth of the ellipticals and lenticulars (also called S0) population. Furthermore, the fraction of early type galaxy is a function of the distance from the cluster center, increasing towards the inner parts, where the fraction of spirals drops down (Whitmore et al.1993^[242]).

This relation seems to be universal and holds over six orders of magnitudes, from small groups to richest clusters (Postman and Geller 1984^[185]). As morphology is a property tightly correlated with other physical parameters, such as luminosity, color and star formation, also these properties are connected to the environment. In fact a color-density relation (Hogg et al. 2004^[119]), and star formation-density relation (Gomez et al. 2003^[98]) were found. Since both spirals and S0 have a rotationally supported disk, it could be that in a cluster there is some process quenching star formation activity of a late type galaxies and transforming it to a lenticular. So in a cluster the number of the S0 grows because they are descendants of the spirals. One of the hypothesis

that explain this observational trend is the ram pressure stripping⁶ (Gunn and Goth 1972^[105]): the gas of the spirals moving in the dense environment of the cluster experiences a pressure from the wind of the intracluster medium

$$P \approx \rho \cdot v \quad (1.1)$$

where P is the ram pressure, ρ is the density of the intracluster medium and v is the relative velocity between galaxy and medium. This pressure can remove all the interstellar gas if it is strong enough to overwhelm the force of gravity of the galaxy thus truncating its star formation activity and hence changing its morphological type. Another explanation for the lower number of spirals in clusters comes from a theoretical study by Toomre (1977)^[218], that proposes that mergers of spirals lead to the formation of an elliptical galaxy. Simulation of two equal mass spiral spirals were performed (e.g. Barnes & Hernquist 1991^[15], Barnes 1992^[14]), showing that at the end of the process a De Vacouleurs radial mass profile⁷, $r^{1/4}$, remains. Simulations of a binary merger with different mass ratios have been studied extensively (Bendo & Barnes 2000^[13], Naab & Burkert 2003^[169]), confirming that these are good candidates for the formation of intermediate and giant ellipticals.

In this context, emblematic is the case of the brightest central galaxies (BCG), sometimes called central dominant or cluster dominant (cD) galaxies, near the center of the clusters, whose evolution is driven through growth by mergers, tidal stripping or galactic cannibalism (Gallagher & Ostriker 1972^[95]; Ostriker & Tremaine 1975^[179]; White 1976^[241]; Malumuth & Richstone 1984^[150]; Merritt 1985^[161], Moore et al. 1996^[165]; Gregg & West 1998^[103]; Willman et al. 2004^[243]; Read et al. 2006^[189]). cDs are elliptical-like galaxies, but with a size many times larger and an extremely high luminosity, even if, as we shall see in the next section, many of their properties are considerably different from those of normal ellipticals. Furthermore there are many clues that cD's have had a different evolution from giant ellipticals in less dense environments. Current cosmological models find that BCG assembled half of the stellar mass in the last 5 Gyr via gas-poor mergers (De Lucia & Blaizot 2007^[70]); hence it is possible to find signatures of these events even in the BCG at the present epoch ($z \sim 0$).

The current model for the formation and evolution of massive galaxies in clusters, among which BCG represent a particular population, is the **two-phase galaxy assembly**, according

⁶Ram pressure is a pressure exerted on a body moving through a fluid medium, caused by relative bulk motion of the fluid.

⁷The De Vacouleurs profile shows how the surface brightness of an elliptical galaxy I changes as a function of the distance from the center of the galaxy r .

to which the present size of a massive galaxies is built in two steps (e.g. Arnold et al. 2011^[8]). At the early epoch, at higher redshift, these galaxies grow through an intense star formation activity and through major mergers (e.g., Shankar et al. 2010^[205]). Because theoretical studies show that the amount of gas occurred in major mergers in the past was larger than at the present day, these mergers produced efficient starbursts (Khochfar & Silk 2006^[132], Naab et al. 2007^[171]), and an higher fraction of gas leads to more dissipation and hence to the formation of compact galaxies (e.g., Robertson et al. 2006^[191]; Khochfar & Silk 2006b^[134]); so in this first phase the inner parts of the massive galaxies were built. Afterwards some process heated the gas in galaxies quenching the star formation (e.g., Granato et al. 2004^[102]; Menci et al. 2006^[158]), maybe feedback processes from an active galactic nuclei (e.g., Somerville et al. 2008^[209]). In a second phase, in a more recent epoch, the bulk of the mass of a massive galaxy is accreted. Some hints of this accretion process come from the increase observed in the number density of galaxies with masses around $10^{11} M_{\odot}$ or larger from $z \sim 3$ up to $z \sim 1$ (Fontana et al. 2006^[89]; Marchesini et al. 2009^[151]; Ilbert et al. 2010^[126]; Conselice et al. 2011^[53], Cassata et al. 2011^[42]), and from a measure of the size of massive galaxies at $z \sim 1.5$ and their counterpart of the same mass at $z = 0$, showing that a larger fraction of galaxies in the past were smaller (Daddi et al. 2005^[67]; Trujillo et al. 2007^[220]; Toft et al. 2007^[217]; Zirm et al. 2007^[249]; Van Dokkum et al. 2008^[226]; Buitrago et al. 2008^[37]; Cimatti et al. 2008^[47], van der Wel et al. 2008^[225]; Franx et al. 2008^[94]; Damjanov et al. 2009^[68] ; van der Wel et al. 2009^[224]).

The evolution at low redshift is dominated by minor mergers, but because of the amount of gas available is lower than at higher redshift, these *dry* mergers do not lead to star formation, but contribute to the increase in size and mass (e.g., Ciotti & van Albada 2001^[48]; Loeb & Peebles 2003^[146]; Domínguez-Tenreiro et al. 2006^[76]; Boylan-Kolchin et al. 2006^[33]; Khochfar & Silk 2006^[132]; Bell et al. 2006a^[20], 2006b; Naab et al. 2007^[171]; Naab et al. 2009^[170]; Bezanson et al. 2009^[26]; Van Dokkum et al. 2010^[228]; Ruszkowski & Springel 2009^[197]; Hopkins et al. 2009^[121]).

According to this scenario, massive galaxies underwent through many interaction with their satellites in the last Gyr. For this purpose the research of such signatures in the nearby cluster has becomes, in recent years, a major player in testing models of formation and evolution and in understanding the importance of dense environments on the galaxies.

1.2 Evolution of the BCG

In the previous sections I described some aspects of the galaxy evolution in the clusters, stressing the differences with respect to less dense environments. In this section I focus on the evolution of the brightest central galaxies or BCGs, which are the most luminous and massive galaxies in the universe. BCGs are located near the center of the massive clusters⁸. and show a very active history of mass assembly (Ruszkowski & Springel 2009^[197], Edwards et al. 2012^[83], Lidman et al. 2012^[144], Laporte et al. 2013^[140], Ragone-Figueroa et al. 2018^[188]), which can be naturally explained in the hierarchical scenario.

BCGs are early-type galaxies and some of their properties resemble those of normal elliptical galaxies, for example their surface brightness profile is fitted very well with a $r^{-1/4}$ De Vaucouleurs profile (Graham et al. 1996^[100]), similar to that of the ETG (Trujillo et al. 2001^[221]; Graham & Guzman 2003^[101]; Aguerri et al. 2004^[1]; Kormendy et al. 2009^[137]), but BCGs have an additional exponential halo (e.g. Iodice et al. 2016^[128], 2017^[127])

Although there are some similarities with normal E galaxies, on the whole BCGs are very different from the typical elliptical galaxies. For example, they do not follow the standard scaling relations of normal ellipticals. In particular they show a luminosity excess in the Faber-Jackson relation⁹ (Lauer et al. 2007^[141]; von der Linden et al. 2007^[233]; Bernardi et al. 2007^[24]; Bernardi et al. 2009^[25] and references therein) and this is a clear evidence that BCG form and evolve in a very different way than that of the normal ETG (e.g., Lin & Mohr 2004^[145]; Brough et al. 2005^[36]; De Lucia & Blaizot 2007^[70] and references therein).

BCGs have been found to be a rather homogeneous population (Sandage 1972a^[199]; Gunn & Oke 1975^[104]; Hoessel & Schneider 1985^[118]; Postman & Lauer 1995^[184]) and, due to their little scatter in absolute magnitude, they have been also used as standard candles¹⁰ (Sandage 1972a^[199]; Postman & Lauer 1995^[184]).

Early theoretical studies proposed star formation in X-ray driven *cooling flows* as an explanation for the large masses of the BCGs (Silk 1976^[208]; Cowie & Binney 1977^[63]; Fabian 1994^[85]), but recent observations of the nearby clusters carried out with Chandra and XMM-Newton in the X-rays showed that the cooling flow rates are too low. Other works proposed the accretion

⁸In reality not all galaxies located near the center of a cluster are also the most luminous in the cluster, but I will use the convention to call these galaxies BCG.

⁹The Faber-Jackson relation is an empirical law observed in elliptical galaxies which relates the total luminosity of the galaxy L to the central velocity dispersion σ in this way: $L \sim \sigma^4$.

¹⁰Standard candles are objects with a known absolute magnitude, hence from a measure of their relative magnitude it is possible to calculate their distance with good precision.

through dynamical friction and tidal stripping from cluster of galaxies as the main mechanism in the formation of BCGs (Ostriker & Tremaine 1975^[179]; McGlynn & Ostriker 1980^[155]; Merritt 1985^[161]). However, this mechanisms must to be ruled out in the clusters because the relative velocity between galaxies is so high, about thousand of km/s , that the cross section for galaxy-galaxy interaction is too low (Ostriker 1980^[178]).

In the context of the Λ CDM model, i.e. the current cosmological model, the hierarchical scenario explains the formation of the massive structures through the accretion of smaller ones, and seems capable to explain the formation and evolution of the BCGs too. Indeed, in this scenario, groups of galaxies will form before massive structures like galaxy clusters, and since in the groups the relative velocity between galaxies is lower (hundreds of km/s), galaxy-galaxy mergers are much more efficient. These mergers are likely to produce elliptical-like galaxies. Indeed theoretical studies and numerical simulations show that mergers of two galaxies of similar mass, even spirals, produce at the end of the process, a galaxy with De Vaucouleurs (1977) $r^{1/4}$ radial mass profile which is also pressure supported (e.g. Toomre 1977^[218]; Barnes & Hernquist 1991^[15]; Barnes 1992^[14]; Bendo & Barnes 2000^[13]; Cretton et al. 2001^[64]; Naab & Burkert 2003^[169]; Bournaud et al. 2005b^[32], Bois et al. 2010^[31]).

Using numerical simulations and semi-analytic techniques De Lucia & Blaizot (2007)^[70], showed that most of the stars in the BCGs formed at early epoch (50% at $z \sim 5$, 80% at $z \sim 3$) in different, smaller galaxies (figure 1.4). Thus most of the stars that belong to extended halos of the BCGs at the present epoch were not born "in situ", but they were accreted from satellite galaxies through *dry mergers*¹¹. Stellar population synthesis models also showed that most of the stars on the BCGs formed prior $z \sim 2$ (Thomas et al. 2005^[216]; Treu et al. 2005^[219]; Jimenez et al. 2007^[129]), this is consistent with low measured values of the star formation rate of the BCGs at lower redshift (e.g. Lidman et al. 2012^[144], Choi et al. 2014^[46], Webb et al. 2015^[235]). De Lucia & Blaizot also demonstrated that BCGs assembled rather late and that about half of the currently observed mass of the BCGs has been accreted in the last 5 Gys ($z \sim 0.5$; which implies that the accretion process is still ongoing). Another evidence of the ongoing mass assembly comes from the comparison of the BCGs stellar masses and surface brightness profile at different redshift (Whiley et al. 2008^[238]; Bernardi 2009^[25]; Collins et al. 2009a^[52]; Valentinuzzi et al. 2010^[223]; Ascaso et al. 2011^[9]; Stott et al. 2011^[213]).

In synthesis the evolution of the BCGs is consistent with the two-phase galaxy assembly

¹¹The term *dry* means that this mergers occur without star formation because is not involved a great amount of gas, opposite to the *wet* mergers which are gas-rich mergers and so trigger the star formation.

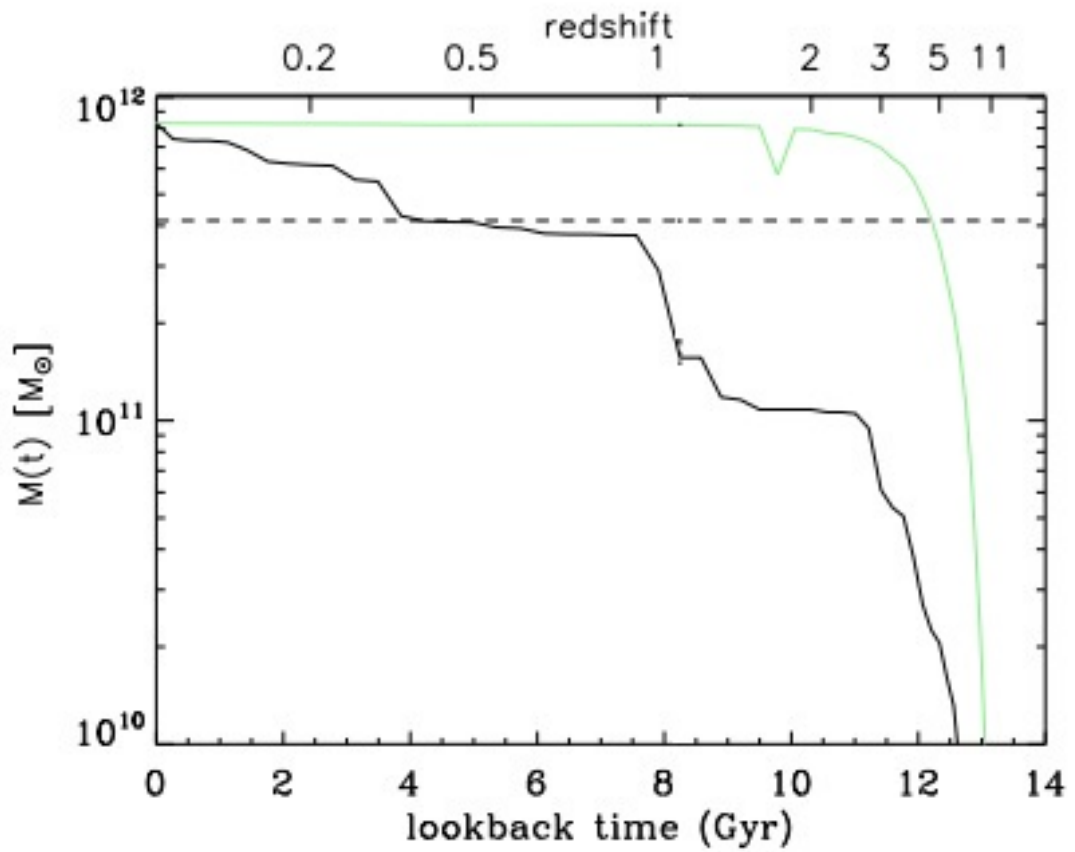


Figure 1.4: Assembly histories of the BCG. The black line shows the stellar mass of the cD while the green line shows the mass of all the progenitor in function of the time. The horizontal dashed line represent half the current stellar mass of the BCG. Image taken from De Lucia & Blaizot (2007).

scenario (see section 1.1): an early epoch growth via gas-rich mergers (or *wet*) and a final assembly where most of the mass is accreted, at lower redshift, through *dry* mergers (e.g. Khochfar & Burkert 2003^[133]; Hopkins et al. 2008^[120], Lidman et al. 2012^[144], Webb et al. 2015^[235]), with early-type satellite of quite red colours and a small gas fraction (De Lucia & Blaizot 2007^[70]). Thus, most of the accreted material at low redshift comes through *minor* mergers. Recent N-body simulations performed by Amorisco (2018)^[2] confirmed that the accretion events contributing to the mass assembly are due to low satellite-to-host virial mass ratio.

Since most of the evolution of a BCG comes through mergers, in particular *minor* mergers at the present epoch, it may be invaluable to observe such events to test and better constrain models for the formation and evolution of these galaxies, which are also tied with the formation and evolution of the cluster themselves. Therefore in recent years, the study of the signature of minor mergers in the local universe, like halo shells, tidal streams or other stellar substructures, has become an important tool to probe the assembly histories of galaxies (e.g., Helmi et al. 1999^[111]; Ibata et al. 2001^[123]; Belokurov et al. 2006^[21]; Tal et al. 2009^[214]; Martinez-Delgado et al. 2010^[152]; Cooper et al. 2011^[55]; Mouhcine et al. 2011^[166]; Xue et al. 2011^[245]; Bate et al. 2014^[17]).

Unfortunately, the debris of minor mergers are very faint, with a surface brightness below 27 *mag/arcsec*, hence it is not simple find them with traditional photometric methods and calls for deep and wide observations with a careful data reduction. In the last section of this chapter I shall discuss another way beyond purely photometric observations to find and study footprints of minor mergers, thus enhancing the probability to catch these substructures.

1.3 Intracluster population

As mentioned before, brightest central galaxies are the most massive galaxies located near the center of the richest clusters. As I discussed in the previous sections, the current cosmological model, the Λ CDM, explains the formation of structures within the hierarchical scenario, where massive systems formed through the agglomeration of smaller structures in a process called merger tree and BCGs grow by assembling mass in merger events and/or tidal stripping, a process that is still ongoing. Some of the stripped material is gravitationally bound to the central dominant or to other bright galaxies in the cluster but is likely that some fraction of it is freely moving in the common potential well of the cluster.

Now we know, especially thanks to surveys of the nearest clusters (Fornax and Virgo)¹², and via cosmological simulations (e.g. Napolitano et al. 2003^[174], Murante et al. 2007^[75]), that an intracluster population of objects exists, mainly made of stars and globular clusters (GCs), not bound to any galaxy (Arnaboldi et al. 2002^[3], Zibetti et al. 2005^[248]; Gonzalez et al. 2007^[99]; Arnaboldi & Gerhard 2010^[5]; Tutukov & Fedorova 2011^[222]; Mihos 2015^[164]). The whole of these objects forms the so called intra-cluster light (ICL), a diffuse and very faint component, that explains part of the extended surface brightness profile of a cD. The fraction of ICL over the total light of the cluster increases at greater distances from the center of the BCG (Zibetti et al. 2005^[248]; Gonzalez et al. 2007^[99]; Iodice et al. 2016^[128]; Spavone et al. 2017^[210]), but it is very hard to disentangle the intra-cluster population from objects bound to the galaxy.

Simulations confirm that this component can be generated from the stripping in the outskirts of the satellite galaxies (Contini et al. 2014^[54]), from galaxies which interact with the cluster tidal field (Moore et al. 1996^[165]; Willman et al. 2004^[243]), from mergers between BCG and other galaxies (Murante et al. 2007^[75]; Puchwein et al. 2010^[74]), or from the complete destruction of dwarf or low surface brightness galaxies, a process called *cannibalism* (Gnedin 2003^[97]). Hence, the galaxy halo is the ideal place where to look for remnants of merger events and studying these regions may provide hints on the mechanism driving the formation and evolution of the clusters. Furthermore, the longer dynamical time at larger galactocentric radii preserves these structures for a longer time.

Unfortunately, observing the intracluster light in the galaxy halos turns out to pose quite a few challenges due to its diffuse nature and its small surface brightness ($\mu \sim 26 - 27 \text{ mag/arcsec}^2$), in the g -band.

A solution to this difficult situation can be found in the use of luminous tracers belonging to the underlying stellar population, such as GCs or planetary nebulae (PNe). Due to their characteristics (intrinsic luminosity or emission line dominated spectra) these tracers are easily observable (as far away as $\sim 50 \text{ Mpc}$; Richtler et al. 2011^[190]) and their velocity can be measured with discrete precision, thus providing important kinematic informations. In the next two subsections I shall focus on the GCs and PNe, respectively, on their main physical properties and on some aspects of galaxy evolution that we know thanks to detailed studies of these objects.

¹²The Virgo cluster is the nearest galaxy clustered located at a distance of about $\sim 16.5 \text{ Mpc}$

1.3.1 GCs as tracers of the intracluster population

Ashman & Zepf in "Globular cluster systems" (1998)^[11], produced an excellent description of the GCs as individual objects and as systems as well. Beyond a detailed analyzes of the Milky Way GCs, they described also the properties of GCs systems in other galaxies and how they can be used to constraint models of the formation and evolution of galaxies. I refer to this book throughout the whole section.

Globular clusters are predominantly round objects made of million of stars, strictly packed together and having an high central density. They have always been a useful tool to obtain hints about formation and evolution of the galaxies, since, due to their very old age (they are among the oldest objects in the universe), they provide a fossil record of the galaxy properties in the formation epoch, thus avoiding the need to push away at higher redshift to observe the epoch of the birth of the Galaxy.

Furthermore, the stellar population of GCs can be approximated with good precision by a single stellar population (SSP)¹³; thus, it is simpler to compare their global properties to SSP models, avoiding further complications posed by an active history of star formation. Finally, they are very luminous objects, hence we can observe them up to distance where individual stars are not observable anymore, and they are ubiquitous, given that almost every galaxy seems to be surrounded by a system of globular clusters. In particular, bright, early-type galaxies, have a very rich system of globular clusters.

All these features make globular cluster systems an easily accessible tracers in clusters of galaxies. For example the excess of the specific frequency S_N (introduced by Harris and van der Bergh 1981^[108]), which is the number of globular clusters per unit luminosity and it is defined as

$$S_N \equiv N_{GC} 10^{0.4(M_V + 15)} \quad (1.2)$$

found in the cDs is among the main evidences that they had a very active mass assembly history. In figure 1.5, where it is shown the specific frequency of cD galaxies compared to the average S_N of normal ellipticals galaxies, it is evident that there is a remarkable rise in the S_N -by a factor of about ~ 5 - going from the bright ellipticals to the central dominant ones (Elmegreen 1999^[84]). This can be explained with the above mentioned stripping scenario. In this model, central dominant galaxies have increased their specific frequency by stripping globular clusters

¹³Single stellar population is an assembly of stars that are coeval and have the same initial chemical composition; because of its simplicity SSP are the basic tools used to understand observational properties of complex systems like globular clusters or galaxies.

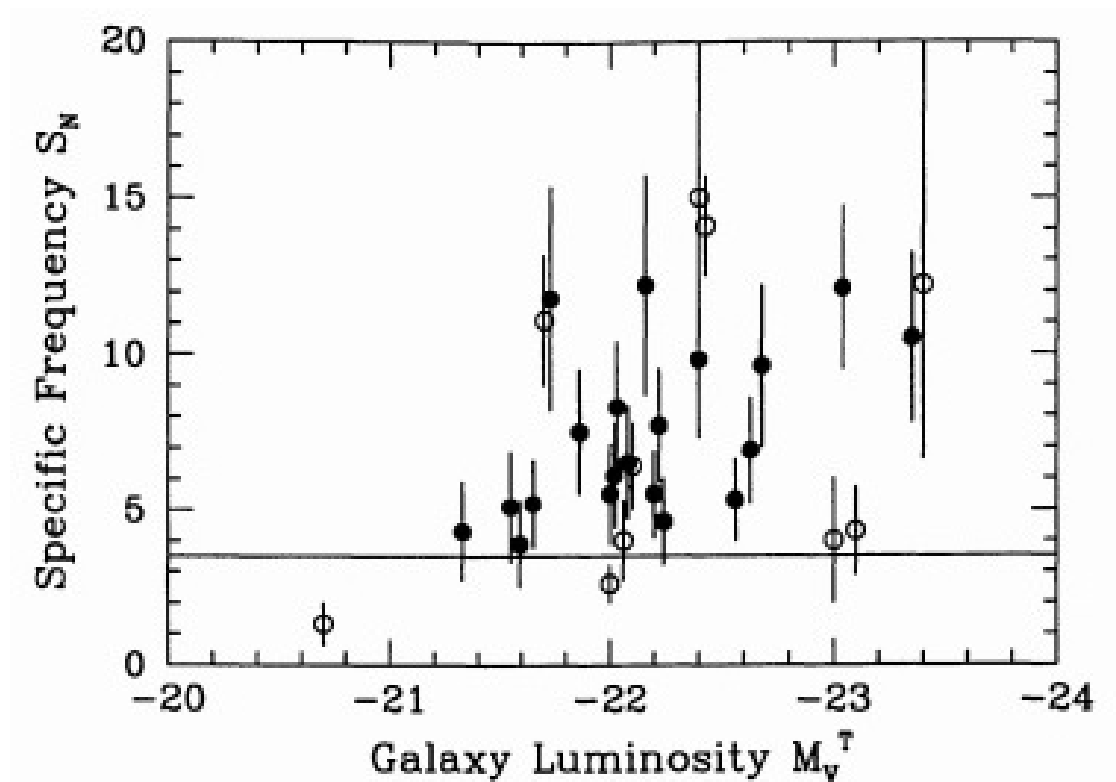


Figure 1.5: Specific frequency (Number of globular clusters per unit luminosity) as function of the total absolute magnitude in V-band, for cD galaxies. Open circles are cD from Harris et al. (1997b), while solid dots are cD from Blakeslee et al. (1997). The solid line at $S_N = 3.5$ is the average specific frequency of normal (non cD) ellipticals. Image taken from Harris et al. (1998).

from the outer region of the neighboring galaxies, thus leading to a lower S_N (Forte et al. 1982^[92]; Côté et al. 1998^[60]).

Further tools of investigation about the history of a galaxy cluster come from the intra-cluster population of GCs, since in this region it is possible to probe the cluster potential using the system of satellite galaxies like dwarfs or ultra compact dwarfs (UCD), and the longer dynamical time of these regions preserves the kinematical and photometric informations about recent or past merger events. Indeed, in the interactions between cD galaxies and other members of the cluster, GCs are tidally stripped from the outskirts of a galaxy enriching the halo of the central dominant or, as I said before, becoming part of the intracluster medium (Murante et al. 2007^[75]; Contini et al. 2014^[54]).

The first to speculate about the existence of a subpopulation of intra-cluster GCs were White (1987)^[240] and West et al. (1995)^[236]. Today we know many systems of globular clusters in nearby galaxy clusters, that not belong to any galaxy member of the cluster (e.g. Romanowsky et al. 2012^[194], D'abrusco et al. 2016^[66]).

From the photometric studies of the globular cluster systems in outer galaxies it clearly emerges the presence of a color bi-modality in the population of the GCs (Ostrov et al. 1993^[180]; Lee & Geisler 1993^[143]). The figure 1.6 shows just an example of this trend.

It is widely accepted that this bi-modality arises from a bimodal metallicity¹⁴, as it can be inferred from the bimodal distribution of the metallicity of the Galactic GCs (Côté 1999^[59]).

Furthermore, elliptical galaxies have a color gradient, i.e. they are redder near the center and tend to become bluer at higher galacto-centric distances (e.g. Bridges et al. 1991^[34]; Ostrov et al. 1993^[180]; Lee & Geisler 1993^[143]). Recent studies confirmed this trend, stressing that red globular clusters are mainly concentrated around the galactic center, and have a similar radial density profile of the stars. Bluer ones, instead, are more spatially extended (e.g. Schuberth et al. 2010^[202]; Pota et al. 2013^[186]; Coccato et al. 2013^[50]; D'abrusco et al. 2016^[66]). Although recently the reality of a metallicity induced bi-modality has been questioned because of the result of a non-linear color-metallicity relation (Yoon, Yi & Lee 2006^[247]; Blakeslee, Cantiello & Peng 2010^[27]; Yoon et al. 2011a^[246]), observations demonstrate that a real physical distinction between these two subpopulation exists (Côté 1999^[59]; Brodie & Strader 2006^[35]; Peng et al. 2006^[183]; Chies-Santos et al. 2011a^[44]; Forbes et al. 2011^[91]).

Therefore, any theory of galaxy formation and galaxy evolution must take into account that

¹⁴Metallicity is a dimensionless quantity used to measure the abundance of elements different from hydrogen and helium. It is defined as the logarithm of the ratio of the element abundance compared to that of the sun.

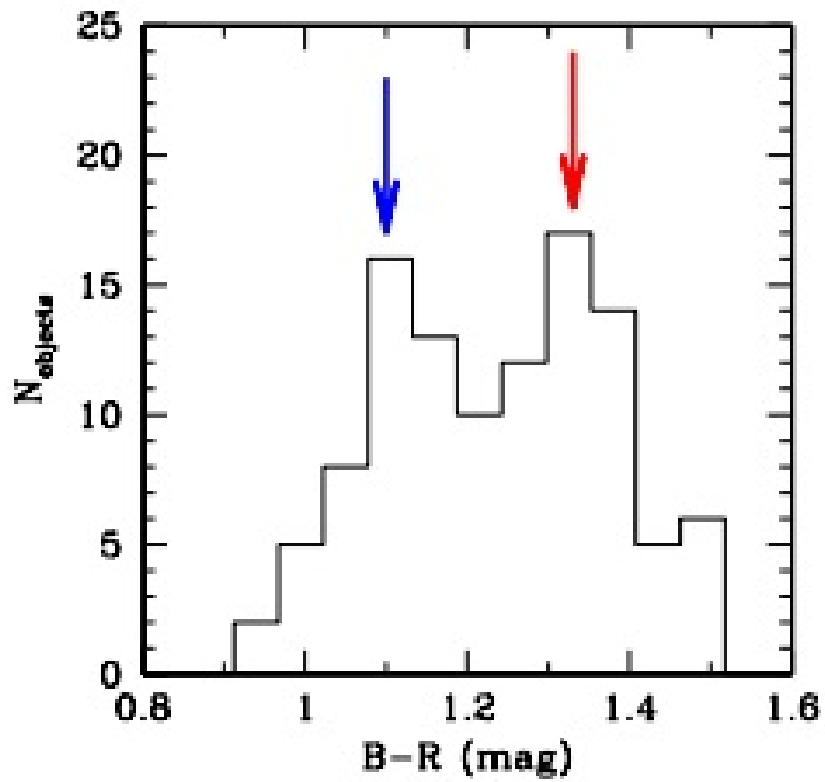


Figure 1.6: Color histogram of the globular clusters for the S0 galaxy NGC 5866, based on ACS/HST data. It is evident the bimodality of the distribution; the estimated position of the two peaks are shown with a blue and red arrow. Image taken from Cantiello & Blakeslee (2012)^[39]

there are two subpopulation of globular cluster: one is redder, metal-rich and traces the radial distribution of stellar light of the galaxy, the other one is bluer, metal-poor and forms a fraction of the intracluster population.

Three scenario have been proposed to explain the formation of two distinct subpopulation of GCs:

- **Major merger scenario:** a merger between two gas-rich galaxies with a pre-existing population of blue and red GCs. This merger can trigger star formation and the formation of new red GCs (Ashman & Zepf 1992^[10]; Bekki et al. 2002^[18]).
- **Multiphase dissipational collapse scenario:** GCs form in two distinct star formation episodes that the galaxy undergoes. Thus, blue GCs formed in the first star formation episode when the collapsing cloud was metal-poor. Red GCs form in a second moment when the gas has been enriched by the final products of the first generation of stars. Some of the blue GCs can also be stripped from satellite galaxies (Forbes et al. 1997a^[90]). This is consistent with the two phase assembly scenario.
- **Dissipationless accretion scenario:** Red GCs form from a monolithic collapse in the early epoch, whereas blue GCs are accreted from satellites through mergers or tidal stripping (Côté et al. 1998^[60]).

Currently there is still a debate on these three scenario, although the more accredited is the multiphase scenario.

It can be safely stated, however, that globular clusters are tightly correlated with the formation and the evolution of the cluster, moreover the possibility to observe these objects at great distances and at large galactocentric radii where the stellar light is fainter and the possibility to measure velocity with great precision even at large galactocentric radii, makes them remarkable tools to understand the accretion history of the cluster.

1.3.2 PNe as tracers of the intracluster population

Planetary nebulae (PNe) are evolved stars with an initial mass between $0.8 \leq M_{\odot} \leq 8$. In other words, they belong to the same old-intermediate population of stars that form the early-type galaxies. Close to the end of their life, these stars expell the outermost layers which are then ionised by the ultraviolet radiation emitted by the hot core. The envelopes of the PNe are easily observable, because of almost 15% of the absorbed light from the central star is re-emitted at

the specific frequency of the green OIII at 5007 Å (Dopita et al. 1992^[77]; Schönberner et al. 2010^[201]). Thus PNe can be easily observed and velocities can be measured also in nearby galaxy clusters with high precision just using a passband narrow filter. Furthermore, they can be traced out to large galactocentric radii where the lower surface brightness makes impossible to do line absorption spectroscopy. All these features make these objects good tracers of the underlying stellar profile of the ETG, indeed their kinematics and radial profile fits very well with those of the stars (Douglas et al. 2007^[78]; Coccato et al. 2009^[49]; Cortesi et al. 2013a^[57]), as we expect from the fact that they are just evolved stars. They are also good tracers, as well as the globular clusters, of the intracluster population, i.e. in the regions where the recent history of mass assembly is still preserved because of longer dynamical times avoid that substructures originated from interactions between galaxies have reached the equilibrium yet.

Therefore the intracluster population of planetary nebulae and globular cluster can be used to probe properties of galaxy halos (e.g. Napolitano et al. 2001^[173], Coccato et al. 2009^[49]; Herrmann & Ciardullo 2009^[115]; Teodorescu et al. 2010^[215]; Schubert et al. 2012^[203]; Pota et al. 2013^[186]), dark matter content (e.g. Côté et al. 2001^[62]; Romanowsky et al. 2003^[193]; Napolitano et al. 2009^[177]; de Lorenzi et al. 2009^[69]; Napolitano et al. 2011^[176]; Richtler et al. 2011^[190]; Deason et al. 2012^[72]), and can be used to understand the evolution of galaxies in nearby clusters.

1.4 Galaxy phase-space properties of discrete kinematical tracers

Additional evidence for the hierarchical assembly scenario in the Λ CDM cosmology model (e.g. White & Rees 1978^[239]; Cooper et al. 2011^[55]) comes from the discovery, in the last decade, of stellar streams and other substructures in the halos of the nearby galaxies; substructures which are the remnants of merger events. Among of the most important example are the Sagittarius stream in the Milky Way (Ibata et al. 1997^[125], 2001b^[123]; Majewski et al. 2003^[149]), and other substructures detected around M31 (Andromeda galaxy; e.g. McConnachie et al. 2009^[154], Ibata et al. 2001a^[124]). Within the local group of galaxies, these substructures can be studied using individual stars (e.g., Koch et al. 2008^[135]; Gilbert et al. 2009^[96]; Starkenburg et al. 2009^[212]; Xue et al. 2011^[245]); but this is not possible at greater distances since individual stars are not resolved. This problem can be overcome using other kinematical tracers like GCs or PNe which

can be detected up to tens of Mpc and at several effective radii from the center of the galaxy. Several PNe and GCs studies showed that these objects can provide evidence for the existence of accretion remnants (Forte et al. 1982^[92]; Muzzio 1987^[168]; Cote et al. 1998^[60]; Hilker et al. 1999^[117]).

Early investigations of such substructures were based on photometric observations, but this is challenging due to the faint surface brightness of the remnants, typically below $\mu \sim 27$ mag/arcsec². In the last few years deeper and more accurate spectroscopy has allowed to include kinematic informations of the debris in order to go beyond the purely photometric studies and look into the phase space of positions and velocities. Using kinematic tracers as GCs and PNe, it is therefore possible to probe the dynamic and kinematic of the clusters up to regions where the potential of the cluster begins to dominate over that of individual galaxies. In these regions it is possible to study substructures in the phase-space because they have not reached the equilibrium yet (Napolitano et al. 2003^[174]; Arnaboldi et al. 2004^[6]; Bullock & Johnston 2005^[38]; Arnaboldi et al. 2012^[7]; Coccato, Arnaboldi, & Gerhard 2013^[50]; Longobardi et al. 2015a^[147]). Indeed, in the galaxy halos the dynamic time-scales are much larger, so at several effective radii from the center of the cluster substructures are preserved in the kinematics and retain the signature of the accretion mechanism in the phase-space for a longer time. This allows them to be used to understand the formation and evolution of the cluster (e.g. Romanowsky et al. 2012^[194]) itself.

Using GCs and PNe as kinematic tracers of the halos of galaxies it has been shown the presence for substructures that are a clear evidence of minor merger or accretion events, that contribute to the mass assembly in the galaxy halos in early-type galaxies (Cote et al. 2003^[61]; Romanowsky et al. 2009^[192], 2012^[194]; Shih & Mendez 2010^[207]; Schuberth et al. 2010^[202]; McNeil et al. 2010^[157]; Woodley & Harris 2011^[244], Foster et al. 2014^[93]).

Numerical simulations and analytical models of orbit kinematics help to understand the pattern of the substructures in the phase space: shells and tidal streams are located in narrow diagonal tracks in the position-velocity diagram, and this could be explained in terms of a near radial infall of objects with almost the same initial potential energy. The patterns in the phase space can be influenced by many factors (e.g., Hernquist & Quinn 1988^[113], 1989^[114]; Johnston 1998^[131]; Helmi et al. 1999^[111]; Helmi 2004^[110]; Rudick et al. 2009^[196]). The most important parameter that drives the kinematics of these substructures is the mass ratio. More massive satellites feel a greater dynamical friction, and therefore, in the case of a larger mass ratio, the orbits shrinks quickly and the bulk of the stripped material is deposited at low galactocentric

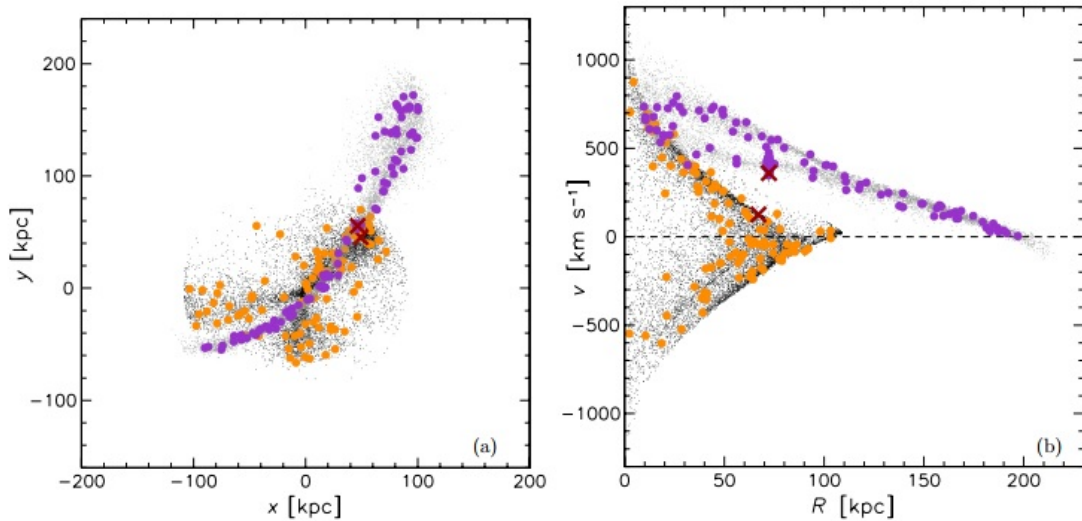


Figure 1.7: Simulations of two satellites with different initial apocenters infalling in a cluster plus BCG potential. It is shown both positional and phase space. In each simulation, subsamples of 100 and 10^4 particles are plotted as large and small dots, respectively, representing initial apocentric distances of 90 and 200 kpc (using small black and large orange dots, and small gray and large purple dots, respectively). The red \times symbols show the locations of the progenitor nuclei, The snapshots shown correspond to 3.5 *Gyr* (~ 10 -20 dynamical times) after the initial apocenters. In the first case, there are sharp features in phase space even when the tidal debris is well mixed in positional space (which happens more rapidly for a smaller initial apocenter). Image taken by Romanowsky et al. (2012).

radii (e.g. Amorisco 2017b^[2]). Furthermore due to the larger size and higher velocity dispersion, massive satellites produce, in the phase space, more diffuse streams. As the orbit shrinks, it becomes more radial (higher eccentricity) until all the memory of the previous motion is lost for $M_{\text{sat}}/M_{\text{host}} \geq 1/20$ (Amorisco 2017b). On the other hand, dynamical friction has a smaller effect on less massive satellites, so their debris are located at larger galactocentric radii (e.g. Amorisco 2017b^[2]) and, moreover, their orbits are less affected, especially for mass ratio $M_{\text{sat}}/M_{\text{host}} \leq 1/50$, and preserve most of the initial angular momentum (Amorisco 2017b^[2]). The angular momentum and the apocenters of the orbit also play an important role in shaping the structures left in the phase space. Orbits with low angular momentum bring satellites to a close passage to the cD and thus they are easily disrupted; this produces shell structures in the position space and chevron-like features in the phase space. Instead orbits with higher pericenter feel less dynamical friction and these satellites form a narrow tidal stream in space and/or in the phase space. The figure 1.7 shows both in the positional space and in the phase space two independent simulations of two infalling satellites with different initial apocenters, made by Romanowsky et al. (2012)^[194]. These simulations recover the kind of patterns described above.

By following the evolution of these cold substructures in a simulation, it can be found that

they mix up after several dynamical times because of the triaxality of the real potential or to the interactions with other satellites.

Using the phase-space as an additional feature to detect cold substructures is therefore an invaluable tool to understand the mass assembly history of the cluster, where just photometric observations fail due to the faint surface brightness of the debris of merger events.

Chapter 2

The Fornax cluster

2.1 Introduction

In this chapter I describe the main properties of the cluster being studied in this work: the Fornax cluster (figure 2.1).

Located in the southern hemisphere, in the Fornax constellation, and centered roughly at $\alpha \sim 3^h 35^m$ and $\delta \sim -35.7^\circ$ this cluster is among the nearest clusters to the Milky Way, and after the Virgo cluster, its northern counterpart, which is the nearest and surely the most studied cluster, is the largest concentration of galaxies at a distance $\leq 20 \text{ Mpc}$ from our galaxy. The distance modulus measured by Blakeslee et al. (2009)^[28]¹ is $(m - M) = 31.51 \pm 0.15 \text{ mag}$, corresponding to a distance of $d = 20.0 \pm 1.4 \text{ Mpc}$, making possible to study it with a higher level of detail not possible for more distant clusters. Identified for the first time as a galaxy cluster by Shadley in 1943, its proximity has motivated many surveys.

Thanks to the most recent surveys, the Fornax Deep Survey (FDS), and the Next Generation Fornax Survey (NGFS), it was unveiled that Fornax hosts a large population of dwarf and ultra compact galaxies (Munoz et al. 2015^[167]; Hilker 2015^[116]; Schulz et al. 2016^[204]), an intracluster population of PNe (e.g. Napolitano et al. 2003^[174]), and GCs (Bassino et al. 2006^[16]; Schuberth et al. 2010^[202]; D'Abrusco et al. 2016^[66]; Cantiello et al. 2017^[40]). Furthermore there are clear evidences on past or recent merger events in the Fornax core (e.g D'abrusco et al. 2016^[66]; Iodice et al. 2017^[127]).

¹Blakeslee et al. (2009) used the surface brightness fluctuations method for determining extragalactic distances, a method developed by Tonry & Schneider in 1988.



Figure 2.1: This image is a color composite mosaic (from the u , g and i bands, of the central 2×1 degrees² in the core of the Fornax cluster. NGC1399, the cD galaxy, is the brightest object on the left side. North is up and east is on the left. Image taken from Iodice et al. (2016).

In the next section I describe the main properties of the galaxies located in Fornax, while in section three I discuss about its globular clusters and the recent discoveries obtained studying the intracluster population of GCs in the Fornax core. In the last section of this chapter I explain the importance of digital surveys of nearby clusters like Fornax to make progress on the theories of galaxy formation and evolution.

2.2 Galaxies

The Fornax cluster is regular in shape and dynamically evolved; it is a relatively poor², but dense cluster. Some of the main properties of the cluster are reported in the table 2.1, compared to the properties of the Virgo cluster, a larger and richer but less dense cluster. Its total enclosed mass at a radius of 1.4 Mpc is $(7 \pm 2) \times 10^{13} M_{\odot}$ and was measured by Drinkwater et al. (2001a)^[80] from galaxies radial velocities; hence the total luminosity, obtained integrating the blue light from all galaxies within this radius is $2 \times 10^{11} L_{\odot}$, yielding a mass-to-light ratio 300 ± 100 , a normal value for clusters (Bahcall 2000^[12]).

²The richness of a cluster is a quantitative measure associated with the total number of galaxies belonging to the cluster.

Table 2.1: Basic properties of the Fornax cluster.

Property	Fornax	Virgo
Mass	$(7 \pm 2) \times 10^{13} M_{\odot}$	$(4 - 7) \times 10^{14} M_{\odot}$
Distance (Mpc)	19.3	16.5
$\langle v_R \rangle$ (km/s)	(1493 ± 36)	(1094 ± 42)
$\langle \sigma_v \rangle$ (km/s)	(374 ± 26)	760
r_c (Mpc)	≈ 0.25	≈ 0.6
n_o (gal Mpc^{-3})	≈ 500	≈ 250
N	235	1170
$f_{E+dE+S0+dS0}$	0.87	0.8
$\langle kT \rangle_X$ (keV)	1.20 ± 0.04	2.58 ± 0.03
$\langle Fe \rangle$ (solar)	0.23 ± 0.03	0.34 ± 0.02

Notes. In the first column are listed the cluster properties in the table and are the mass, distance, average heliocentric radial velocity, velocity dispersion, King model core radius, central galaxy density, number of members with $B \leq 18$ and within $3.5r_c$, the fraction of these that are E, dE, S0 or dS0, and the average temperature and Fe abundance of the intracluster medium as derived from X-ray observations (excluding the inner cluster regions); in the second and third columns there the property values in the Fornax and Virgo cluster, respectively.

Currently, the most exhaustive catalog is the Fornax Cluster Catalog (FCC) by Ferguson (1989a) ^[86], obtained with a survey of about 40 *degrees*² using large-scale plates from the 2.5 m Las Campanas telescope; this catalog lists about 240 members most of which very likely belong to Fornax. As in most other clusters, the bulk of the galaxies are early-type galaxies, and late-type galaxies are more present in the outer regions of the cluster (Drinkwater et al. 2001 ^[80]) (see also section 1.1).

Using a sample of 108 galaxies, Drinkwater et al. (2001) ^[80] performed the first dynamical analysis on Fornax. The total sample has a mean velocity of 1493 ± 36 *km/s* and a velocity dispersion of 374 ± 26 *km/s*. Although there are small differences in the mean velocity or velocity dispersion of early-type (356 ± 31 *km/s*) and late-type galaxies (405 ± 45 *km/s*), a significant difference exists between the dwarf galaxies (429 ± 41 *km/s*) and the giants (308 ± 30 *km/s*), suggesting that the dwarfs form a distinct population. The difference in the velocity dispersion is similar to the predicted ratio of $\sqrt{2} : 1$ by Colless & Dunn (1996) ^[51] for infalling and virialized objects, thus probably the dwarf is a population of infalling objects while the giants population is virialized.

The Fornax cluster can be divided in two main substructures, the main subcluster is centered on the cD NGC 1399 and has a velocity dispersion of $\sigma_v = 370 \text{ km/s}$, whereas the other one ("Fornax-SW") is centered 3° to the South-West direction, has a velocity dispersion of $\sigma_v = 377 \text{ km/s}$ and it is dominated by NGC 1316 (=FornaxA). Fornax-SW has an higher fraction of late-type galaxies, is a region of intense star formation and probably is not virialized (Drinkwater et al. 2001^[80]). Most likely this subcluster is infalling for the first time towards the main cluster at velocities of $100 - 500 \text{ km/s}$. This solution is also supported by a large amount of neutral hydrogen present in Fornax-SW, that hardly could have survived a previous close passage through the main cluster (Drinkwater et al. 2001^[80]).

In the core of Fornax, recent studies revealed the signatures of recent interactions involving the cD NGC 1399 and other bright galaxies located in the core. In particular Iodice et al. (2017)^[127] detected a very faint ($\mu_r \sim 28 - 29 \text{ mag/arcsec}^2$) and diffuse intra-cluster light (ICL) located between the cD and the bright galaxies NGC 1387, NGC1379, NGC1381, at distances of $10 \leq R \leq 40 \text{ arcmin}$ ($\sim 58 - 230 \text{ Kpc}$) from NGC 1399 (figure 2.2). The total luminosity in the g -band of the ICL is $L_g \sim 8.3 \times 10^9 L_\odot$. Comparing the properties of this ICL with those predicted by N-body simulations that model ICL formation (Rudick et al. 2009^[196]), the most likely scenario for the origin of the ICL in the core of Fornax is tidal stripping of stars and GCs from the outskirt of galaxies in a close passage. The similarity between the fraction of the luminosity in the ICL with respect to the total light of cD ($\sim 5\%$) and the fraction of blue GCs respect than the total population of blue GCs ($\sim 4 - 6\%$) is a clear evidence of an intracluster population in the Fornax core.

Other hints on recent interactions in the core of Fornax have been obtained from the kinematics of tracers of the stellar population like GCs and PNe and will be described in the next section.

2.3 Extragalactic globular clusters (EGCs)

As already discussed in section 1.3.1 system of globular cluster provide an important device to obtain informations about the formation and the evolution of a galaxy. The Milky Way and the other galaxies in the Local group³ provide a natural starting point to test model of galaxy evolution using the properties of their system of globular clusters, but this limited the statistics

³The Local group is a galaxy group that consist of more than 50 galaxies. Besides the Milky way, other important members are M31 (Andromeda galaxy) and M33 (Triangulum galaxy).

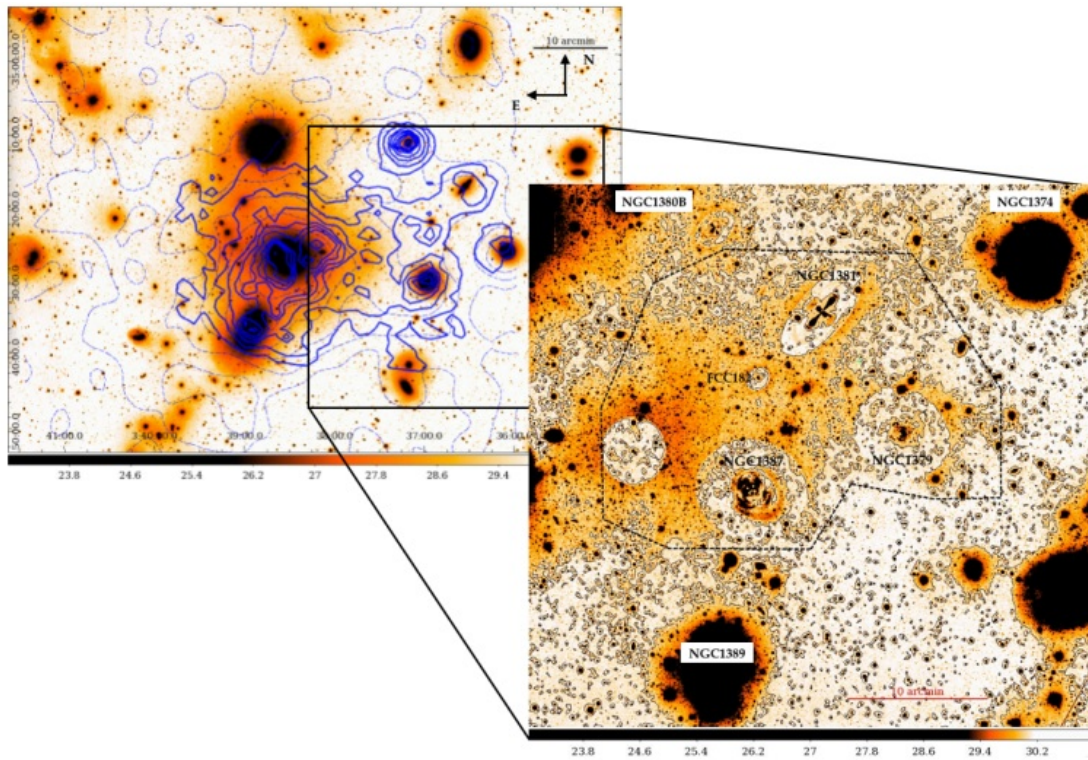


Figure 2.2: In the left panel it is shown the central regions ($2 \times 1 \text{ degrees}^2$) of the Fornax cluster in the r -band surface brightness levels. This image also displays the spatial distribution of the blue GCs derived by D'Abrusco et al. (2016) (in blue, see also section 2.3). In the right panel is zoomed the regions on the west side ($40.9 \times 42.7 \text{ arcmin}$, $\sim 237 \times 248 \text{ Kpc}$), after a subtraction of the bright galaxies. The black contours are the surface brightness levels ($\mu_r = 29.8 - 30.2 \text{ mag/arcsec}^2$).

to low density regions and late-type galaxies. Hence, in order to progress in the understanding of galaxy evolution, and to gain a broader knowledge on denser environments, there is the need to complement such studies with observations of GCs beyond the Local group. Nearby clusters offer the advantage to be close enough to allow the detection of large samples of GCs and therefore investigate the relationship between the galaxies and their system of globular clusters over a broad range of galaxy properties and environments. Thus the observations of extragalactic globular clusters in nearby clusters like Fornax have been used to study some of the trends already found in the Local group, such as the color-magnitude relation of GCs (e.g. Mieske et al. 2010^[163]), their luminosity function (e.g. Villegas et al. 2010^[232]), their color gradients (e.g. Liu et al. 2010) or the reliability of the half-light radii of the GCs as distance indicator (e.g. Masters et al. 2010^[153]).

Very interesting was the discover, in the Fornax core, of an intracluster population of GCs (e.g. Bassino et al. 2006^[16]) in regions where the dynamical timescale is longer than that at small galactocentric radii, and it is easier to find kinematic signature of recent interactions between galaxies useful to reconstruct the evolutionary history of the cluster. Complementary to photometric only studies (e.g. Iodice et al. 2017^[127]), the properties of GCs have revealed such signatures also in the region surrounding the cD NGC 1399. A lower specific frequency ($S_N \sim 2$) with respect to typical values for cluster ellipticals ($S_N \sim 5$, see figure 1.5), for the GCs system of NGC 1404 support the scenario of a tidal stripping of GCs in a close passage to the cD (e.g. Bekki et al. 2003^[19]). Other evidences of such interactions were found by Napolitano et al. (2002)^[172] using the velocity structure of PNe as kinematical tracers.

By using ~ 3000 candidate GCs in the central $\sim 8.4 \text{ degrees}^2$ of the cluster, D’abrusco et al. (2016)^[66] discovered a density over-abundance of GCs in a region of about $\sim 0.5 \text{ degrees}^2$ ($\sim 0.06 \text{ Mpc}^2$) in the Fornax core.

This over-density enhanced extends into the W-E direction, connecting the cD NGC 1399 to other bright galaxies in the core of Fornax NGC 1387, NGC1404, NGC 1380 and NGC 1380b. A similar asymmetry was also observed in the X-ray halo emission of NGC 1399 (Paolillo et al. 2002^[181]). This structure is more conspicuous in the distribution of blue GCs (figure 2.3), and is spatially coincident with the ICL revealed by Iodice et al. (2017^[127]; see also section 2.2).

As the build-up of the ICL discussed in the previous section, also the origin of this extended structure supports the scenario of a tidal stripping of GCs from the outer region of galaxies in a close encounter with the BCG or with the central regions of the cluster potential well. Other two isolated over-densities, mostly composed of blue GCs, discovered by D’abrusco et al. (2016)^[66],

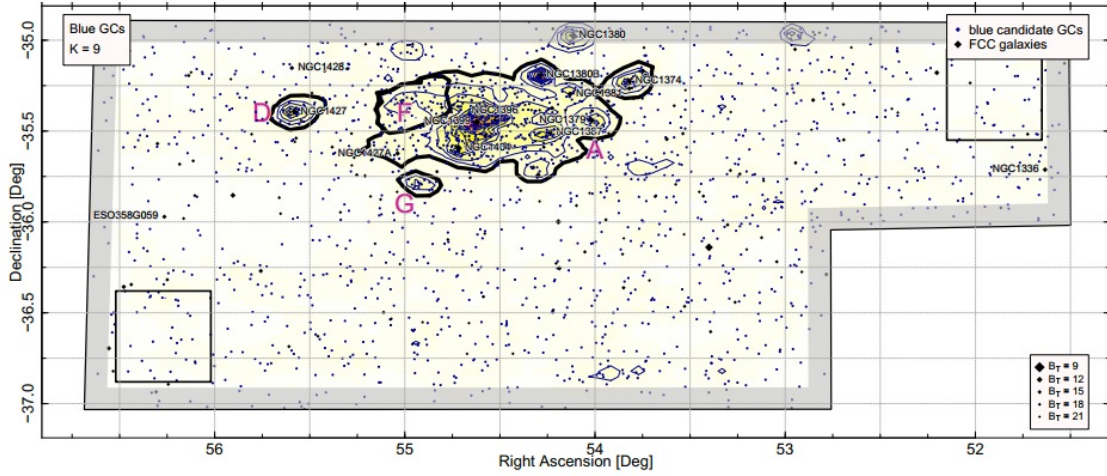


Figure 2.3: Density maps of the spatial distribution of blue candidate GCs. Black diamonds are galaxies of the FCC, size coded according to their B_T magnitude. This image displays the overdensity in the W-E direction and the other two structure called F and G. Image taken by D’abrusco et al. 2016.

(called F and G in figure 2.3) are not spatially coincident with any bright galaxy in the core of Fornax and could have originated from accretion events too.

Beyond the spatial distribution of the GCs, their kinematics can be used to reveal the accretion history of the cluster, as described in section 1.4.

2.4 Relevance

To understand all processes driving the formation and the evolution of galaxies is challenging, and is one of the major problem in astronomy. As already discussed, cluster of galaxies are important tools to test the theories of galaxy evolution. In the last decades, there were many progresses in our knowledge of the main mechanisms driving the evolution of galaxies in the context of the Λ CDM cosmology model, but there are still many questions which remain unanswered. To this purpose, nearby cluster offer a unique opportunity to observe and study denser environments in such high detail impossible to achieve in more distant clusters. Now I give a brief description of some of the advantages in studying nearby clusters like Fornax, focusing on the aspects connected to this work.

1. **Extragalactic globular clusters (ECG):** Due to their high luminosity these objects are easily detectable to the Fornax distance, and since they are ubiquitous -giant early-type galaxies may contain thousand of GCs (e.g., Harris, Pritchett & McClure 1995^[107]; Blakeslee

et al. 2003^[29])- it is possible to have a large and homogeneous catalog to study the role of dense environments on the global properties of GCs. The discovery of an intracluster population of GCs, and PNe as well, makes it possible to reveal the dynamic of the cluster from the radial velocities of these objects, and to study the kinematics in the galaxy halos, i.e. in the region where we expect to find signatures of recent interactions.

2. **Dwarf and Low surface brightness galaxies (LSB):** Dwarf galaxies are the most abundant population in the galaxy cluster, and moreover their low mass make them easily influenced by denser environments. Furthermore, the accretion of the BCG in the last Gyr occurs through mergers with low satellite-to-host mass ratio (see section 1.2), hence studying the dwarf population it is important to obtain informations about the recent mass assembly of the BCG and the origin of the intracluster light.

In addition to the rich population of dwarf galaxies in clusters, recently there was the discover of a particular class of galaxies with large radii and very low surface brightness, the so called *low surface brightness galaxies* (Koda et al. 2015^[136]; Mihos et al. 2015^[164]; van Dokkum et al. 2015^[227]; Munoz et al. 2015^[167], Venhola et al. 2017^[231]). These objects are really hard to detect in distant clusters, so nearby clusters like Fornax allow to study this new and particular class of objects.

3. **Signatures of merger events:** The discovery of several stellar substructures in the Local group, signatures of past or recent merger events (e.g., Helmi et al. 1999^[111]; Ibata et al. 2001^[123]; Tal et al. 2009^[214]; Martínez-Delgado et al. 2010^[152]; Cooper et al. 2011^[55]), has provided a direct evidence of the build-up of massive galaxies from the accretion of smaller stellar systems. Beyond the Local Group the detection of such substructures is harder because remnants of merger events have a low surface brightness. Thanks to tracers of the stellar population, like GCs and PNe, it is possible to trace the kinematics of clusters out to several galactocentric radii; and with the increase in the precision of velocity measurement of these objects, the observations are sensitive to smaller satellite-to-host ratio ($M_{\text{sat}}/M_{\text{host}} \sim (\Delta v/\sigma)^2$).

Chapter 3

Data

3.1 Fornax Deep Survey

This work is based on the Fornax Deep Survey (FDS), a joint project based on Guaranteed Time Observations for the surveys Fornax Cluster Ultra-deep Survey (FOCUS; P.I. R. Peletier) and VST Early-type GALaxy Survey (VEGAS; P.I. M. Capaccioli and E. Iodice, from 2016). The goal of the FDS is to observe the whole Fornax Cluster, out to its virial radius ($\sim 0.7 Mpc$, Drinkwater et al. 2001^[80]), to study the structure and evolution of its galaxies, from the most massive to the dwarf systems and find signatures of its ongoing assembly. This is achieved with a variety of observations, which include deep photometry, and multi-object and integral-field spectroscopy.

Imaging observations were taken at the ESO La Silla Paranal Observatory with the VLT Survey Telescope or VST. The VST is a 2.6m wide-field optical survey telescope (Schipani et al. 2012^[200]), equipped with the wide-field camera OmegaCam, having a field of view of 1×1 deg² and operating in the optical wavelength range from 0.3 to 1.0 μm (Kuijken 2011^[139]). The mean pixel scale is 0.21"/pixel. Complementary to the optical data, observations in J and in K infrared bands are performed with VISTA/VIRCAM (with limiting magnitudes $K_s = 23.4$ AB mag, and $J = 23.4$ AB mag, respectively).

As mentioned before, one of the aim of the FDS is to investigate the evolutionary history of the cluster. In order to do so, the survey has been designed to perform deep and large-scale multi-band imaging to reach the regions of the faint stellar halos of all galaxies within the virial radius. These are the regions where footprints of mass assembly are still present. These halos, whose complex kinematics has been revealed through the detection of globular clusters

and planetary nebulae, show complex structures in the form of tidal tails or shell, which are the imprint of a gravitational interaction, like merger events or tidal stripping. As such, they are ideal laboratories to unveil the formation history and the evolution of a cluster (see Bender et al. 2015^[22]; Longobardi et al. 2015^[147], and references therein). These structures have a very low surface brightness, typically below $\mu_R \sim 27 \frac{mag}{arcsec^2}$, hence deep imaging is mandatory to study the signs of galaxy interactions.

In order to achieve the low level of surface brightness which are typical of these structures, a remarkable effort was made with the VEGAS survey, a multiband survey in the southern hemisphere (Capaccioli et al. 2015), which has produced remarkable results (e.g. Iodice et al. 2016^[128], 2017^[127]; Spavone et al. 2017^[210]).

Another important survey of the Fornax cluster is The Next Generation Fornax Survey (NGFS; Munoz et al. 2015^[167]). This is a multi-wavelength survey, in optical and near-infrared bands, of 50 deg^2 around the NGC1399, out to the cluster virial sphere ($R_{\text{vir}} \sim 1.4 \text{ Mpc}$) (Drinkwater et al. 2001^[80]). NGFS uses for the optical wavelengths the Blanco 4-meter telescope at Cerro Tololo Interamerican Observatory (CTIO) mounted with the Dark Energy Camera (DECam; Flaugher et al. 2015^[88]); while for the near-infrared observations NGFS uses the VIRCAM (Sutherland et al. 2015) mounted on the VISTA 3.7-meter telescope of the European Southern Observatory (ESO) The aim of the NGFS survey is to detect point sources at $S/N = 5$ down to $u = 26.5$, $g = 26.1$, $i = 25.3$, $J = 24.0$, and $K = 23.3$ AB mag. NGFS has partially worked as a partner survey for FDS and, among other things, it provided near infrared photometry to help with the selection of GC candidates for spectroscopic follow-up (see Sect. 3.1.2)

3.1.1 Photometry

The FDS survey strategy has been optimized in order to achieve a uniform deep multiband (u , g , r and i) photometry, reaching a depth of the imaging dataset of about $\sim 30 \text{ mag}/arcsec^2$ in the g -band (Iodice et al. 2016^[128], 2017^[127]). These are unprecedented surface brightness levels on such a large scale multi-band observations and, as such, they are making possible to study the light distribution of the very faint galaxy halos out to $8 - 10$ effective radii R_{eff} (hundreds of kiloparsecs), where the surface brightness reaches very low values (below $\mu = 27 \text{ mag}/arcsec^2$) and streams and tidal tails from the small satellites, like the disrupting dwarf galaxies, are expected to be detected (see e.g. Cooper et al. 2009).

This is an important piece of information to understand the evolution of the cluster because

these are the smoking gun of the mechanisms that contribute in the current mass assembly of clusters.

The diffuse intracluster light has its origin from stars stripped from minor mergers from other galaxies (Napolitano et al. 2003^[174]; De Lucia & Blaizot 2007^[70]; Puchwein et al. 2010^[74]; Contini et al. 2014^[54]; Cui et al. 2014^[65]). The debris of the interactions have a very low surface brightness, the long tidal tails, results of major merging events, are seen at a surface brightness fainter than $24 - 26$ mag/arcsec² (depending on the band-pass), while small substructures have lower level of surface brightness.

The Fornax Deep Survey provides a uniform view of the Fornax cluster and of all its members, from the giant ellipticals to the intracluster population made of GCs and PNe with the aim to shed some light on the evolution of the cluster.

3.1.2 Spectroscopy of GCs

In this section, the selection of GCs in Fornax for the multi-object spectroscopic follow-up is described. The reference literature papers (and catalogs), where the data presented in this section are based on, are Bergond et al. (2007)^[23], Schuberth et al. (2010)^[202] and Pota et al. (2018)^[187]. In Pota et al. (2018) all data are discussed and homogenized, hence here the main details of the catalogue assembled by Pota et al. (2018) are discussed. The interested reader can refer to the original papers for a deeper description of the individual datasets.

Pota et al. (2018) describes a large follow-up of the cluster core, aimed at expanding the spectroscopical coverage of the area with respect to previous literature. Data were acquired from October 2014 to January 2015, in Period 94 (Program ID: 094.B-0687, PI: M. Capaccioli); and spectroscopic observations were performed with the VISIBLE MultiObject Spectrograph (VIMOS, Le Fèvre et al. 2003), mounted on the VLT-UT3 Melipal telescope at the ESO Paranal observatory in Chile. The VIMOS spectrograph was used in multi-object mode and was equipped with a MR grating with a spectral resolution $R = 580$ or 12 \AA FWHM and a dispersion of 2.5 \AA pix. The filter used is a CG475, which cuts off wavelengths bluer than 4750 \AA . Slits had a width of $1'$ and the pixel scale in the spatial direction was $0.205 \text{ arcsec/pixel}$. All masks were observed in three exposures of 30 minutes, to obtain a total of 1.5 hours. The seeing had a median of 0.85 arcsec , ranging from a minimum of 0.66 arcsec to a maximum of 1.15 arcsec .

Since the GC sample from Schubert et al. (2010)^[202] occupies a limited region in the combined 2-colour giK_s diagram, in Pota et al. (2018)^[187] the procedure to select GC candidates was to delimit a polygon around the objects distribution in this colour space.

Therefore the selection of GC candidates was based on VST/OmegaCAM photometry in the de-reddened g and i bands from FDS (D'Abrusco et al. 2016^[66]; Iodice et al. 2016^[128]), and VISTA/VIRCAM photometry in the K_s band from the NGFS.

Finally, they covered the central square degree around NGC1399 with a total of 25 VIMOS masks, shown in figure 3.1, along with the observations performed by Bergond et al. (2007)^[23] and Schuberth et al. (2010)^[202]. It is possible to see from the figure that the observations by Schubert et al. (2010) delimit a small central region around NGC1399 ($\sim 18arcmin$), while observations by Bergond et al. (2007) are more radially extended, covering a region of about 1.5 degrees in right ascension and about half a degree in declination.

The final mask design (i.e. slit allocation) consisted of 4340 unique spectroscopic targets, 2643 of them (about 61%) are within the limited polygon defined above to select GC candidates in the giK_s colour-colour space. The remaining slits were used to observe known stars and background galaxies, and some of them are used to duplicate targets, in order to understand uncertainties and possible systematics in the radial velocity measurements. They performed a cut-off at high and low magnitudes, in particular they just used just a range of $17.0 \leq i \leq 23.0$, to avoid contamination by foreground stars and a too low signal-to-noise spectra,

The final area covered by the VIMOS observations includes NGC 1399, the cD galaxy of Fornax, and other large galaxies like NGC 1404, NGC 1387 and NGC 1380.

From a total of 6700 spectra obtained (this number is greater than the total number of the slits because from one slit can be extracted multiple spectra), Pota et al. (2018) performed a redshift estimation to compute the heliocentric velocity of the objects (for a precise description of this measure I refer to section 3.1).

A separation of the various types of objects: Fornax objects, GCs, UCDs and galaxies physically bound to the cluster, from galactic stars and background galaxies must be performed in order to avoid contaminations among the different subsets. In particular, it was necessary to reject all object that were not connected to the Fornax cluster. Following the same procedure used by Schuberth et al. (2010), they performed a separation based on the systemic velocity of the objects, keeping objects in the velocity range of $450 \leq v \leq 2500 \text{ km/s}$ as Fornax objects (850 datapoints), and rejecting objects with $-450 \leq v \leq 450$ (956 datapoints). Finally only objects with a high signal-to-noise were retained leading to a final catalogue of 387 Fornax cluster objects.

To this catalog Pota et al. (2018) added objects found in literature, from the catalog by Bergond et al. (2007) and Schubert et al. (2010).

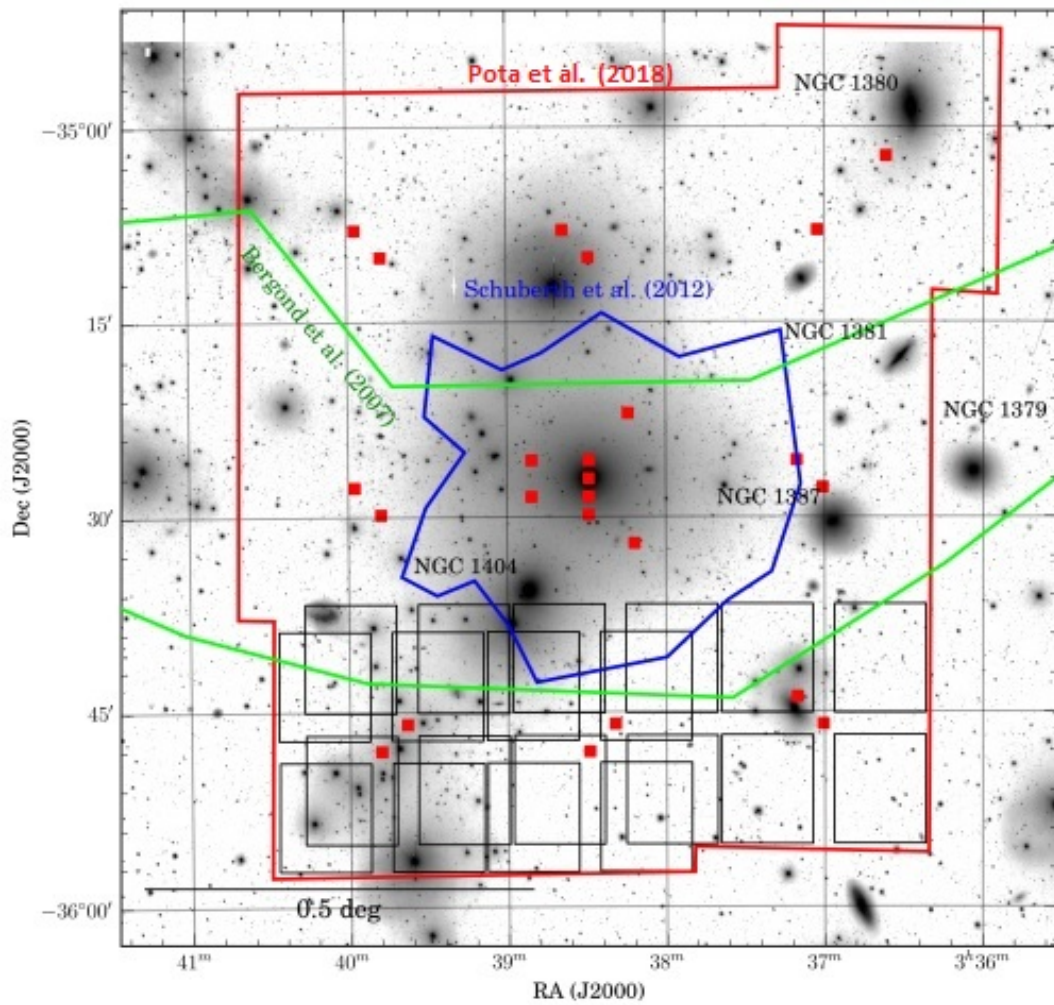


Figure 3.1: This image shows the regions covered by all 25 VIMOS pointing (whose centers are marked with red boxes) in red, along with other regions covered by Schubert et al. (2010) in blue and Bergond et al. (2007) in green. The background image is a mosaic of several VST/OmegaCAM pointings in the g-band. At the center there is the cD NGC 1399, and other galaxies are also labeled. The footprints of some VIMOS masks are shown on the bottom. Image taken from Pota et al. (2018).

In order to avoid duplicates I removed all objects that had a literature counterpart, considering as duplicate GCs all those within 0.4 arcseconds from Pota's GCs and with radial velocity comprised within 1 sigma, finding 48 duplicates that have been removed from the final catalogue. In the section 3.2 I describe the whole catalogue of globular clusters and some of their properties.

3.1.3 Selection of PNe

In this section the observations of planetary nebulae used in this thesis are described. This is a collection of PNe from Spiniello et al. (2018)^[211] and McNeil et al. (2010)^[157]. Again, an interested reader can refer to the original papers for a detailed description of the individual datasets.

In Spiniello et al. (2018) the observations made with FORS2 at the 8-meter Very Large Telescope (VLT) of the European Southern Observatory (ESO), and acquired in P96 (096.B-0412(A), PI: M. Capaccioli) from November 2015 to December 2016, are described together with the strategy of the data reduction and analysis of the telescope data. A total of 50 hours of observing time, with seeing usually below $0.8''$, covering an area of $\sim 50' \times 33'$; $\sim 1300''$ in the East-West direction from the center of NGC1399 and $\sim 1000''$ in the North-South direction. The region complements the area already observed by McNeil et al. (2010). In figure 3.2 the 20 FORS2 pointings observed during the observing run are shown, each of them consisting of three exposures for a total of ~ 2050 seconds on target.

The 1400V grating with a mean dispersion of $0.6396 \text{ \AA}/\text{pixel}$ and the OIII/3000+51 filter, centered on the redshifted [OIII] 5007 line (with the SR collimator, $\lambda_{\text{central}} = 5054 \text{ \AA}$, $FWHM = 59 \text{ \AA}$).

The identification of PNe from the [OIII] emission is based on the proper classification of emission-line objects that belong to three main classes:

- PNe: they are monochromatic sources.
- Lyman- α galaxies: these are galaxies at $z \sim 3$, but they are associated with a continuum so it is simple remove them from the catalogue.
- OII emitters at $z \sim 0.347$: at this z these emitters have the [OII] doublet that falls in the narrow band filters, but the high resolution of the grism 1400V enables to resolve the doublet.

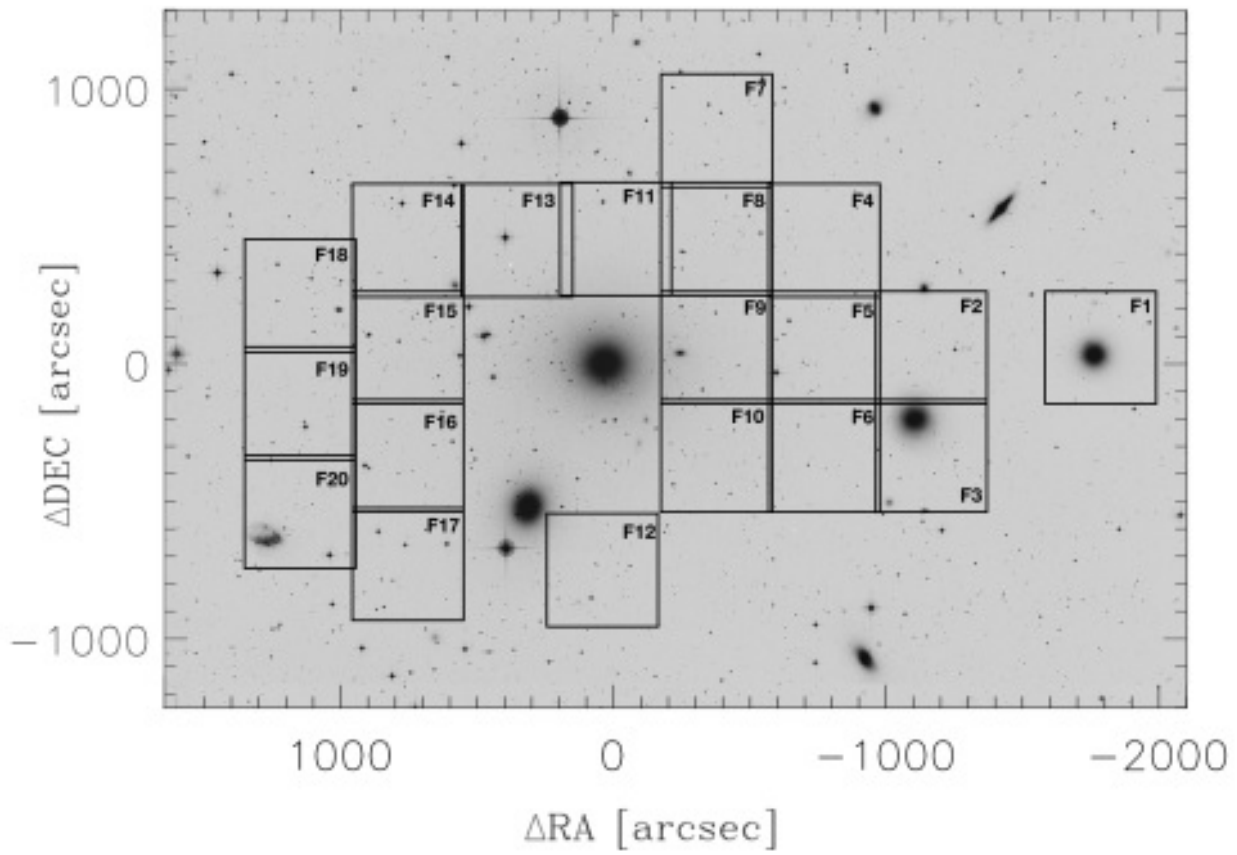


Figure 3.2: Image of the Fornax cluster centered around NGC1399. This image shows the 20 FORS2 pointings (black boxes) obtained in the observations. Image taken from Spiniello et al. (2018).

From the shift of the [OIII] emission with respect to a calibrated frame it is possible to obtain the velocity of the PNe. The uncertainties in the velocities range from 30 to 45 km/s .

3.2 The catalog of GCs

In this sections the catalogue of globular clusters from Pota et al. 2018, whose selection is described in the 3.1.2, is discussed in more details. the catalogue consists of 1183 objects, 387 new GC from Pota et al. (2018)^[187], 665 from Schubert et al. (2010)^[202] and the remaining 131 from Bergond et al. (2007)^[23]. The catalog reports the position of every GC (i.e. Right Ascension, RA, and Declination, DEC, in Equatorial coordinates) and heliocentric velocity corrected radial velocities (or redshifts) and related errors (in km/s). The systemic velocity of GCs is 1443 ± 18 km/s , which is consistent with the systemic velocity of the cD (NGC 1399, i.e. 1425 km/s , reference). This sample also comprises objects bound to other giant ellipticals in Fornax, as NGC 1387, NGC 1404 or NGC 1380. In chapter 4 a method to isolate GCs belonging to these systems will be discussed.

In the figure 3.3 the plot of radial velocity vs (g-i) color for all GCs is shown, along with other sources observed, such as galactic stars or background galaxies. It is apparent from the figure that using colors to split GCs from contaminants is not sufficient to have a clean separation, whereas using also kinematic information allowed the authors to separate Fornax members from background galaxies or Galactic stars.

Once they are separated from stars and other contaminants, GCs can be used to perform extended kinematical studies of the core region of the Fornax cluster. The usual assumption is that the cluster is spherical symmetric and one can use circular annuli to compute the typical kinematical quantities. The main observable interesting for hot systems (i.e. gravitational systems dominated by random motions, like elliptical galaxies and galaxy clusters), is the velocity dispersion, defined as

$$v_{\text{rms}} = \frac{1}{N} \sum (v_i - v_{\text{sys}})^2 - (\Delta v_i)^2 \quad (3.1)$$

Figure 3.3 shows the velocity dispersion of blue globular clusters with $(g - i) \leq 0.85$ mag is higher than velocity dispersion of red ones ($(g - i) \geq 0.85$ mag); a property already observed in many other giant galaxies (e.g. Pota et al. 2013).

The figure 3.4 displays the root-mean square velocity of all 1183 objects in the final catalogue as function of the distance from the center of NGC1399. The root-mean squared velocities

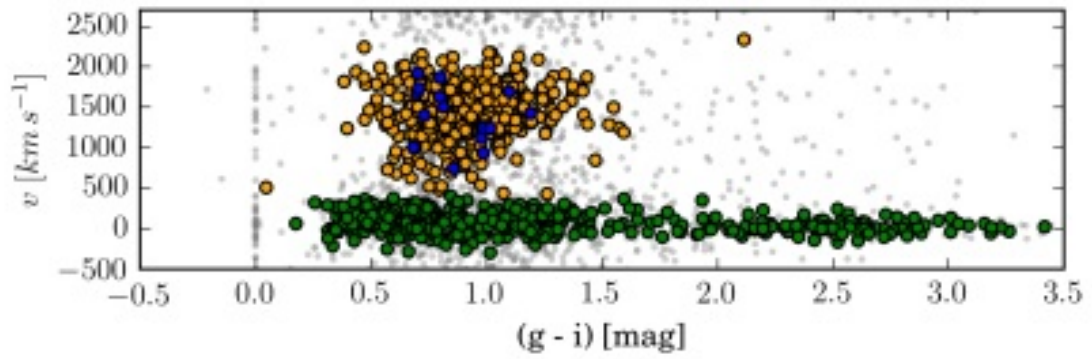


Figure 3.3: Plot radial velocity vs $(g-i)$ color. Yellow and blue circles are, respectively, GCs and UCDs. Contaminants are also shown in green, while grey dot are all sources observed with VIMOS. Image taken from Pota et al. (2018).

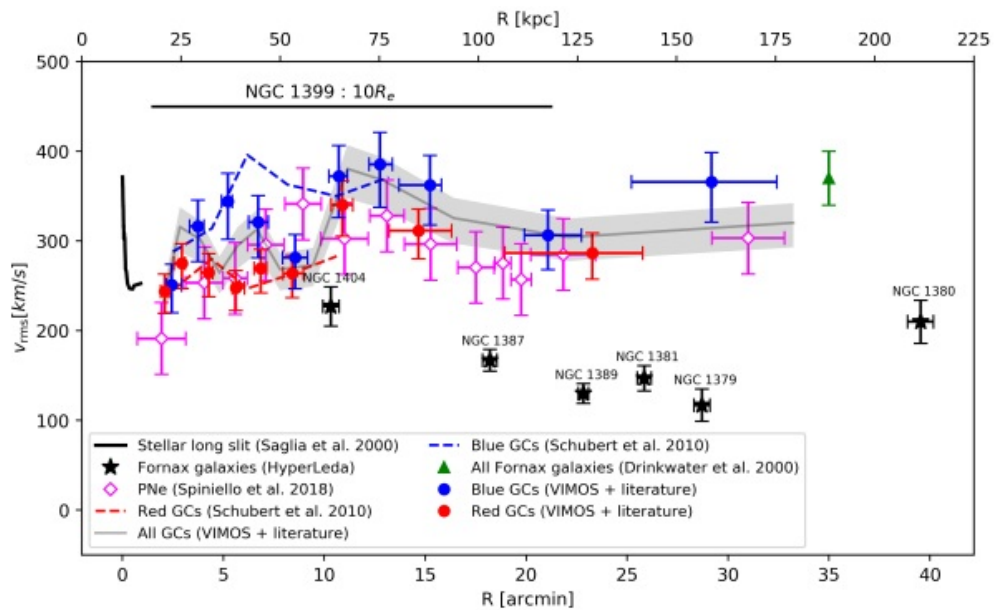


Figure 3.4: Root-mean square profile in the Fornax core. The grey line is the profile of the final catalogue of GCs, while the blue and red points are the blue and red GCs, respectively. Blue and red dashed lines represent the root-mean square of GCs from Schubert et al. (2010). Black solid line is the central stellar velocity dispersion obtained by Saglia et al. (2000). Green triangle shows the velocity dispersion of the Fornax galaxies obtained by Drinkwater et al. (2000).

depends on the ordered motions and the random motions as well, thus it is tied to the total kinetic energy and is defined as:

where v_i is the radial velocity of the i -th globular cluster and Δv_i is its uncertainty; v_{sys} is the systemic velocity of NGC1399 that is 1425 km/s . The figure 3.4 shows the root-mean square profile for all objects of the final catalog, the GCs from Schubert et al. (2010)^[202], the PNe from Spiniello et al. (2018)^[211], the stellar velocity dispersion of NGC1399 (Saglia et al. 2000^[198]) and all Fornax galaxies (Drinkwater et al. 2000^[81]). In the innermost regions, the velocity dispersion of GCs is consistent with the stellar velocity dispersion measured by Saglia et al. (2000)^[198] within 1 arcmin galactocentric radius. At $R \sim 10 \text{ arcmin}$ ($\sim 50 \text{ Kpc}$) there is a steep rise in the velocity dispersion of GCs and PNe as well, and then the root-mean square profile flattens to value determined from other Fornax galaxies (Drinkwater et al. 2000)^[81]. Therefore at $R \geq 10 \text{ arcmin}$ the kinematics of both GCs and PNe is dominated by the cluster potential, and hence this distance represent the transition from the innermost region where the kinematics is ruled by the potential of NGC1399, to the outermost regions where there is the beginning of the intracluster population of objects whose dynamics is governed by the cluster potential.

When separated in two distinct photometric population, using the threshold of $(g-i) = 0.85 \text{ mag}$, the figure 3.4 shows that the velocity dispersion profile of blue GCs is higher, at all galactocentric distances, than that of red ones and that of PNe; thus red GCs have a profile similar to that of the stars as described in the section.

3.3 The catalog of PNe

The total number of PNe detected by Spiniello et al. (2018)^[211] is 1452. From those I excluded objects around NGC1379, the black box flagged as 1 in the figure 3.2, for a total of 150 PNe. To these I added McNeil's objects too, 184 PNe, so obtaining a final catalog of 1495 PNe. As already discussed in section 3.1.3, the PNe in the catalog of McNeil are centered around NGC1399, thus these are a complement to the objects detected by Spiniello et al. (2018).

Since uncertainties in the velocity of this sample range from 30 to 45 km/s , I used an average value of 37.5 km/s as error on the velocities.

From figure 3.4 we can see the root-mean square radial profile for the PNe (magenta diamonds), obtaining similar results to those of the GCs. At distances $R \leq 250''$ PNe match very well the central stellar dispersion measured by Saglia et al. (2000)^[198] and the dispersion of the red GCs found by Schubert et al. (2010)^[202]. This is the region where the potential of

NGC1399 dominates and PNe and red GCs trace very well the kinematics of the cD, a result obtained for many giant galaxies too (e.g. Pota et al. 2013^[186]). At intermediate distances, $250'' \leq R \leq 1000''$, there is a steep rise in the velocity dispersion of PNe, very similar to that of GCs (see section 3.2), as already discussed in the previous section at this galactocentric radius there is the transition between the colder kinematics region dominated by the potential of the central galaxy to the warmer kinematics region governed by the cluster potential. Indeed in the outermost regions, at $R \geq 1000''$ the velocity dispersion of the PNe flattens out to the value of the dispersion of the Fornax cluster reported by Drinkwater et al. (2000)^[81].

3.4 The dwarf galaxies

In this section I discuss the catalog by Munoz et al. (2015)^[167] of dwarf galaxies in the Fornax core. I refer to that paper for a more detailed description of the observations and image processing. Observations were part of the Next Generation Fornax Survey (NGFS) and they detected 158 new dwarf galaxies in the central part of the Fornax cluster. They used a multi-passband in the *u*-, *g*-, *i*-band, wide-field observations using the Dark Energy Camera (DECam; Flaugher et al. 2015^[88]) mounted on the 4-m Blanco telescope at Cerro Tololo Interamerican Observatory. Most of the new dwarf galaxies are low surface brightness objects, with the faintest of them having an absolute magnitude of $M_i = -8.0 \text{ mag}$. They also discovered a population of Ultra Diffuse Galaxies (UDGs), a type of galaxies with very low stellar mass ($\sim 6 \times 10^7 M_\odot$) but with large radii (1.5-4.6 Kpc); these features make the UDGs very hard to detect ($\mu \sim 26.0 - 28.5 \text{ mag/arcsec}^2$).

The figure 3.5 shows all new dwarf by Munoz et al. (2015)^[167] as red circles, along with dwarf galaxies already detected by Ferguson (1989)^[86] as small gray circles and other galaxies detected by Mieske et al. (2007)^[162] as large gray circles. This image displays the central region, 3 deg^2 , of the Fornax cluster, corresponding to $\sim 350 \text{ Kpc}$ radius from NGC 1399, located at the center of the image.

The surface brightness of this sample ranges from $\mu_i = 22.0$ up to $\mu_i = 28.0 \text{ mag/arcsec}^2$, and the half-light radii ranges from $r_e \simeq 90 \text{ pc}$ up to $r_e \simeq 2.5 \text{ Kpc}$. The sample of the dwarf galaxies was divided in two classes: nucleated and non nucleated. Both classes have an exponential light profile and show a size-luminosity relation, although the slope is shallower for the nucleated dwarf galaxies. I included a description of the whole catalogue by Munoz et al. (2015)^[167], although for my purposes I will use just those objects dwarf that are in the field covered by the catalogues

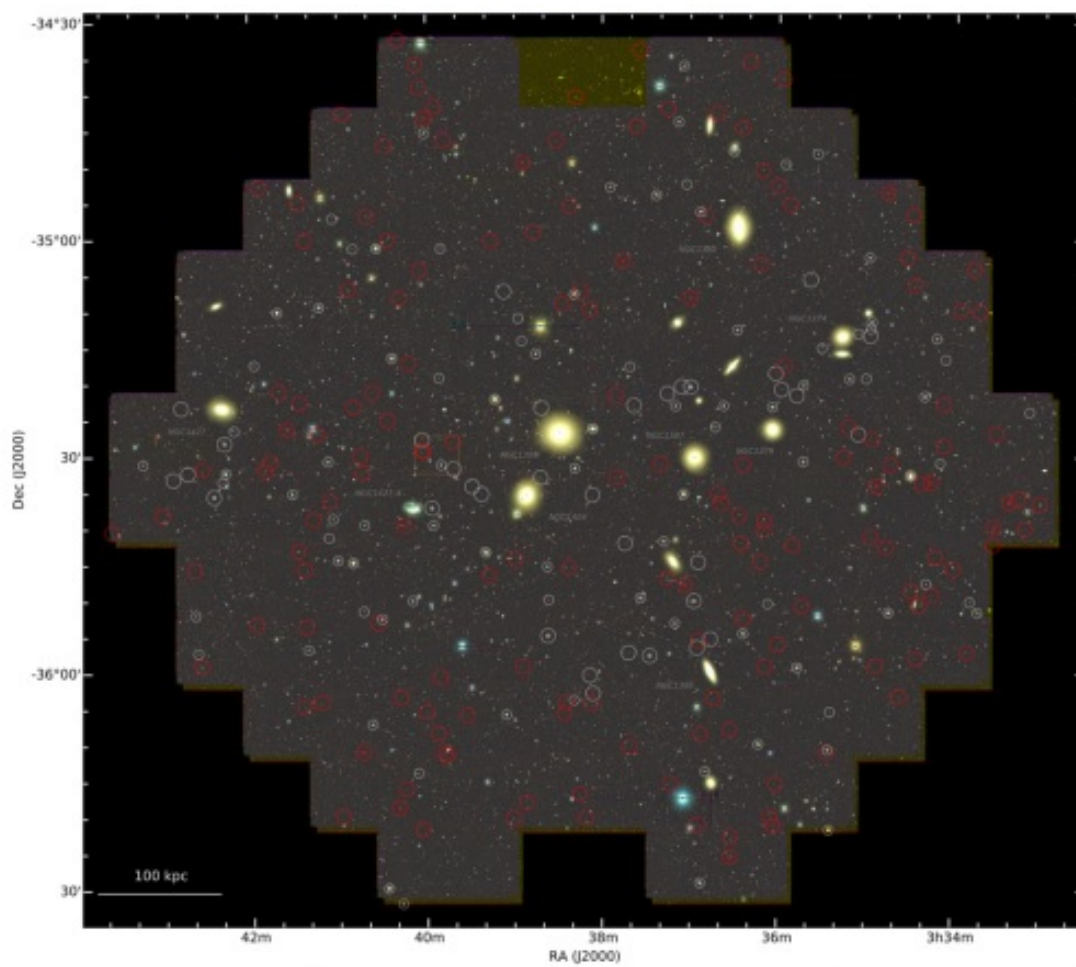


Figure 3.5

of GCs and PNe described in the previous sections.

Chapter 4

Data analysis

4.1 Introduction

Even though interactions and mergers are important processes in the growth of massive structures, the probability to observe them directly, as ongoing events, is fairly low in the nearby universe. On the other hand, one can look for indirect evidences, e.g. searching stellar substructures in galaxy haloes, or even beyond, in the intracluster regions, under the form of debris of past or recent merger events. These are unique piece of information to study the mechanisms supplying mass in the assembly history of galaxies. In particular, being these events generally located in the halo regions of galaxies, the longer dynamical time can leave the signatures of recent events preserved and useful to study them in details (Bullock & Johnson 2005^[38]).

Complementary to photometry, spectroscopy is a necessary piece of information since these substructures should maintain kinematic signatures of the interaction (West et al. 2004^[237]). Kinematics itself is the fundament for any dynamical analyses aimed at inferring the mass of the galaxies involved in the interactions.

However, spectroscopic measurements of the stellar halos of galaxies are very challenging because their low surface brightness ($\mu \sim 27 \text{ mag/arcsec}^2$ or fainter) and their diffuse nature. Hence, the use of kinematic tracers like planetary nebulae or globular clusters is often a viable alternative to obtain velocity measurements and to study the outskirts of galaxies where it is very hard to measure the absorption line from spectroscopy (PNe; Hui et al. 1995^[122]; Arnaboldi et al. 1996^[4]; Méndez et al. 2001^[159]; Napolitano, Arnaboldi, & Capaccioli 2002^[172]; Romanowsky et al. 2003^[193]; Douglas et al. 2007^[78]; de Lorenzi et al. 2009^[69]; Coccato et al.

2009^[49]; Napolitano et al. 2009^[177], 2011^[176]; Richtler et al. 2011^[190]; Forbes et al. 2011^[91]; Pota et al. 2013^[186]; Longobardi et al. 2015a^[147]; Hartke et al. 2017^[109]) (GCs; Côté et al. 2003^[61]; Romanowsky et al. 2009^[192]; Schuberth et al. 2010^[202]; Woodley & Harris 2011^[244]; Romanowsky et al. 2012^[194]; Foster et al. 2014^[93]; Veljanoski et al. 2016^[229]; Pota et al. 2018^[187]; Longobardi et al. 2018^[148]).

GCs and PNe are observable out to large distances from the galaxy centers (Durrell et al. 2003^[82]; Merrett et al. 2003^[160]; Shih & Mendez 2010^[207]; Cortesi et al. 2011^[56]; Richtler et al. 2011^[190]) and their velocity can be measured with good precision in the nearby galaxy clusters, make them very useful to underline stellar substructures. Furthermore, their kinematical information allows us to go beyond purely photometric observations and characterize the phase-space (of projected positions and line-of-sight velocities) to look for typical signatures expected in these interactions, like tidal streams or chevron-like pattern described in the section 1.4 (e.g., Johnston et al. 2008^[130]; Romanowsky et al. 2012^[194]).

In this chapter I present a new method to search signatures of merger events in the phase space defined by discrete tracers in the core of massive clusters. In particular we will use the case of the Fornax cluster (see chapter 3) where several studies have provided evidences of active galaxy interactions (e.g. D’abrusco et al. 2016^[66]; Iodice et al. 2017^[127]; Spiniello et al. 2018^[211]; Sheardown et al. 2018^[206]). I focused the research on cold substructures, as the one expected to be produced by tidal stripping with dwarf galaxies, which are most abundant galaxies in the universe (e.g., Ferguson & Binggeli 1994^[87]).

Using GCs and PNe as kinematic tracers, we look for substructures correlated in the space of positions and in velocity, and showing a low velocity dispersion (in practice, the standard deviation of the distribution of their line-of-sight velocities), typical of dwarf galaxies (Kourkchi et al. 2011^[138]). In the section 4.2 I will describe some properties of the GCs and PNe. In the section 4.3 I will describe the algorithm used to find these cold substructures, and a simulation used to validate the method proposed. In the section 4.4 I will discuss the goodness of the algorithm testing it on two simulated streams, while in the section 4.5 I present a statistical analysis of the sub-structure candidates the method has found, In the section 4.6 I finally compare spatial positions of the substructures with the latest dwarf catalogs in Fornax (Munoz et al. 2015^[167], Venhola et al. 2018^[230]). In the last section of this chapter I will describe the galmer simulations, a database of thousand simulations of interacting pairs.

4.2 Datasets

I will start by describing some of the main properties of the PN and GC catalogs adopted for the search of substructures in the phase space, in particular I will discuss their distribution in RA, DEC and in the velocity space.

As described in chapter 3, after having applied some appropriate selection criteria, the total number of GCs of our sample is 1183, while our sample of PNe is composed of 1495 objects. Then, the total sample of tracers we will use in the following analysis is made of 2678 objects where GCs represent the 44% of the whole catalog and the PNe the 56%. Figure 4.1 show the position in RA and DEC of the objects and the space made by the clustercentric radius (distance from the center of NGC 1399) vs radial velocity, of the GCs and PNe, respectively. This is a form of reduced phase space, where the position is given by the radius, R , and the velocity is the component along the line-of-sight of every tracers. In the following, we will briefly refer to this as *phase-space*. In the phase-space we also plotted the mean velocities and the velocity dispersion at 1σ and 2.5σ . These were calculated dividing the whole sample in distance bins, such that in each bin the number of the particles is about the same (~ 120).

Looking at the 2D distribution of GCs, this is rather spherically uniform, with a number density of objects increasing towards the center of the cluster. On the other hand, it is evident from the figure 4.1c that PNe have a non homogeneous distribution. This inhomogeneity is due to different reasons: first the position of the 20 FORS2 pointings were not placed symmetrically around the cluster center, but they were driven by the local light density measured in the deep photometry by Iodice et al. 2016^[128]; second, the different observational conditions (seeing) and the failure of some exposure made the intrinsic depth of each pointing different and consequently also the detection limit of the PNe. Hence, the number of identified PNe in each pointing varies not only because of the intrinsic differences of the density of PNe, but also due to the ability of finding them down to the same magnitude limit. In principle, one should have selected all PNe down to the same magnitude in all fields to obtain a complete sample. However, since we did not have an accurate photometry of the sources (PN photometry was beyond the purpose of this thesis) and since we wanted to increase the chance of identifying faint features (which demands the largest possible number of tracers), we decided to keep the full sample at the cost of spatial non homogeneities which will make the chance of finding substructure lower in less complete area.

In the section 4.3.1 I will discuss a simulation of cluster tracers made on the basis of the

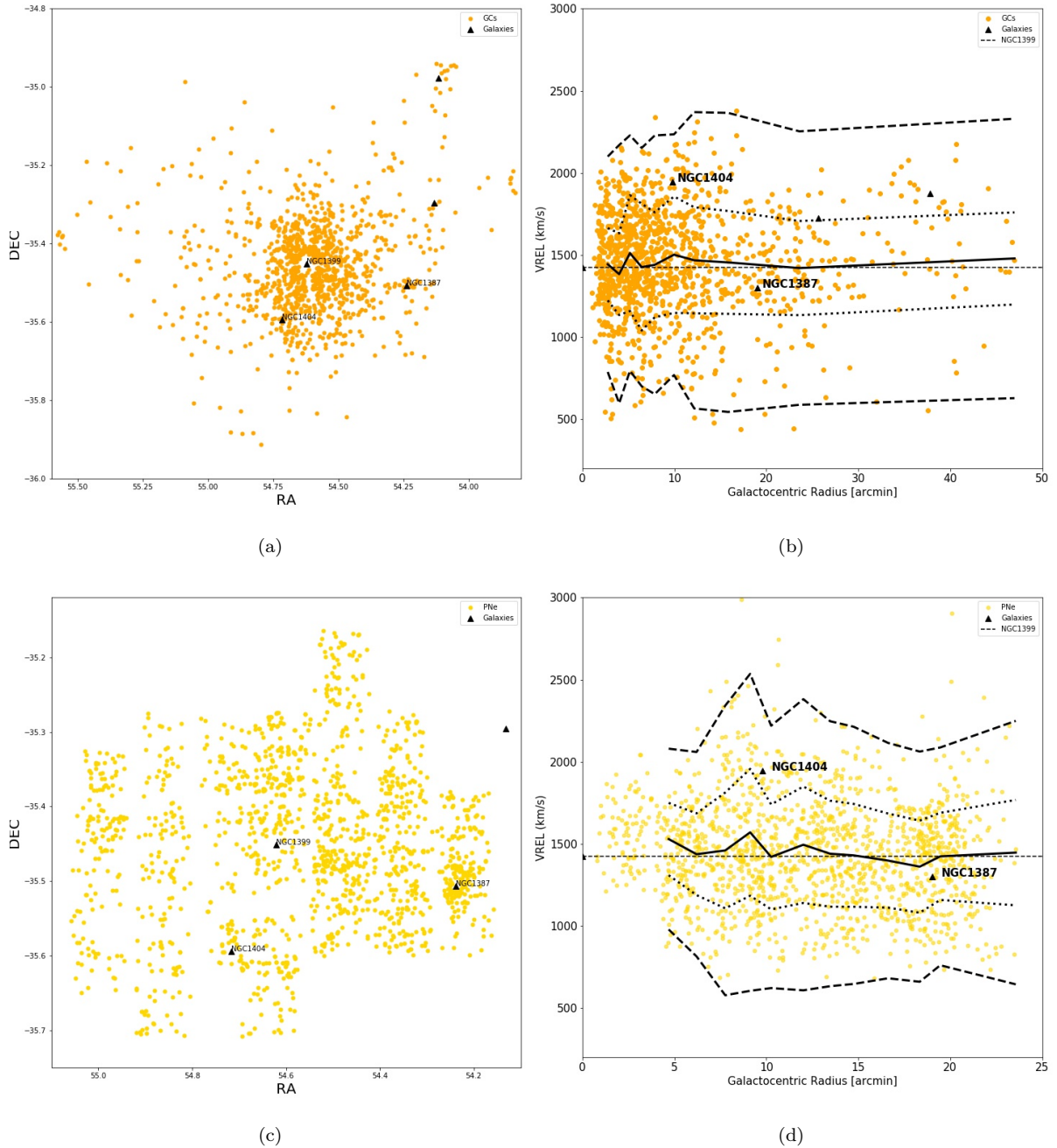


Figure 4.1: (a) - (b) Distribution of the GCs in RA, DEC and in the phase-space, respectively. In (b) there are, overlapped, the mean velocity of the particles (solid line), the velocity dispersion at 1σ (dotted lines) and the velocity dispersion at 2.5σ (dashed lines). (c) - (d) Same plots, but for the PNe. Black triangles are galaxies in the field. The dashed horizontal line in the phase space is the systemic velocity of NGC 1399 (1425 km/s)

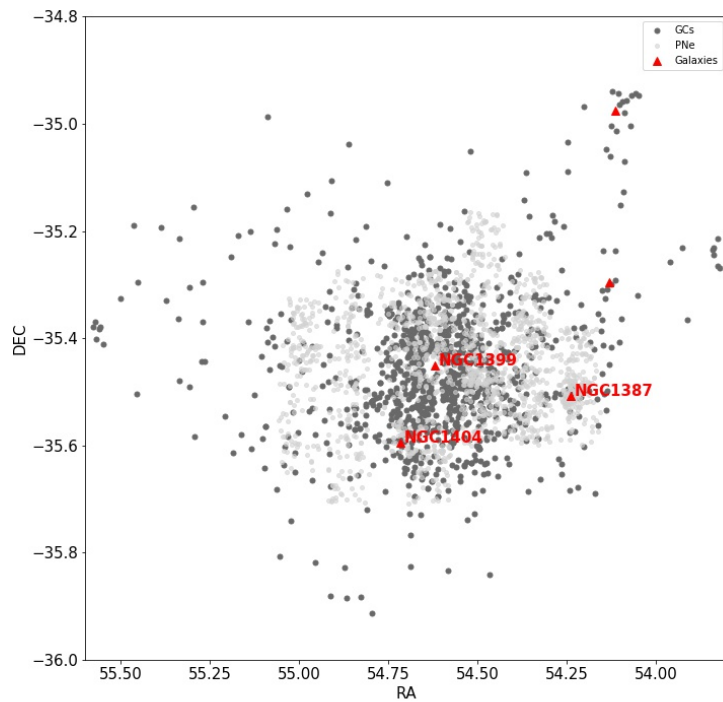
recipe by Napolitano et al. (2001)^[173] in order to test the method proposed in this thesis and to estimate the percentage of spurious substructures. As I will discuss later, this simulation is based on a 3D spherical potential and cannot reproduce the inhomogeneity of the real sample.

This impacts upon the accurate estimate of the spurious detection in real PN data, as I will discuss later. Here, it is important to remark this aspect of the analysis, which we expect to improve in forthcoming developments of this research. There are other differences in the two samples, which result even clearer from Fig. 4.2 where I show the GC and PN samples together. GCs are observed out to ~ 45 arcmin from NGC 1399, while the PN observation extended at a maximum distance of ~ 25 arcmin. There are galaxies, though, like NGC 1387, which mainly have PN detected. Overall PNe do not have a clear decreasing density with the radius outside the bulk of the NGC 1399 system (see discussion about the number density as a function of the radius below).

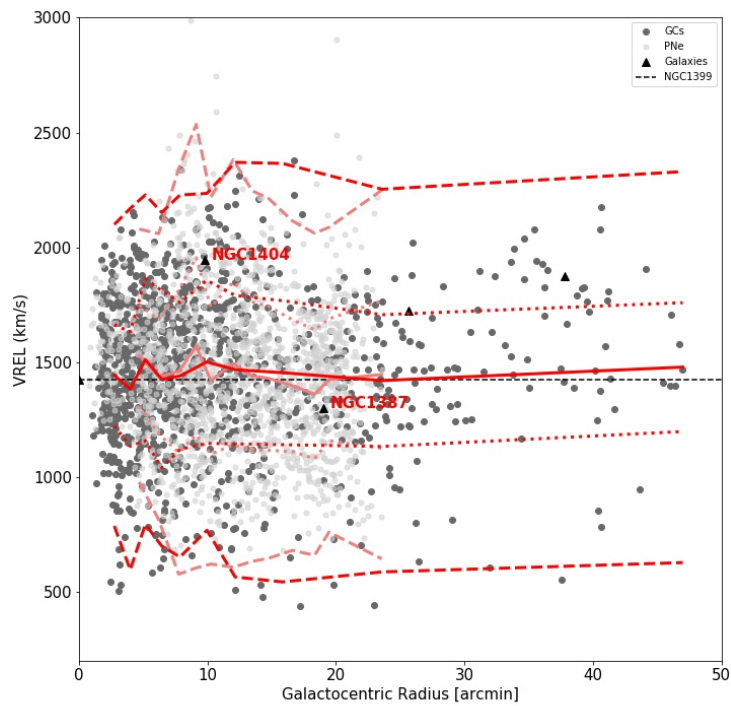
Looking at the phase spaces, either for the separated samples in Figs. 4.1 (b-d), or the cumulative phase space in Fig. 4.2b, besides some inhomogeneities in the radial distribution of the PNe which comes for their spatial inhomogeneities, the two samples show a larger dispersion in the center and a decreasing dispersion going toward larger radii. Both samples have a significant numbers of objects around and even exceeding the $\pm 2.5\sigma$ levels (shown as long-dashed lines in all figures above), i.e. there are likely a lot of tracers which are not bound to the main galaxy and are instead free flying into the cluster potential (i.e. they are intracluster objects, see also Pota et al. 2018^[187] and Spiniello et al. 2018^[211]). Overall the two samples do not show large differences in terms of mean velocity and velocity dispersion (continuous and short dashed lines respectively in Fig. 4.2, bottom). However I will discuss this in a more quantitative way in the next Section.

I just want to remark, in figure 4.1a, that the objects around NGC 1387 ($\sim 19'$ from NGC 1399) have an average velocity higher by about 100 km/s with respect to that of NGC 1387 (1302 km/s, de Vaucoulers 1991^[71]), a result already found by Spiniello et al. (2018)^[211]. We take into consideration this difference in the generation of the simulated cluster.

Finally, in Fig. 4.3 we show the distribution of the cluster-centric radii of the two subpopulation, in order to quantify the differences in their spatial distributions. It is clearer from this figure that PNe (in blue) have been detected up to a distance of about 25 arcminutes from NGC 1399, while the population of GCs (in red) have been detected up to much larger galactocentric distances ($\sim 45'$). As already mentioned before, the PNe do not show a clearly decreasing density with the radius, indeed the number of PNe is almost constant from 4 up to 20 arcminutes.

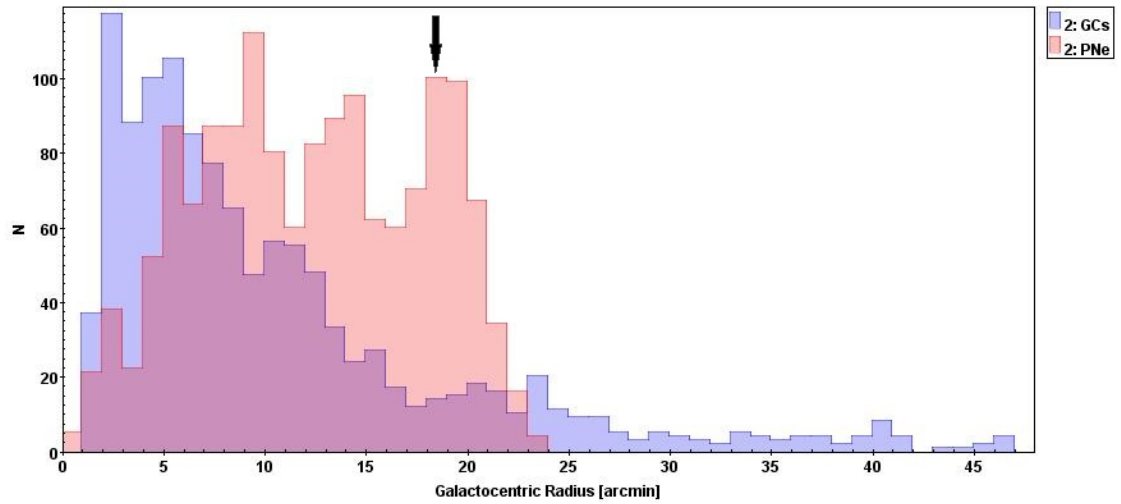


(a)

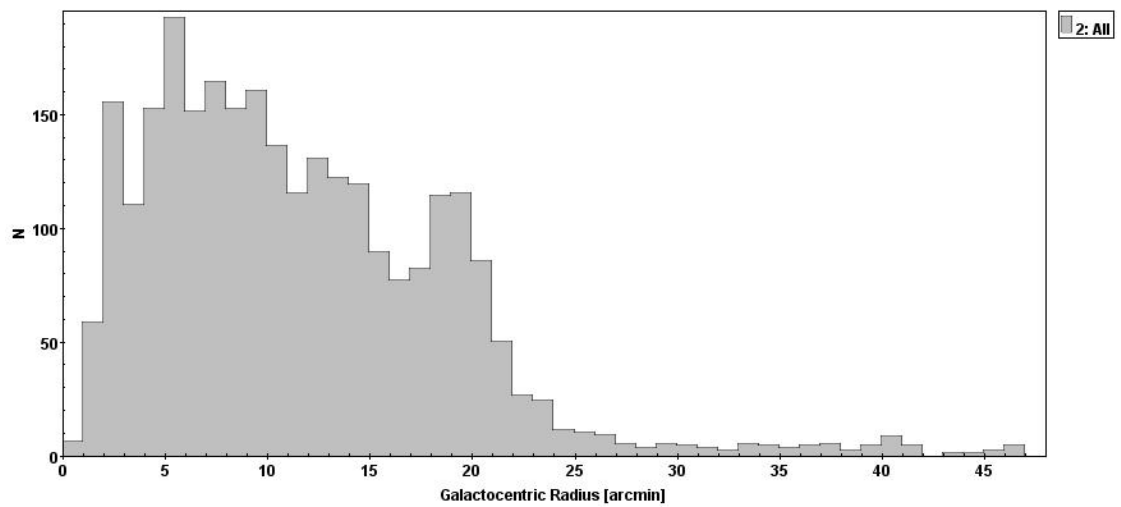


(b)

Figure 4.2: (a): Image of the whole sample of GCs (dark gray) and PNe (light gray) in RA vs DEC. (b): GCs (dark gray) and PNe (light gray) in the phase-space. The lines correspond to the mean velocity of the particles (solid line, dark red for the GCs and light red for the PNe), the velocity dispersion at 1σ (dotted line) and the velocity dispersion at 2.5σ .



(a)



(b)

Figure 4.3: (a) Radial distribution of the GCs (in blue) and PNe (in red) and (b) radial distribution of the whole sample. The vertical arrow shows the position of NGC 1387, which is heavily populated by PNe (and not by GCs in our sample) and sticks out of the overall PN/GC distribution as an evident density peak.

Table 4.1: Parameters and p-values of the Kolmogorov-Smirnov test

GCs	PNe	Radius (arcmin)	p-value
332	327	$5.0 \leq r \leq 9.0$	0.3648
191	363	$10.5 \leq r \leq 15.0$	0.4297
107	352	$15.0 \leq r \leq 18.5$ & $20.0 \leq r \leq 23.0$	0.2380

Notes. In the first two columns there are the number of GCs and PNe in each shell. In the third column there is the inner and outer radius of each shell, while in the last column it is listed the p-value of the K-S test.

The peak at about 20 arcminutes (indicated by the black arrow in the figure 4.3) is due to the numerous PNe detected around NGC 1387 (see also the figure 4.1, bottom). On the other hand, the radial distribution of GCs is much different, showing a constant decline outside the NGC 1399 system. The total radial distribution of both populations reflect the trends described above, hence there is a slight decrease in the number of the objects beyond the 10 arcminutes and then a deep decrease at about 25 arcminutes, the maximum radius of detection of the PNe.

4.2.1 Kolmogorov-Smirnov test

Due to the general similarities of the two subsamples we can think of combining them together to increase the statistics, under the reasonable assumption that PNe and GCs both respond in the same way to the encounters, hence showing the same kinematics if populating the streams we want to spot in the phase-space.

In this section I want to test the hypothesis that PNe and GCs are both extracted by the same parent population, and in order to do so I have performed a Kolmogorov-Smirnov test (K-S test, hereafter) on the two samples. If so, this will justify us to use them as a single test particle population in the stream detection algorithm (see section 4.3).

We expect that, in a stripping event, kinematic differences between GCs and PNe are within velocity uncertainties, hence we could not distinguish these two population from their kinematics, despite intrinsically they can have a slightly different kinematics within the galaxy potential they originally belong to.

Indeed following the discussion in Napolitano et al. (2014)^[175] we can expect the differences in the projected dispersion profile on two population to be originated by the different number density profiles and intrinsic anisotropy of the two population. Assuming a power-law profile $v_{\text{circ}}^2 = V_0^2 r^{-\gamma}$ and $\sigma^2 = \sigma_0^2 r^{-\gamma}$ where $v_{\text{circ}}^2 = GM(r)/r$ and $\gamma \equiv -d \ln \sigma^2 / d \ln r$, the projected

dispersion can be written as (Dekel et al. 2005^[73]):

$$\sigma_{\text{P}}^2 = A(\alpha, \gamma) \left(\frac{(\alpha + \gamma) - (\alpha + \gamma - 1)\beta}{(\alpha + \gamma) - 2\beta} \right) V_0^2 R^{-\gamma} \quad (4.1)$$

where $\alpha \equiv -d \ln j / d \ln r$, $\beta = 1 - \sigma_{\theta}^2 / \sigma_r^2$, with j is the deprojected surface brightness, σ_{θ} and σ_r^2 are the azimuthal and the radial velocity dispersion in the spherical coordinates, respectively; and

$$A(\alpha, \gamma) = \frac{1}{(\alpha + \gamma)} \frac{\Gamma[(\alpha + \gamma - 1)/2]}{\Gamma[(\alpha + \gamma)/2]} \frac{\Gamma[\alpha/2]}{\Gamma[(\alpha - 1)/2]} \quad (4.2)$$

In the assumption of a power-law profile α, β and γ are constant with r for PNe and GCs. In large galaxies given the typical values of these parameters, the difference can be of the order of 10–20% (see e.g. Napolitano et al. 2014^[175]), hence basically within the typical errors of individual dispersion values obtained by PNe and GCs. If we knew these parameters in dwarf galaxies (as done for massive systems) we could predict also for the latter systems what it might be a difference in projected velocity dispersion according to Eq. 4.2.

Unfortunately there are little information on the detailed slope of these populations in low-mass systems, while we have sparse information on the the metal rich and metal poor stellar populations in the local group, which might be used as a reference being PNe and GCs possibly tracers of the former and the latter populations respectively. For instance, Walker & Peñarrubia (2011)^[234] discuss the dispersion predictions of different rich and poor subpopulations assuming realistic profile slopes and anisotropy parameters and show (see e.g. their Fig. 3) that the velocity dispersion difference become very small (of the order of 10% or smaller) outside 1–2 R_e . If we assume that the PNe and GCs basically follow the kinematics of these subcomponent, then we can reasonably expect that the two population should show differences in their velocity dispersion profiles of the same magnitude, hence again within the typical statistical errors. To check that the two tracers are statistical indistinguishable in a more quantitative way, we decided to perform a Kolmogorov-Smirnoff (K-S) test.

A K-S test is a non parametric test used to compare the probability distributions of two samples. It measures the maximum distance between the cumulative distribution of the samples¹; if this distance is below a critical value the two samples likely come from the same distribution. To verify that GCs and PNe follow the same kinematical distribution I defined three shells at different radial distances from NGC 1399, and then I performed a K-S test in each of them. I excluded from this non parametric test the inner region of the cluster ($R \leq 5$ arcmin) and the

¹In statistics, the cumulative distribution function of a random variable X , evaluated in x , is the probability to have a value less or equal to x , or $F_X(x) = P(X \leq x)$

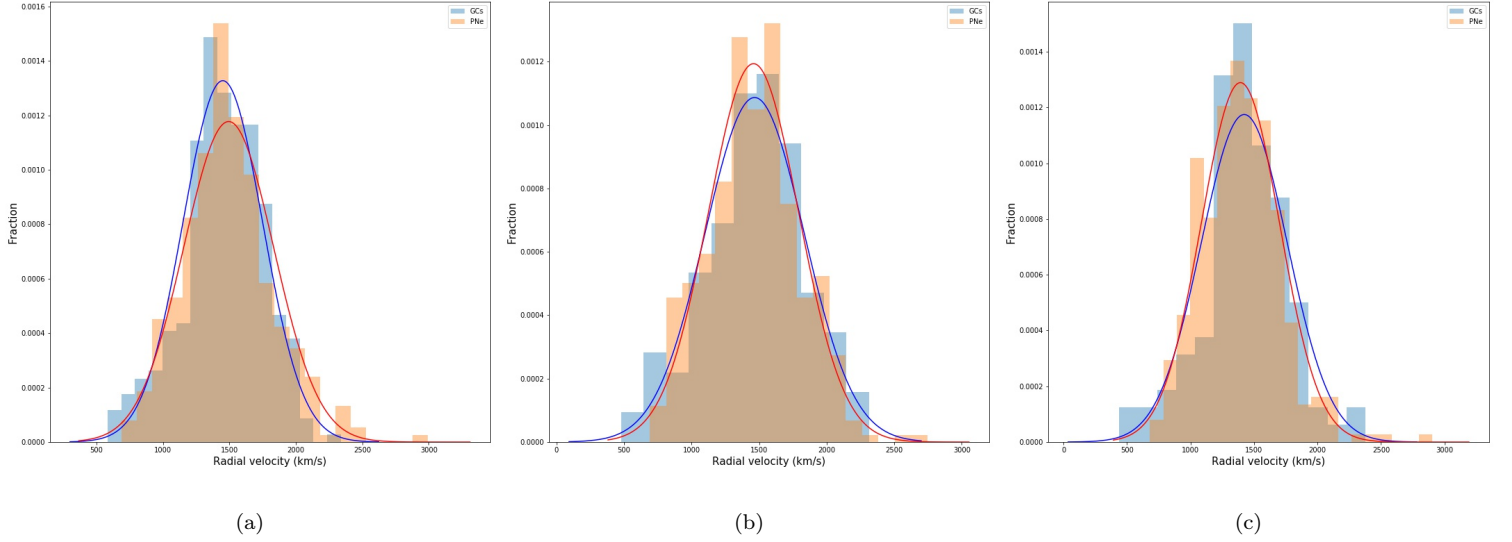


Figure 4.4: Histograms of the fraction of GCs (in blue) and of the PNe (red) per velocity interval in the three shells at different radial distances. Overlapped to these histograms there are the distribution of the two samples.

galactocentric distances where NGC 1387 and NGC 1404 are located because these regions will be excluded in the research of the cold substructures (see section 4.3.5).

The inner and outer radius of each shell were selected in order to have about the same number of particles, although the non uniform distribution of the PNe make difficult to have the same number of GCs if the number of PNe is kept almost constant. Because of PNe are selected out to a maximum distance of about ~ 25 arcmin, there are not further shells beyond this galactocentric radius.

In the table 4.1 I show the results of the K-S test in each shell. In the figure 4.4 it is displayed the histogram of the fraction of GCs (in blue) and of PNe (red) per velocity interval for the three shells and their distribution. The results obtained from the K-S test are consistent with the null hypothesis that both GCs and PNe follow the same distribution. Indeed the p-values for all the shells showed in the table 4.1 are well above the significance level of the 5%; moreover it is also evident from the figure 4.4 that the two distributions are very similar. From now on, we will consider in the algorithm that I will describe in the next section, GCs and PNe as the same test particles, thus increasing the signal-to-noise ratio and enhanced the chance of finding a cold substructure.

4.3 An algorithm to find cold substructures

As I mentioned in the previous section the goal is to find cold substructures correlated both in the position and in velocity; therefore I implemented an algorithm that looks for points close both in the plane made of RA vs DEC and in the plane made of velocity vs distance from the center of the cD. This is based on a nearest-neighbors approach, taking also velocities of particles into account, so that it can find coherent kinematic substructures. The algorithm can be divided in two steps: in the first step it defines as "friends" all points that are close enough in the space of configurations and have a similar velocity; then it inspects all common points belonging to different group of friends in order to check if these groups belong to the same substructure. This allows to find also structures that have a chain-like pattern.

The first part of the algorithm works in this way:

1. it takes a point (hence 'origin') in the space of configurations, and find the k nearest neighbors;
2. it measures the mean velocity \bar{v} , and the velocity dispersion σ of the k nearest neighbors;
3. it discards outliers which have a velocity outside $n \sigma$ of the mean velocity \bar{v} ;
4. it iterates point 3 until there are no more outliers or there are no more points;
5. it verifies that the 'origin' has a velocity within 1σ from the mean velocity \bar{v} of the remnant points;
6. it verifies that the total number of points is greater than a threshold value ($N_{\text{tot}} \geq N_{\text{min}}$), if this is true we found a group and we call these points "friends";
7. it measures the mean velocity \bar{v} and the velocity dispersion σ of the "friends";
8. it repeats from the point 1 to the point 7 for all GCs and PNe present in the catalog and stores the different groups of friends.

The adoption of a threshold for the minimum number of objects to define them as a group (the point 6 in the first part of the algorithm) is critical: indeed this is needed to minimize the detection of spurious groups that have similar velocity by chance. We aspect that on k points some of them can have casually a comparable velocity, but this probability decreases by increasing the number "k" of points belonging to the group, hence having a better chance to select a real structure.

The algorithm described above has the advantage that it is able to refine the selection of coherent spatial and velocity substructures, however, it has the disadvantage to be biased toward round geometries being based on a simple metric which uses the distances from every single particles. This reduces the chance to identify chain-like structure, which are likely expected in elongated streams. Here below we have added a second stage in the algorithm aimed at verifying if some of the groups do belong to a single structure, by analyzing their common points. The algorithm performs the following steps:

1. it takes a group and find all the other ones which have common points with it;
2. starting from the group with lower velocity dispersion (σ_1), it compares σ_1 with the velocity dispersion (σ_2) of the other group of friends;
3. if $\sigma_2 \leq \sigma_1 + \frac{\sigma_1}{\sqrt{2N_{tot}}}$ it joins these two groups in a unique structure;
4. it repeats points from 1) to 3) until it inspects all the other groups which have common points;
5. it measures mean velocity v_{fin} , and velocity dispersion σ_{fin} of the final structure;
6. it repeat from the point 1) to the 5) for all group of friends found in the first step;
7. it deletes all substructures with σ_{fin} greater than a threshold value ($\sigma_{fin} \geq \sigma_{min}$).

At the end we have a certain number of substructures with a low velocity dispersion (the cut-off is imposed in the last point in the second step of the algorithm).

This algorithm depends on a number of parameters (k , n , N_{min}) whose values must be chosen in order to maximize the number of real cold substructures (completeness) and minimize the number of spurious ones (purity). In the next sections I will show how the parameters of the algorithm have been set in order to optimize both completeness and purity.

4.3.1 Simulation of the Fornax cluster

In this section I describe the suite of Montecarlo simulations of the core of the Fornax cluster I have used to asses the performances of the algorithm described above. We simulated only the region covered by our objects, that is the regions of Fornax of about 1.8 degrees^2 around the cD, NGC 1399. In this area there are other two bright galaxies besides NGC 1399: NGC 1404, located just below the cD, in the S-E direction at about 9 arcmin; and NGC 1387, at

a distance of ~ 19 arcmin at west of NGC 1399; both of them are early type galaxies. We generated simulated GCs and PNe at the equilibrium in the gravitational potential of these three galaxies, assuming this to be the superposition of the individual galaxy potential with spherical symmetry. We will refer to these particles in the following as “relaxed” particles or component. Following Napolitano et al. (2001)^[173], we have produced the 3D position starting from a 3D density profile and then projected on the 2D (X-Y in our case) sky plane. For each particle we have determined the 3D velocity vector according to the hydrostatic equilibrium equations (see below), which we have projected along the line of sight and finally simulated a radial velocity measurement by randomly extracting the measured velocity from a gaussian having the truth radial velocity as mean and standard deviation equal to the measurement errors. In order to produce these Montecarlo realizations of particles sampling the total potential in the Fornax core, we have assumed for the cluster a total mass of about 10^{14} solar masses and assumed a Hernquist (1990)^[112] density distribution of the stellar-like tracers. This is a good approximation for elliptical galaxies following the de Vaucouleurs law (1948). The luminous mass density is expressed by the formula

$$\rho(r) = C \frac{M_1 a}{2\pi} \frac{1}{r(r+a)^3} \quad (4.3)$$

where M_1 is the total luminous mass, a is a distance scale ($R_e = 1.81534 a$) and C is a normalization constant.

In addition to the stellar mass density we also considered a dark halo whose distribution was assumed to follow a Navarro-Frenk-White profile (NFW); so the potential is derived from the total mass:

$$M_{\text{tot}} = M_1 + M_{\text{dm}} \quad (4.4)$$

We consider a non-rotating system,² and an isotropic velocity dispersion tensor. Hence, the radial Jeans equation, which regulates the equilibrium of spherical gravitating systems, writes:

$$\frac{d(\rho\sigma^2)}{dr} = -G \frac{M(r)\rho(r)}{r^2} \quad (4.5)$$

This allowed to obtain the 3D velocity dispersion of the tracers and generate a full 3D phase space. As briefly anticipated above, we then simulated an observed phase-space by projecting the tracer distribution on the sky plane and derive the line-of-sight velocity of the individual particles. In order to simulate a velocity measurement, we took into account the typical velocity

²Although it was measured a rotation of blue GCs in the radial range between 4 and 8 arcminute, the kinematic of the outskirts of NGC1399 is dominated by the random motions (Schubert et al. 2010^[202], Coccato et al. 2013^[50])

Table 4.2: Parameters of the simulated cluster

Galaxy	Number of Points	Effective ^a Radii (arcsec)	Velocity ^b Systemic (km/s)	Velocity ^b Dispersion (km/s)
NGC1399	2380	138	1425	320
NGC1387	150	42	1302 ^c	160
NGC1404	45	24.5 ^c	1947	247

Notes. In this table there are the parameters of the simulated galaxies. In the second column there are the number of the points simulated for every galaxy. In the columns 3 there is their effective radii; finally in the columns 4 and 5 there are, respectively, the systemic velocity of the galaxies and their velocity dispersion

^a Values taken from Caon, Capaccioli, D’onofrio (1994)

^b Values taken from Nasa Extragalactic Database (NED)

^c These values have been adapted to obtain a more realistic reproduction (see below in the text)

error in order to randomly extract the observed velocities (we refer to the original Napolitano et al. 2001^[173] paper for more details about the Montecarlo simulation). With the projected X and Y position and the radial velocity we could mimic different mock observations to test our stream detection procedure. We have been careful to check that the position and phase-space closely resemble the real one.

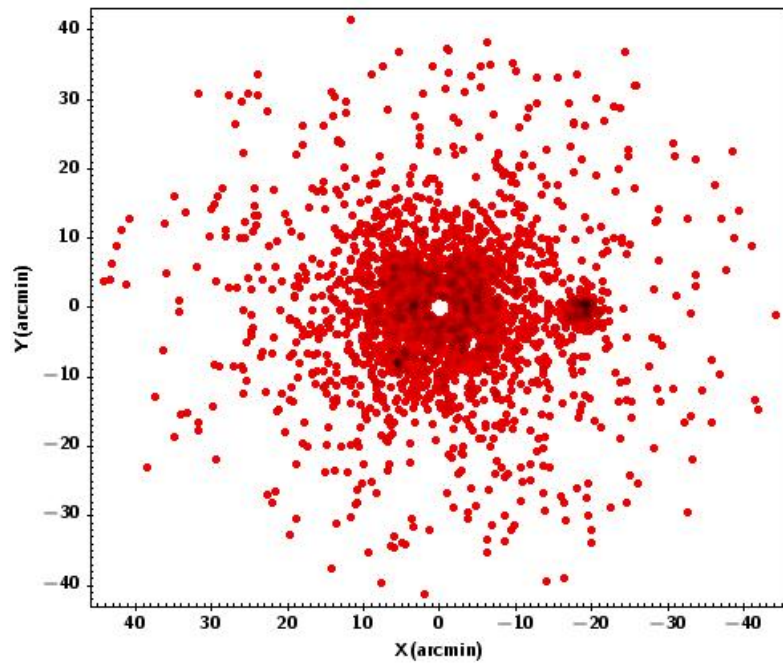
The parameters of the three simulated galaxies are reported in table 4.2.

Of the total number of particles included in the simulations, i.e. 2575 similarly to the totality of PNe nad GCs in the area, the number of points for each satellite galaxy was obtained with a cross-match with the real data (i.e. counting the number of plausible particles bound to the galaxies), while both effective radii and velocity dispersion were taken from literature.

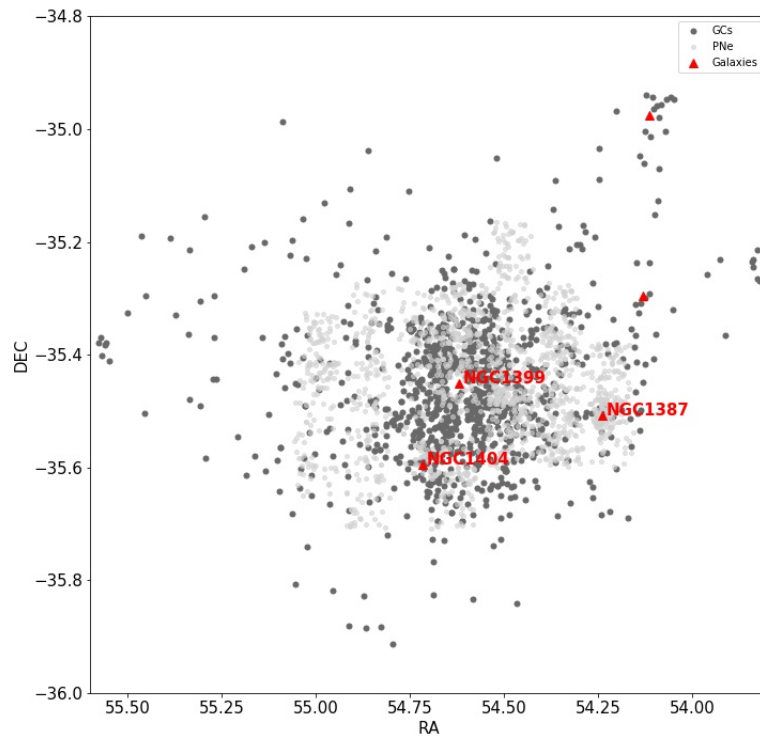
We used a mean measurement error on the velocities of 39 km/s , very similar to the velocity uncertainties in the real sample, which have an average of about 37.5 km/s . In figures 4.5 we show the simulated points with positions computed with respect to the simulated cluster center, while in the bottom panel we show the real data. In figure 4.6 shows the same points in the phase-space (black circles), overlapped with the real data (red circles).

To obtain a realistic reproduction of the PN and GC system around NGC 1404, we need to adopt an effective radius (i.e. the characteristic scale of the light distribution) larger than the usual estimate from literature from (Caon, Capaccioli, D’onofrio 1994)^[41], but used a $R_e \sim 100''$, more consistent with the one from Corwin et al. 1985^[58] (i.e. $\sim 80''$).

We found another inconsistency between the simulations and the real sample in the points



(a) Points of the simulation with NGC1399 at the origin of coordinates. NGC1404 is just below the cD and NGC1387 is at $X = -20$ arcmin



(b) Positions of the real sample of GCs (dark gray points) and PNe (light gray points). Red triangles are the galaxies in the field.

Figure 4.5: (a): relative positions of the simulated points. (b): positions in RA and DEC of the real sample.

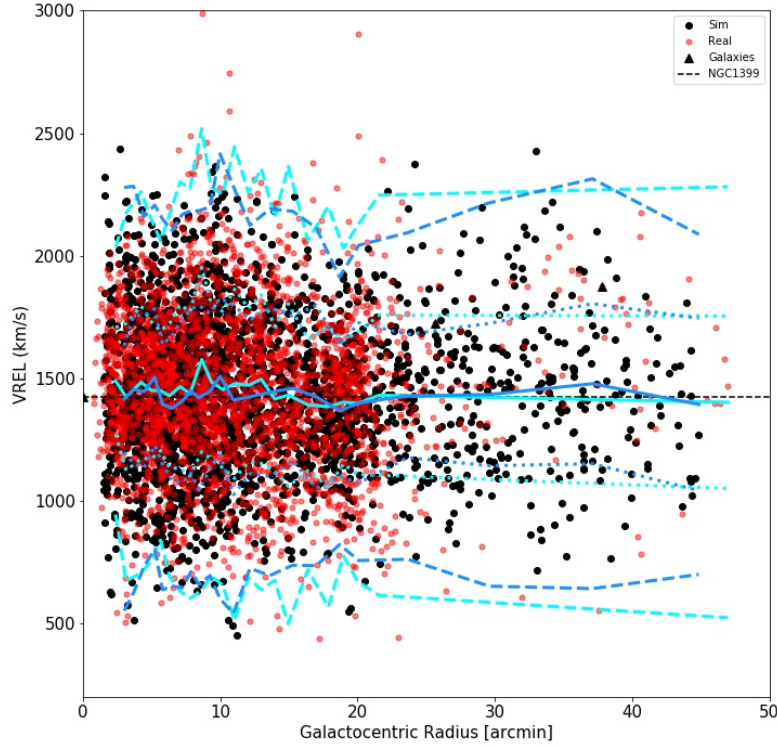


Figure 4.6: Phase-space with real data (open red diamonds) overlapped with points of the simulation (black circles). On the x-axis the distance from NGC1399 in arcminute and on the y-axis velocities of the points in km/s . The continuous cyan and blue lines represent the mean velocity as a function of the radius of the real and simulated particles, while the short-dashed and long-dashed lines represent the 1σ and 2.5σ profiles of the same datasets. It is evident that real data and simulations have very close global properties as a function of the radius. The dashed black line represents the systemic velocity of NGC1399 ($1425 km/s$)

surrounding NGC 1387; they were shifted downward in the phase-space respect to real particles. We explain this difference with an inferred velocity of PNe higher by about $\sim 100 km/s$ than the systemic velocity of the galaxy which is tabulated in the literature (see section 4.2 and Spiniello et al. 2018^[211]). Indeed in this area we have a larger number of PNe than GCs, respectively 117 (88%) and 16 (12%) within three effective radii from NGC 1387; thus we add $100 km/s$ to all simulated points around NGC 1387 in order to fit the real objects. The final result of all these fine tuning calibration of the simulated sample is shown in Figure 4.6 where we can see that there is a good superposition between simulated and real points in the surrounding regions of these two galaxies, within 10 arcminutes for NGC 1404 and ~ 19 arcminutes for NGC 1387. Overall the phase-space similarity of the real and simulated data are also demonstrated by the nice overlap between their mean velocity lines and the 1σ and 2.5σ profiles (see also Figure caption).

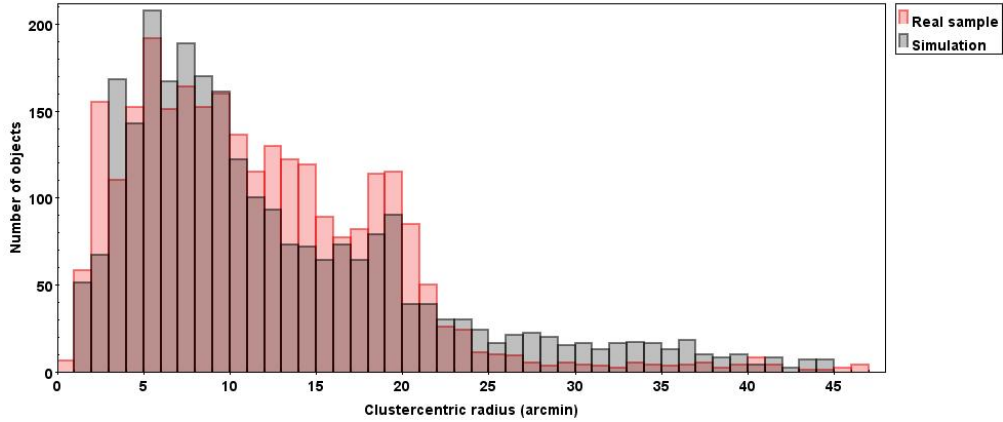


Figure 4.7: Histogram of the number of particles in function of the distance from the center of NGC 1399. Simulation are shown in black, whereas real data are red.

In the figure 4.7 the number of the real (red rectangles) and simulated points (black rectangles) as a function of the distance from NGC 1399 are compared. There is a good agreement between the two samples, although there is an excess of points in the real data between 12 and 21 arcminute, probably due to the inhomogeneity of PNe sample (see section 4.2). We will keep this in mind in the case there will be a segregation of stream detection in this specific area, which might be a warning that there is an underestimate of spurious substructures in the simulated datasets.

On the other hand, there is a slight overabundance of points in the simulation from 24 arcminutes and further, this is possibly due to the fact that there are no PNe detected in this area (see figure 4.1c), which we did not impose in our simulation. However, due to the small differences, we do not believe this is affecting the prediction of spurious detection at these distances.

Furthermore, we also see differences in the range between 2 and 3 arcminute, which is difficult to take into account in the simulation, since we do not have an accurate detection function in the very bright center, but this is not important because this area is excluded from the search of the substructures (see next Sections).

Finally, from Fig. 4.6, showing the phase space of the simulation and the real datasample, we also see that, despite the differences in the radius distribution due to the inhomogeneities discussed above, there is a substantial similarity between the simulation and real data velocity distribution at all radii. Only, the real data seem to have more scattered particles, possibly because the real cluster is not properly at the equilibrium like the simulated systems we have produced by construction with our Jeans equations.

Since there are no streams or interactions in the simulated dataset, the synthetic particles are just points moving in a 3-D spherical potential of the galaxy, and the number of the structures that we expect to find is zero. All the detected groups are indicative of the number of contaminants that we could find if we would run this in real data. In fact every subgroup found in the simulation is not determined by a real substructure in the phase-space, but it is a random combination of connected particles. By varying the free parameters and applying the algorithm to the simulation with no real streams we can find the set-up needed to minimize the number of spurious substructures.

4.3.2 Selection of the parameters

In this section I describe how to choose the free parameters (k , n , N_{\min}) of the algorithm, in order to maximize the number of real substructures in the sample and minimize the incidence of the false detections. To do that, I used the simulation of the cluster described in the previous section to select the best set of parameters to be used on real data. Since we have discussed the difficulty of the simulation to reproduce the inhomogeneities of the real data, we will use a conservative approach by considering as a lower limit the number of spurious detection found for a given parameter set-up. For this reason, in order to minimize the spurious detections in the real data, we will use as viable parameters the ones that produce no spurious detection if the algorithm is ran on the simulations without the addition of any simulated stream (see next section).

Indeed, the algorithm has been ran on this simulation varying the parameters in the following ranges:

- $10 \leq k \leq 30$
- $1.3 \leq n \leq 2$
- $4 \leq N_{\min} \leq 17$

This choice allowed us to search either small substructures, that we aspect to find with a low k and a low N_{\min} , or more large and spatially extended groups with a greater values of both k and N_{\min} .

To reduce the possibilities of finding spurious substructures I excluded from this research the inner regions of the three galaxies; indeed there is an high probability that in these areas the algorithm finds false cold substructures that actual belong to one of the bright galaxy in Fornax.

Furthermore it can happen that, because of the high density in these regions, there are some objects that are close either in the position or in the phase space owing to an accidental two-dimensional projection; hence the algorithm can reveal as a real substructure points that actual are far in the line of sight. Additionally, we expect the outskirts of galaxies to preserve kinematic information of accretion events, due to a longer dynamical time that prevents substructures to quickly mix in the cluster potential (Bullock & Johnston 2005^[38]).

So I searched for subgroups only in the outer regions beyond $5'$ from NGC 1399 and beyond two effective radii from the other galaxies ($49''$ for NGC 1404 and $84''$ for NGC 1387).

I want to stress that with a nearest-neighbors approach it could happen that if the origin point is close to these borders, we could have a subgroup that may be accidentally classified as cold because the hotter component is outside the observed area; in order to avoid these border effects we will exclude also these very borderline regions.

As cut-off in the maximum value of σ_{\min} I used 40 km/s and 50 km/s , values comparable to the dwarfs velocity dispersion, because we are looking for tidal debris with this kind of galaxy population. Indeed, we expect that the dwarf disruption is the most common event still going on in the local universe which contributes to the intracluster stellar population and the assembly of large stellar haloes around galaxies. The remnants of these events preserve their kinematic properties for a longer time than those of massive satellites (see section 1.4). Furthermore massive galaxies produce more diffuse substructures due to a higher velocity dispersion and a larger sizes, so they are harder to unveil in the phase space (see section 1.4).

4.3.3 Setting-up the best parameter range of the stream finding algorithm

The next step was to find the best values for free parameters. The overall plan is to use the same parameter set-up on simulation and real data and select the parameter combinations that minimize the number of contaminants. By varying the values of the parameters as I described above, I considered as good all those which find no substructures in the simulation, which due to the nature of this one, are false groups.

In order to reduce the parameter space I have started to test the parameter combination on a first simulation (i.e. the one shown in Figures 4.5) to find the parameter values that clearly produced too much spurious detection to be used.

With this approach I found 13 good set of parameters with a $\sigma_{\min} \leq 40 \text{ km/s}$. These are

listed in Table 4.3, where the parameter set is shown together with the number of time these structure occur over 100 re-simulation of the same cluster described in the previous Section (see next Section for more details). In fact, as discussed in the next Section, we have repeated the same exercise on a suite of 100 simulations in order to estimate the occurrence of spurious detection, which are our main contaminant in the automatic stream search.

As a first general consideration, there is a strong dependence on the N_{\min} , as we expect owing to the diminishing probabilities to have spurious groups when this number is increased; while these results are almost independent from the other two parameters (k and n).

Indeed, in almost any way I changed them there is at least a value of N_{\min} where we have no more structures in the simulation.

On the other hand, it is harder to obtain good set of parameters with $\sigma_{\min} \leq 50 \text{ km/s}$: After applying this cut-off I found five good set of parameters; in this cases it is more common to find false substructures, and there is a dependence also on the other parameters (k, n).

4.3.4 Validation of selected parameters

The procedure described in the Section 4.2.2 followed to select candidates of good sets of parameters, but this is just a first step to find out the reliability of these sets, that will enables us to state which substructure that we will find in the real sample is not spurious. In this section I focus on the evaluation of the robustness of the sets of parameters found before, and I give a measure of their reliability.

Obviously a single simulation is not enough to detect truly reliable sets, indeed we have to test the robustness of these sets of parameters against the statistical fluctuations that occur over a large enough number of simulations. Hence the next step is to test the parameter set-up in Table 4.3 and analyze their stability; this is necessary to evaluate the goodness of the substructures found in the real data or the probability that they are just false detections. We start using a threshold of 40 kms^{-1} for the velocity dispersion of the final stream candidate (see Section 4.2.2).

As anticipated we used 100 simulations to measure the number of times a given set of parameters produced false groups. Looking now closer to the results reported in Table 4.3 it is evident that not all sets of parameters produce a reliability to detect real cold substructures and that some of them are highly unreliable. By reliability here we indicate the probability over 100 simulations (with no simulated substructures) that a parameter set-up produces no false detections.

These results clearly show that there are a number of parameter combinations that produce

Table 4.3: Parameter of the algorithm and their reliability when the cut-off in the velocity dispersion is $\sigma = 40$ km/s.

$k - n - N_{\min}$	Occurences ^a	Reliability (%) ^a
10 - 1.5 - 7	3	97
10 - 1.8 - 7	44	56
10 - 1.3 - 6	6	94
10 - 2.0 - 8	1	99
12 - 1.3 - 6	24	76
15 - 1.3 - 6	52	48
15 - 1.5 - 8	24	76
15 - 1.5 - 9	5	95
20 - 1.5 - 9	33	67
20 - 1.3 - 8	7	93
25 - 1.8 - 12	16	84
30 - 1.3 - 8	53	47
30 - 1.8 - 13	13	87

Notes. In the first column there are the values of the free parameters, where k is the number of nearest neighbors, n is the number of sigma used to remove the outliers and N_{\min} is the minimum number of points to consider them as "friends". In the second and third columns there are the number of times that a set found at least a spurious substructure and its reliability, defined as the number of times that the set do not find any substructure. In the last column there are the real structures that each single set detects.

^a Since the probability to have false groups on N simulations follow a Poissonian, errors are $\sqrt{N} = 10$, that is 10%.

Table 4.4: Parameter of the algorithm and their reliability when the cut-off in the velocity dispersion is $\sigma = 50$ km/s.

$k - n - N_{\min}$	Occurences ^a	Reliability (%) ^a
10 - 1.5 - 7	30	70
15 - 1.5 - 8	58	42
20 - 1.8 - 11	35	65
25 - 1.8 - 14	45	55
30 - 1.8 - 14	61	39

Notes. In the first column there are the values of the free parameters, where k is the number of nearest neighbors, n is the number of sigma used to remove the outliers and N_{\min} is the minimum number of points to consider them as "friends". In the second and third columns there are the number of times that a set found at least a spurious substructure and its reliability, defined as the number of times that the set do not find any substructure. In the last column there are the real structures that each single set detects.

^a Since the probability to have false groups on N simulations follow a Poissonian, errors are $\sqrt{N} = 10$, that is 10%.

at least a false detection in a large fraction of simulations, however the majority of set-ups produces spurious detection in less than half of the Montecarlo re-simulations.

In particular, we have two sets of parameters that have a reliability lower than 50% (i.e. that produce false detections for more than 50 % of the extractions over the 100 simulations); four parameter combination below 70 %; four between 70% and 90% and five larger than 90%. In general 50% probability is an acceptable risk to take for the automatic detection of streams in real data, i.e. assuming that half of the detected substructures might turn to be spurious. However, since we saw this is possibly a lower limit in the fraction of the spurious detection (or an upper limit on the reliability) we have decided to take instead the 70% as a more conservative threshold. In the following we will discuss the streams found in real data (if any) with the parameter set-up corresponding to reliability larger than 70%.

We have repeated the same automatic detection of spurious substructures, this time using a dispersion threshold of 50 kms^{-1} , with the results reported in Table 4.5. In this case the combination that returned a reliability of the order of 70% is only one, i.e. $k = 10$, $n = 1.5$, $N_{\min} = 7$.

4.3.5 Results on real data

In this section I discuss in details all substructures found in the real sample using the set of parameters validated on simulations in the previous section. Here I follow the same steps used

for the simulations, starting by excluding points within $5'$ from NGC 1399 and within two effective radii from NGC 1404 and NGC 1387.

I begin with the description of the structures found using a cut-off on the velocity dispersion of $\sigma = 40 \text{ km/s}$, which provided 13 sets of reliable parameters to adopt for the stream finding.

With these sets of parameters, the algorithm has found three different substructures, each of them occurring more than one time in different parameter set-ups. The results are summarized in Table 4.5.

Although these substructures are recurrent for the majority of the points belonging to them, depending on the specific parameter combination some of the objects can be jump in or out of the selection and the number can slightly change from one set-up to the other.

In the figure 4.8 these three cold substructures are plotted in RA-DEC and in the phase-space against the other ungrouped particle in their surrounding. Since the groups can change depending on the particular parameter set-up, in these figures I have plotted only the points belonging to the substructure found from parameter set-up gave the lower velocity dispersion.

In the following I will brief discuss the details of these three cold substructures, leaving a statistical characterization of them to a later section.

S1:

This structure occurs 11 times on 13 different sets of parameters, using any value of k and n ; and it is the one that shows up more than any other. It varies from a minimum number of points $N_{\text{tot}} = 7$ (when k is 10), to $N_{\text{tot}} = 13$ (when k is 30). Its dispersion of velocities ranges from $\sigma = 30.35 \text{ km/s}$ when $k = 15, 30$; and $N_{\text{tot}} = 9$ to $\sigma = 39.65 \text{ km/s}$ when $k = 10$ and $N_{\text{tot}} = 8$. It is located just beyond 5 arcminutes in the North-West direction from NGC 1399, and as we can see in the figure 4.8, it has a mean velocity comparable to that of NGC 1399, with some points above and others below its systemic velocity.

S2:

This structure occurs for three different parameter combination, with $k = 15, 30$; and it varies from a minimum of 10 points when k is low, to 14 points when k is high. It is located farther from the cD than other two structures, at a distance of about $15'$, just to the west of NGC 1404, in a region where it was observed an overabundance of blue GCs by D'abrusco et al. (2016)^[66]. Its mean velocity ($V_{\text{mean}} = 1325 \text{ kms}^{-1}$) is lower than the velocity of NGC 1399 ($V_{\text{sys}} = 1425 \text{ kms}^{-1}$) and its velocity dispersion ranges from $\sigma = 32.13 \text{ km/s}$ when $k = 30$ and $N_{\text{tot}} = 14$ to $\sigma = 39.06 \text{ km/s}$ when $k = 15$ and $N_{\text{tot}} = 10$.

S3:

This structure occurs only for two times over the 13 selected parameter set-ups, i.e. for $k = 12$ and $k = 15$. In these two cases it has the same seven points shown in the figure 4.8. This structure is located just beyond five arcminutes in the South-West direction respect NGC 1399. It has a mean velocity ($V_{\text{mean}} = 1509 \text{ kms}^{-1}$) larger than that of the cD and a dispersion of velocity of $\sigma = 36.43 \text{ km/s}$.

Now I describe all the substructures found with a cut-off in the velocity dispersion of $\sigma = 50 \text{ km/s}^3$.

In this case we have identified five reliable sets of parameters which we have applied to the GCs/PNe dataset. I have found three substructures, of which one was already found with the $\sigma = 40 \text{ km/s}$ cut-off (S2) and two other new candidates. These are shown in figure 4.9 in the space of positions and in the phase space and listed in Table 4.5 (actually we have also found a third substructure which looked interesting albeit obtained with a lower reliability set-up, we report a description of it in the following for completeness).

Here below is a brief description of the properties of these new substructures.

S4:

This structure occurs one time with $k = 10$ and has $N_{\text{tot}} = 8$. It is located just beyond 5 arcminutes in the South-West direction from NGC 1399, where it was observed a diffuse patch of ICL from Iodice et al. (2017)^[127]. It has an average velocity slightly greater than that of the cD and a velocity dispersion of $\sigma = 47.7 \text{ km/s}$.

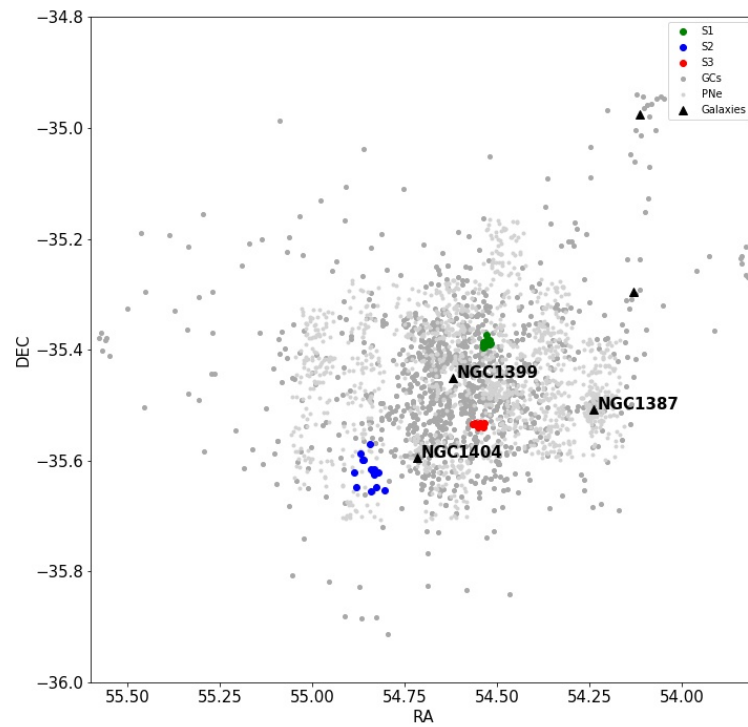
S5:

This structure occurs with $k = 10$ and has $N_{\text{tot}} = 8$. Its position is in the South-West direction at about 10 arcminutes from the cD. It has a mean velocity comparable to that of NGC 1399 and a velocity dispersion of $\sigma = 49.8 \text{ km/s}$.

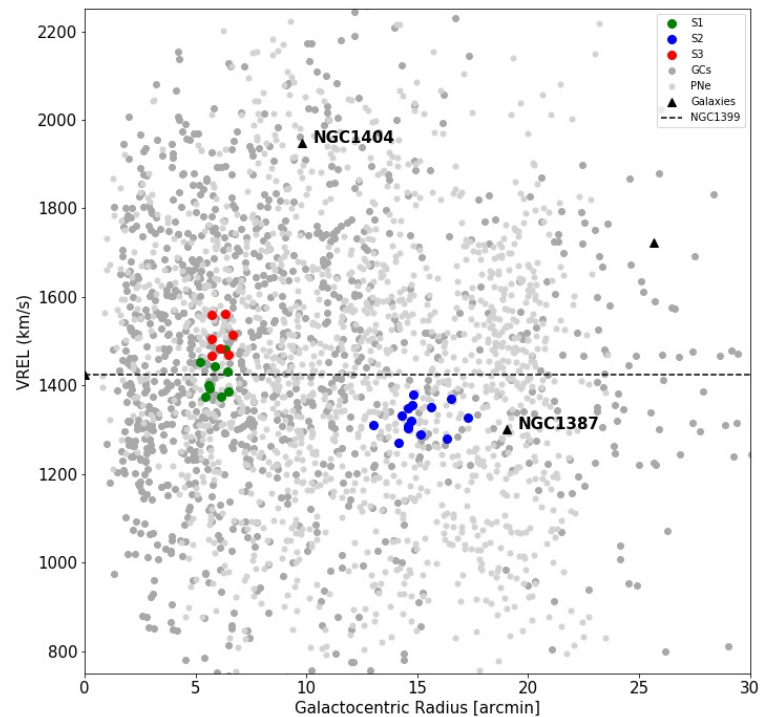
S6:

This structure occurs just one time with $k = 15$ and has $N_{\text{tot}} = 9$. It is located at the East of the cD and has a mean velocity lower than that of NGC 1399, with a velocity dispersion of $\sigma = 48.8 \text{ km/s}$. This structure occur in a set of parameter with a reliability below the threshold of the 70 % so very likely to be a a spurious detection. We will show in the figures in order to have the sense of what a spurious detection can look like.

³It was also attempted a search of substructures with a cut-off in the velocity dispersion of $\sigma = 60 \text{ km/s}$, but this did not produce new substructures with respect that ones found with the other two cut-off. In principle we can try to search for more substructures using larger cut-off in future analysis.

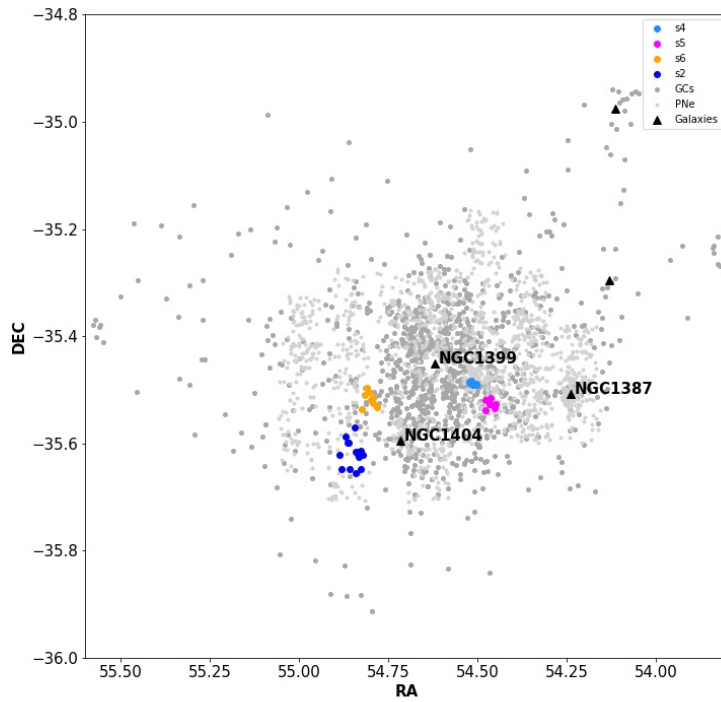


(a) Substructures in RA vs DEC: each of them is shown with a different colour; black triangles are galaxies. GCs are dark gray points while PNe are light gray points. East is on the left side.

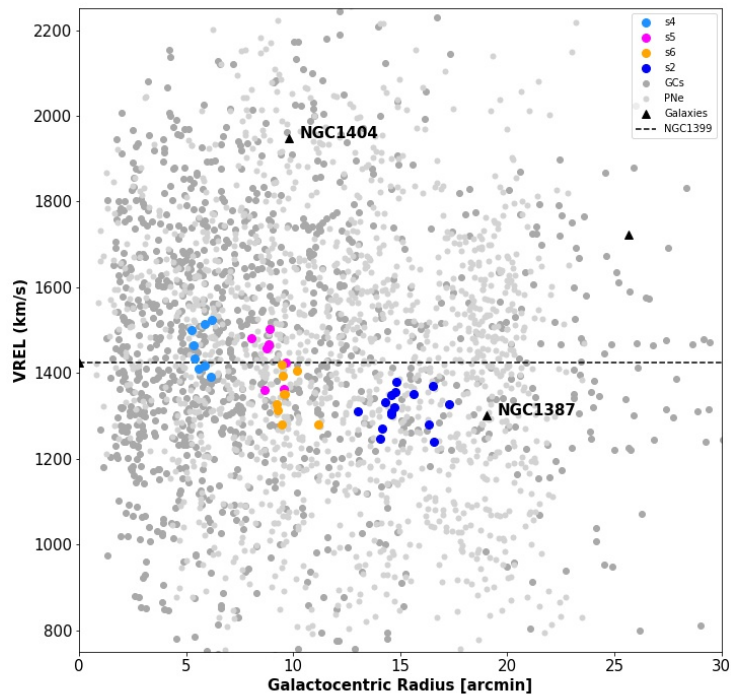


(b) Substructures in the phase-space. On the x-axis there is the distance from NGC1399, the y-axis show velocity of the points. The dashed line is the systemic velocity of NGC1399. The velocities uncertainties are not shown; this have an average of about 37 km/s

Figure 4.8: Substructures with $\sigma \leq 40 \text{ km/s}$.



(a) Substructures in RA vs DEC: each of them is shown with a different colour. GCs are dark gray points while PNe are light gray points. Black triangles are the galaxies in the field. East is on the left side.



(b) Substructures in the phase-space. On the x-axis there is the distance from NGC 1399, the y-axis shows the radial velocity of the points. The dashed line is the systemic velocity of NGC1399. The velocities uncertainties are not shown; this have an average of about 37 km/s

Figure 4.9: Substructures with $\sigma \leq 50 \text{ km/s}$.

Table 4.5: Parameter of the algorithm and their reliability

$k - n - N_{\min}$	Reliability (%) ^a	Structures
$\sigma \leq 40 \text{ km/s}$		
10 - 1.5 - 7	97	S1
10 - 1.3 - 6	94	S1
10 - 2.0 - 8	99	S1
12 - 1.3 - 6	76	S3
15 - 1.5 - 8	76	S1 - S2
15 - 1.5 - 9	95	S2
20 - 1.3 - 8	93	S1
25 - 1.8 - 12	84	S1
30 - 1.8 - 13	87	S2
$\sigma \leq 50 \text{ km/s}$		
10 - 1.5 - 7	70	S4 - S5

Notes. In the first column there are the values of the free parameters, where k is the number of nearest neighbors, n is the number of sigma used to remove the outliers and N_{\min} is the minimum number of points to consider them as "friends". In the second column there is the reliability as computed in the previous section, defined as the number of times that the set do not find any spurious substructure. In the last column there are the real structures ID that each single set detects.

^a Since the probability to have false groups on N simulations follow a Poissonian, errors are $\sqrt{N} = 10$, that is 10%.

4.4 An a posteriori test: recovering simulated substructures

So far we have used the simulations to select the parameter configurations which showed little sensitivity to statistical fluctuation (in a given dataset with no substructures) that might resemble cold substructures, likely streams. This under the assumption that if the algorithm would find any substructure this has a good chance to be real. We did not test, on the other hand, if the algorithm is capable to find a given substructure, if present, and we did not even test whether this depends on the density of datapoints belonging to it. In particular, we do not know whether a stream, with the characteristics we have found in the real data, is detectable by our algorithm, or real data have more complicated random substructures that our simulations could not reproduce. This an a posteriori test that we can do only after having seen what kind of substructures the algorithm has found in the data.

To test this, we have generated two “real” tidal streams with different number of points and different sizes and inserted them on about half of the sets of parameters listed in the table 4.3. The sets on which we check the ability of finding real substructures are listed in the table 4.6. The first stream, hereafter *stream 1* has a length of four arcminutes and a thickness of 2 arcminutes and it is composed by 24 points with a velocity dispersion of 32 km/s and errors in the velocity of 37 km/s, values comparable to the real substructures found with the $\sigma = 40$ km/s cut-off. This artificial stream is similar to some of the streams found in the real data also in size but it is about twice in numbers, in order to check how many of the particles belonging to a real stream are actually recovered. Indeed, we cannot expect that a stream mixed to a relaxed component can have the totality of the particles recovered, hence we want to measure also the completeness of the algorithm “on stream”.

The second stream, *stream 2*, has a length of 2 arcminutes and it is composed by 20 points with the same kinematic values of the first stream.

We put these streams in the 100 simulations used in section 4.3.4, every time changing randomly their position in a range between 10 and 20 arcminutes from the center of the simulation, and their mean velocity in a range of 1275 – 1575 km/s (i.e. ± 150 km/s, with respect to the mean velocity of the simulated NGC 1399, which is 1425 km/s). The reliability of the two streams on each set of parameters are listed in the table 4.6.

There are a few things to remark. First, the algorithm is almost always capable to find the stream, which is a positive confirmation of the effectiveness of its design. Only few cases have a recovery rate (or reliability) $< 10\%$ (depending on the stream), while in all other cases we

Table 4.6: Reliability of finding real substructures

$k - n - N_{min}$	Reliability (%) ^a		Particles recovered	
	Stream 1	Stream 2	Stream 1	Stream 2
10 - 1.3 - 6	34	3	8	6
10 - 1.5 - 7	88	95	9	8
10 - 2.0 - 8	96	98	11	11
12 - 1.3 - 6	43	2	7	6
15 - 1.5 - 9	77	82	13	10
20 - 1.3 - 8	5	8	8	8
25 - 1.8 - 12	100	59	20	14
30 - 1.8 - 13	100	45	20	14

Notes. In the first column there are the sets of parameters tested to find real substructures, in columns two and three we report the results on the stream 1 and the stream 2, respectively. In the last two columns there are the average number of particles recovered for the stream 1 and the stream 2 (approximated to the closest integer), respectively. Stream 1 and 2 are originally made of 25 and 20 particles respectively.

^a Errors on the reliability are 10%.

have a recovery rate $> 30\%$ and we have quite a number of configurations with a rate $> 70\%$. This recovery rate has a different meaning with respect to the one measured earlier, since in this case we have test the effective ability to find a given stream. In principle, this recovery rate is even more stringent than the one tested in absence of streams and, being designed around the characteristic of the real stream we have discussed in the previous section, directly gives the sense of the reliability of the S1–S5 streams seen above. Second, the ability to catch “real” substructures depends mostly on the parameter n ; indeed the results are very similar for those sets with the same values of n , while do not vary within the errors (i.e. the 10% which comes from the Poissonian errors) if we put different k or N_{min} . In particular, the sets with the value $n = 1.3$ yield the worst performances and they are the only ones with a reliability always worse than 70%, although some reasonable success rate are obtained for stream 1 (e.g. 34% with $k = 10$ and 43% with $k = 12$) and much worse rates for stream 2 (generally below 10%).

Much better performances are obtained for the other set of parameters which, as commented above, generally reach a success rate of the order of 75% or higher (up to 100%). Hence, this a posteriori test allows us to restrict the range of parameters that have likely returned real streams.

At least in principle. From the Table 4.5, indeed, the substructures found with $n \neq 1.3$ are S1, S2, S4 and S5 are confirmed to have high significance. On the other hand S3 seems to have a lower reliability, since this is associated to a parameter set-up with a recovery rate of the 40% at the best. This latter is, though, is one of the most promising feature found in the real data being located very close to one of the recently discovered dwarf galaxies in Fornax. Hence its reliability is enhanced by the latter circumstance as we will comment later.

The *stream 1*, possibly because is made of a larger number of objects, has a recovery rate which ranges from 77% with $k = 15$, to 100% with $k = 25, 30$, while the *stream 2* has a lower recovery rate with $k = 10$ and $k = 15$ where the values are of above 95% and 82%, respectively.

However, given the poissonian errors of the order of 10% we can conclude that all the so call reliabilities are consistent with each other, within the errors, regardless the n assumed.

If we take a look at the differences of the results between the two streams, it is evident that with a higher k , it is easier to detect the stream 1, which has more particles, while from $k = 15$ and below it is easier to catch the stream 2.

Finally some comments about the completeness of the recovered substructures (i.e. how many particles are recovered with respect to the original composing the simulated stream). Of course in no case all particles are recovered. The probability to detect points of the streams grows by increasing the value of k , reaching a maximum of about 20 out of 24 points for the stream 1 with $k = 25, 30$, and a maximum of about 14 out of 20 points for the stream 2 with the same values of k . Furthermore sometime the algorithm detected, along with the particles belonging to the real stream, some contaminants, and the probability to find false positive points in the algorithm grows also for increasing k too. Anyway, the number of contaminants is maximum of about three contaminants with $k = 30$. Hence we can conclude that the overall contamination is not severe, although this would represent a minor problem in any case since our first goal is to have a real stream detected.

It is important to stress that in the structures found in the real data, the proper number of points could be slightly different, since the algorithm very probably missed some point belonging to the stream or picked up some contaminants.

4.5 Statistical analysis of the substructures

In the previous section I have discussed in more depth the probability that the substructure that I have found in the real data are real. In this section I describe some general properties, like the

size and the total number of objects, of the substructures found in the Fornax cluster, and their kinematics.

In the table 4.7 there is a general description of each substructure obtained using a velocity dispersion cut-off of 40 km/s and with $\sigma \leq 50$ km/s, as reported in Table 4.6.

In the second column I have reported the total number of objects of the substructures, with the total number of GCs and PNe reported between brackets. In the third and fourth column, there are the mean velocity and their velocity dispersion of the substructures, while in the fifth column there is a measure of their size, defined as the maximum distance among all points of the substructure.

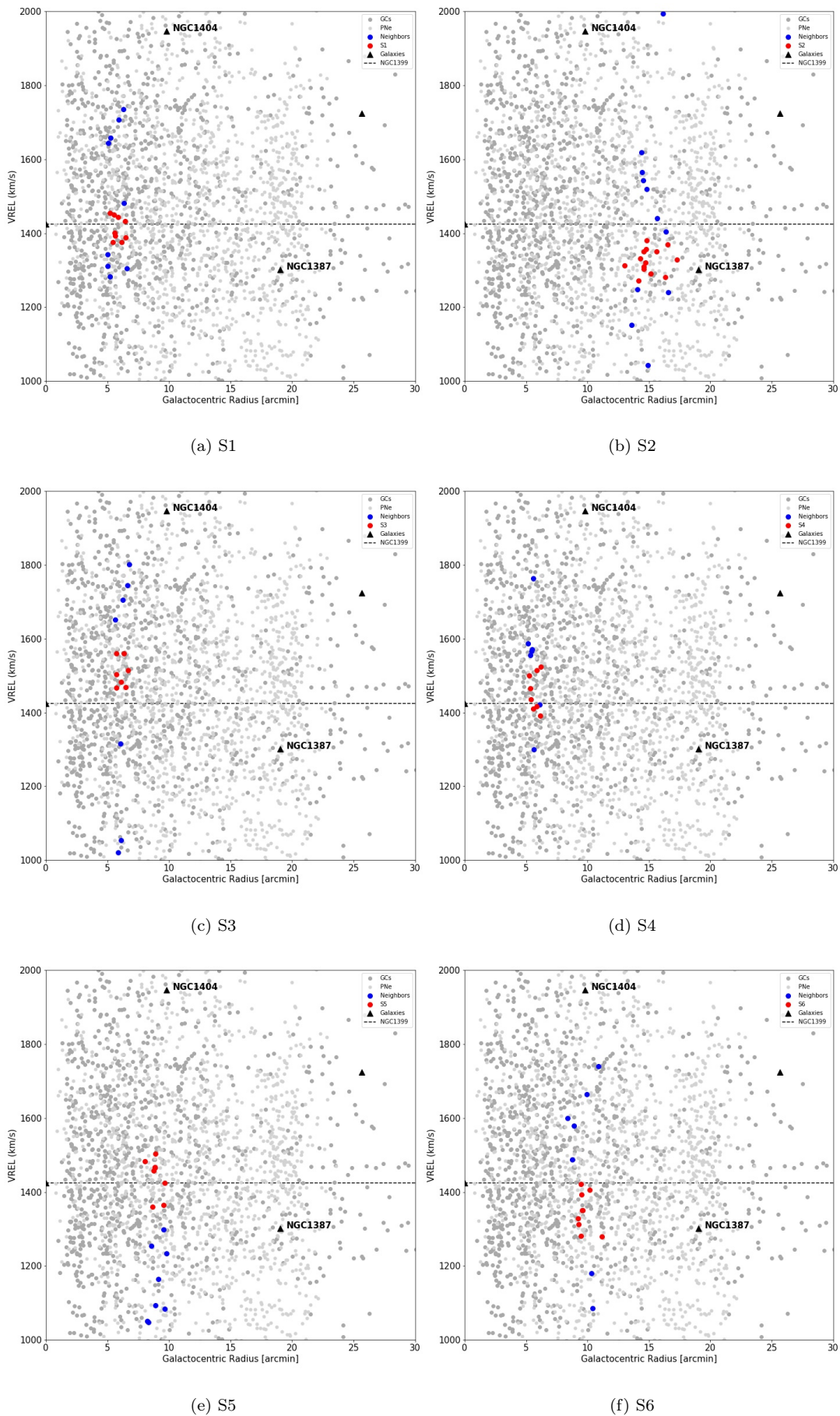
Since streams or tails of disrupted dwarf should preserve their kinematics and so should have a different velocity distribution with respect to the surrounding relaxed component, I compared the kinematics of the substructures to the kinematics of the region in which they are embedded.

Hence I measured the mean velocity and the velocity dispersion of the N , $1.5 \times N$ and $2 \times N$, closest points to each substructure, where N is the total number of objects belonging to the subgroup. These values are listed from the sixth column on of table 4.7. Since some substructure, in particular S1, S2 and S3, occur in more than a set of parameters, the values listed in the table have been measured for the sets which gave the lowest velocity dispersion of the structure.

The substructures have a total number of points ranging from a minimum value of 7 (S3) up to 14 (S2) and, with the exception of S2 whose bulk of points are PNe, the other substructures have a comparable number of GCs and PNe. Their mean velocity and velocity dispersion range from 1325 km/s (S2) and 30 km/s (S1) up to 1508 km/s (S3) and 49 km/s (S5). In particular, S1, S4 and S5 seem to have a mean velocity consistent with the cD, while all the others have $\sim \pm 100$ km/s offset, possibly indicative of some relative velocity. This does not tell much about the nature of a particular structure because in case of a tangential stream of which one sees only the transverse component and the measured radial component is consistent with the systemic velocity of the cluster.

Most structures have a size of about 1-1.5 arcminutes; but S6 and S2 are much more extended, having a length of ~ 140 and ~ 260 arcseconds, respectively (this motivated the adoption of this same typical sizes for the simulated stream in the previous Section).

In figure 4.10 the substructures (red points) along with their N nearest neighbors (blue points) are shown, in the phase-space, to see if subgroups are moving differently with respect to the surrounding regions.

Figure 4.10: Phase space of the structures (in red) and their N closest points (in blue)

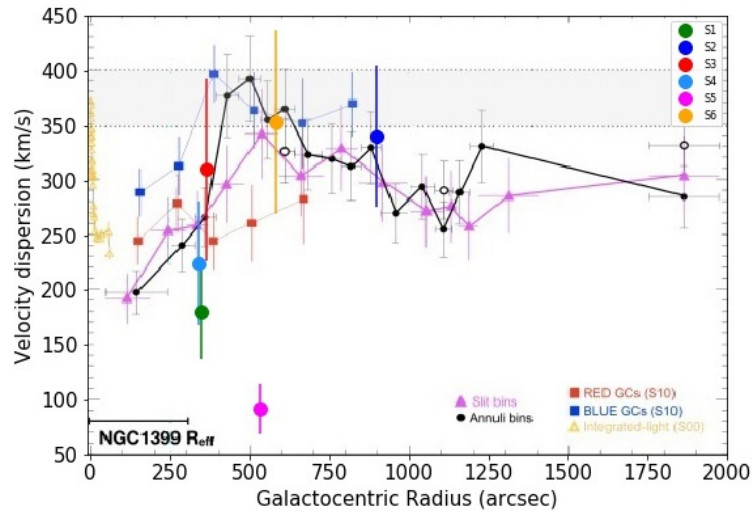
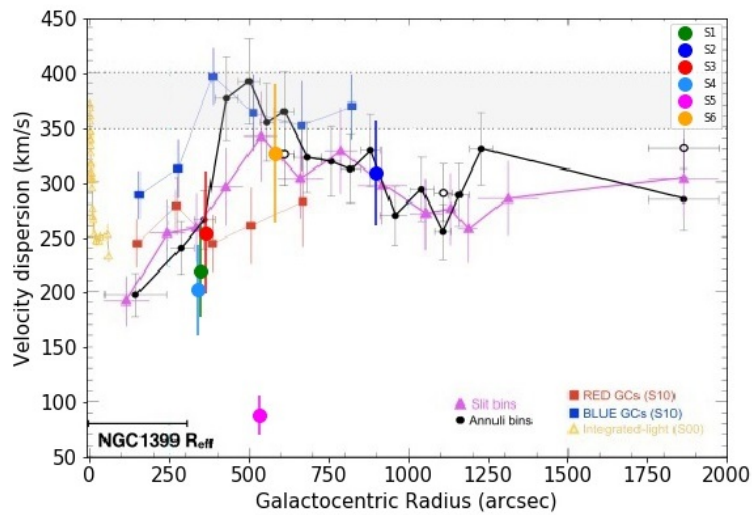
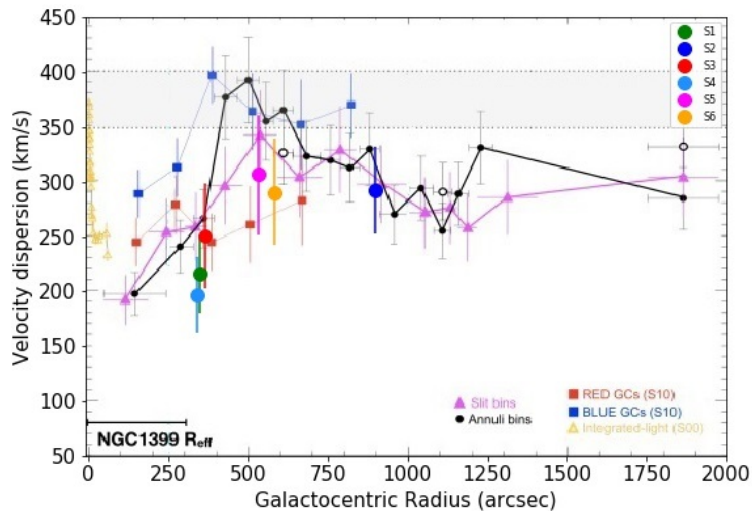
(a) Velocity dispersion of the N closest points(b) Velocity dispersion of the $1.5 \times N$ closest points(c) Velocity dispersion of the $2 \times N$ closest points

Figure 4.11: Velocity dispersion of the neighbors of the structures (colored circles) overlapped with the velocity dispersion of the PNe (magenta triangles) measured by Spiniello et al. (2018), and with the blue GCs (blue squares) and red GCs (red squares) measured by Pota et al. (2018). The yellow triangles is the integrated stellar light profile along the major axis of NGC 1399 from Saglia et al. (2000).

Table 4.7: Properties of the substructures

ID	N. points (GCs - PNe)	v_{mean} (km/s)	σ (km/s)	Size (arcsec)	$V_{\text{Neig.}}$ (km/s)	$\sigma_{\text{Neig.}}$ (km/s)	$V_{\text{Neig.}}$ (km/s)	$\sigma_{\text{Neig.}}$ (km/s)	$V_{\text{Neig.}}$ (km/s)	$\sigma_{\text{Neig.}}$ (km/s)
S1	9 (6 - 3)	1412	30	68	1496	180	1527	220	1500	216
S2	14 (2 - 12)	1325	32	262	1300	340	1299	309	1334	292
S3	7 (4 - 3)	1509	36	89	1470	310	1476	255	1509	251
S4	8 (4 - 4)	1457	48	57	1468	225	1413	203	1414	197
S5	9 (4 - 5)	1440	50	93	1153	92	1183	88	1310	306
S6	9 (6 - 3)	1347	49	140	1327	353	1409	327	1425	291

Notes. Statistical properties of the substructures. In the second column there are total number of points belonging to the structure (separated in parenthesis in GCs and PNe). In the third and fourth column we have the mean velocity and the standard deviation of the structures; in the sixth its size. In the last columns we have the mean velocity and velocity dispersion of the nearest points to the structure, for N , $1.5 \times N$ and $2 \times N$ points, where N is the number of points of the structures.

Uncertainties on the mean velocities are $\frac{\sigma}{\sqrt{N}}$, while uncertainties in the velocity dispersions are $\frac{\sigma}{\sqrt{2N}}$, so errors on the velocity dispersion of the substructures are about 10 km/s while the errors on the velocity dispersion of the neighbors are about 50 km/s. Errors on the mean velocities are about 15 km/s for the structures and in the range 70-100 km/s for the neighbors..

From this figure and from the values reported in table 4.7 it is evident that most substructures have a kinematics which is clearly different from that of the closest neighbors particles, that seem to move following the gravitational potential of the cluster (374 ± 26 km/s; Drinkwater et al. 2001).

There are two exceptions: S1, whose N neighbors have a velocity dispersion of about 170 km/s, although this dispersion becomes higher if we consider more surrounding points (see the last and the third last columns in the table), and S5, whose neighbors have a velocity dispersion of about 93 km/s, again this value tends to increase if we consider more points.

In figure 4.11 I show the velocity dispersion of the closest points of the substructures overlapped with the velocity dispersion of the PNe and GCs in Fornax, whose trend was already discussed in the chapter 3. From the figure it is evident that all but S5 are embedded in regions that are moving following the potential of the cluster. Thus the low value found for the velocity dispersion of the closest points to S1 are, within the errors, consistent with the velocity dispersion profile of the PNe and red GCs.

The mean velocity of the neighbors are consistent with that of the substructures, there is just a deviation from the mean velocity of the neighbors of the structure S5 (evident in the

Table 4.8: Properties of the dwarfs close to the substructures

ID (NGFS)	RA (J2000)	DEC (J2000)	i-mag	i-Mag	R_e (arcsec)	R_e Kpc	Structure
033929-353421	54.8704583	-35.5725883	19.92	-11.59	8.384	0.813	S2
033922-353524	54.8436250	-35.5900222	19.33	-12.18	2.762	0.268	S2
033819-353151	54.5781667	-35.5309278	16.72	-14.79	12.613	1.223	S3
033750-353302	54.4577917	-35.5504389	21.76	-9.75	3.232	0.313	S5

Notes. In the first column there is the ID of the dwarfs close to the substructures. In the columns two and three there are the positions in RA and DEC. The columns four and five show the relative and absolute magnitude in the *i*-band. The columns six and seven show the effective radii of the dwarfs, in arcseconds and in Kpc, respectively. Finally in the last column it is listed the substructures close to the dwarfs.

figure 4.10e), this deviation decreases when we consider more neighbors, but anyway is within the uncertainties on the mean velocity.

In this section we showed that all the substructures have an overall velocity dispersion different from the local kinematics of the relaxed component, which is dominated by the cluster potential. Because of streams of tails of disrupted dwarfs should have a different velocity distribution, this could be an evidence in favour of a physical nature of these substructures.

4.6 Cold substructures vs dwarf galaxies

As the substructures that we are looking for should have their origin from the tidal stripping of dwarf galaxies, a useful test may be to compare the spatial position of the structures that we found with that of the dwarf galaxies in Fornax. In this section I perform this match, using, for the population of dwarf, the catalog by Munoz et al. (2015)^[167] described in the section 3.4.

An overlapping of a substructure with a dwarf will represent a further, and important evidence of a physical origin of the substructure, since it is highly unlikely to find a spurious structure near a dwarf. Furthermore, this association is likely to indicate the progenitor of the observed substructure and call for further investigations to check this evidence in future deeper investigations. We will try to substantiate this working hypothesis using hydrodynamical simulations in the next Section.

In the figure 4.12 the core of the Fornax cluster is displayed along with the position of the

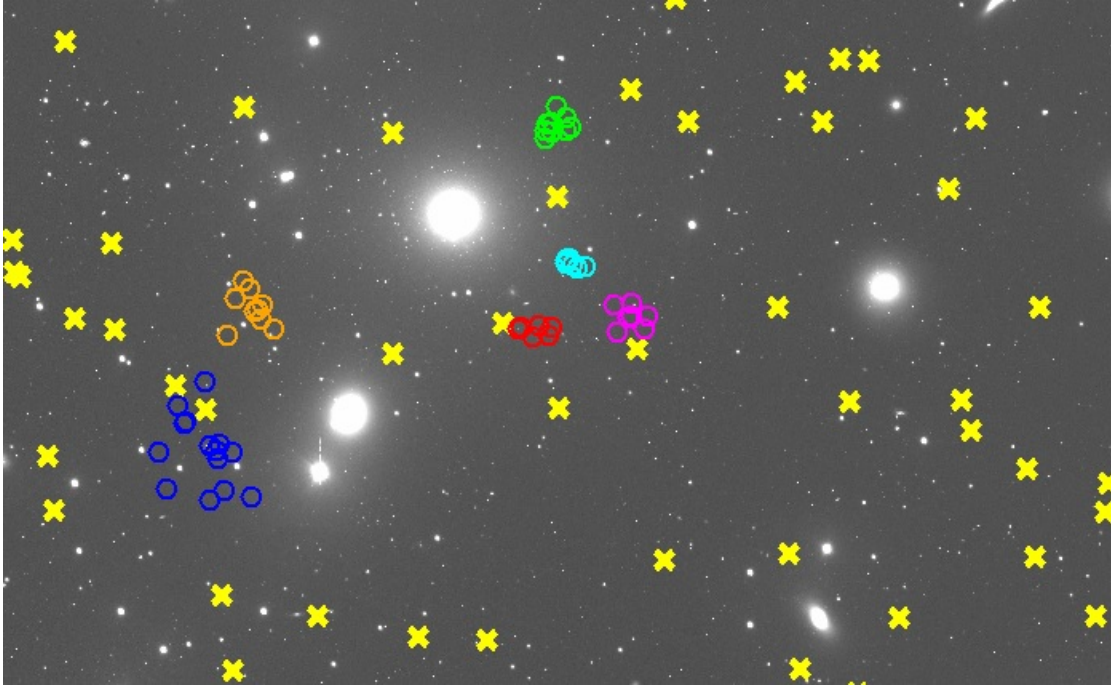
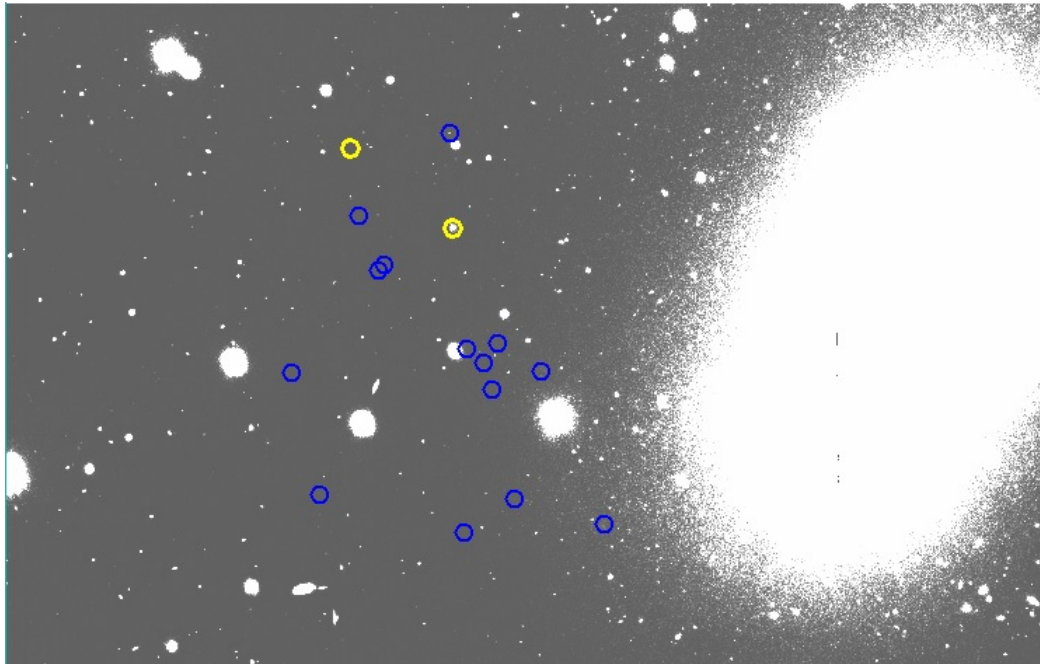


Figure 4.12: Image of the Fornax core along with the position of all the substructures and the dwarf galaxies. NGC 1399 is the galaxy near the center of the image, NGC 1404 and NGC 1387 are also visible just below the cD and in the right side of the image, respectively. Dwarf are yellow crosses in the figure, while substructures are colored circles.

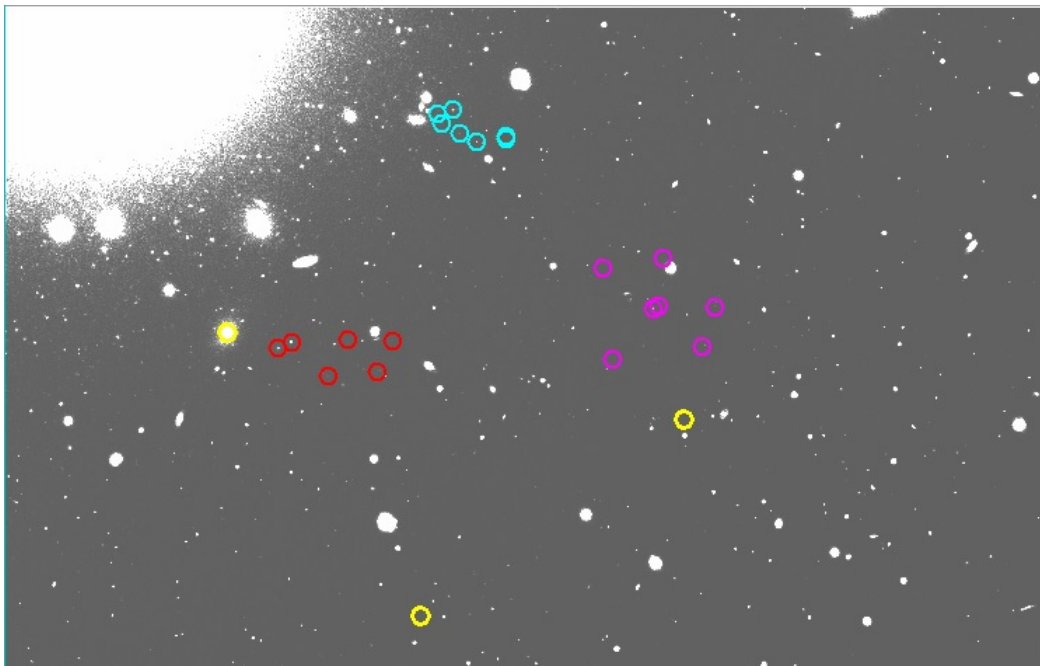
dwarf galaxies (yellow crosses) and the substructures (colored circles, the colors are the same of the figures 4.8 - 4.9).

From the figure it is clear that three of the substructures are very close to a dwarf, in particular the structures named S2 (blue circles), which overlaps with two dwarfs, and S3 (red circles) found with a cut-off in the velocity dispersion of $\sigma = 40$ km/s, and the structure S5 (magenta circles) found with a threshold of $\sigma = 50$ km/s. These represent half of the substructures that we found; the other half is not spatially connected to any known dwarf in the catalog by Munoz et al. (2015). Some of the properties of the dwarf close to the substructures, like their position, their magnitude in the i -band and their effective radii, are listed in the table 4.8.

In the figure 4.13 the area where we found the substructures S2 and S3 and S5 is zoomed, in order to look closer at those dwarfs whose spatial positions are near to the three substructures. While two of the dwarfs, in particular the one visible near S3 (at the left side of the bottom of the figure 4.13), and that near S2 (near the center of the top of the figure 4.13) are clearly visible and indeed are very luminous dwarfs (see also the table 4.8, the third and the first row, respectively), the other two are low surface brightness galaxies (LSB) and have been detected



(a)



(b)

Figure 4.13

only in the last decade thanks the recent surveys, like the NGFS, in the Fornax cluster.

Thus two of the four dwarfs close to the substructures were unknown until the last years, and one can speculate that the substructures we have found would have led to the discovery of these systems, looking by eye to all objects in the area of the detected substructure. Hence, we can argue that this method can be effective to search also for LSBs close to the spatial positions of the cold substructures revealed with our method.

Following the same reasoning, it could be that near the three substructures that do not correlate in the spatial position with any dwarf of the catalog of Munoz et al. (2015) there is a LSB not detected yet. Unfortunately, by looking by eye to the area of the substructure candidates, there were no signs of other possible companion galaxies (included LSBs).

Finally the proximity of S1 and S4 ($\sim 5'$) to the cD can make harder to reveal (if any) the progenitor galaxies which might have originated the substructures, due to the brightness of the cD halo regions. Equally, if these progenitor galaxies have reached the center so closely, they might have been already accreted (Venhola et al. 2017), or being in the process of being totally disrupted.

4.7 Galmer simulations

To conclude our analysis and try to interpret the characteristic of the final detected stream candidates into the dynamics of the accretion of dwarf satellites, we have made use of a suite of publicly available simulations, the Galmer simulations (Chilingarian et al. 2010^[45]).

In this section I describe the database of thousand simulations of interacting pairs with different initial conditions, with the double aim to test our finding method on the substructures generated by these simulations and to compare the phase-space distribution of the particles to those of our real substructures. The Galmer database provide about 1019 simulations of colliding galaxies and more than 70000 snapshots showing the development of these encounters up to 3 Gyr from the begin of the encounter with a bin interval for each snapshot of 100 Myr.

From this database we selected the simulated interaction between a gE0 and a dS0 with a mass aspect ratio of 1:10, the maximum value present in the database (see also Table 4.9). Although the bulk of the dwarfs in the core of Fornax is made of dE0, we used a dS0 because this had the mass and effective radius more similar to the dwarfs in the inner regions of Fornax, in particular with the dwarfs found close to the substructures. We selected an encounter starting with the dS0 at 100 Kpc, and falling toward the gE0 in a prograde orbit with an inclination of

Table 4.9: Parameters of the galmer galaxies

	M_B	M_H	r_B	r_H	N_{star}	N_{DM}
	$[2.3 \times 10^9 M_\odot]$	$[2.3 \times 10^9 M_\odot]$	[Kpc]	[Kpc]		
gE0	70	30	4	7	320000	160000
dS0	1	5	0.6	3.2	32000	16000

33 degrees and a pericentral distance of 16 Kpc. The parameters of the simulated galaxies are listed in the table 4.9.

From this simulation we extracted the projected positions and the radial velocities of the stellar points at 1.6 Gyr and at 2.1 Gyr from the begin of the encounter; the former is a snapshot of the dwarf after the first close encounter with the giant, while the latter is temporarily located in the second close encounter between the two galaxies.

From these two snapshots I have randomly selected 100 points from the stellar component of the dwarf (i.e. about the expected number of GCs and PNe belonging to a dwarf with a similar mass, see e.g. Romanowsky et al. 2012, Buzzoni et al. 2006) excluding from this selection points near the center of the dwarf, poorly sampled by GC and PNe which generally populate the outskirts of galaxies.

This give us the phase space of a realistic population of PN+GC particles of a disrupting dwarf to Then I put these points to one of our simulations, with the center of the ent like the one we have in the Fornax core. These include both particles still bound to the dwarf and the ones that have stripped. To do that I have located the center of this Galmer dwarf in a projected position in the Montecarlo simulated NGC 1399 very similar to the relative position of the dwarf galaxies we have associated the detected streams in real data (i.e. S2 and S5). To these I have just adjusted the mean velocity to 1525 km/s ($1425 + 100$ km/s, where 1425 km/s is the velocity of the simulated cD). Using some of the set of free parameters described in the section 4.3.4 I analyzed the ability of the algorithm to catch the tidal of the dwarf and the positions of the substructures in RA and DEC and in the phase-space. The structures detected in this way are displayed in the figures 4.14, 4.15 for the snapshot at 1600 Myr and in the figure 4.16 for the snapshot at 2100 Myr.

From the figures it is clear that the out the 100 selected the points the algorithm is capable to detect the points near the center of the dwarf, while just in a case (with $k=30$) it is caught the long tide of the dwarf. Looking at the phase space it can see the the substructures do not

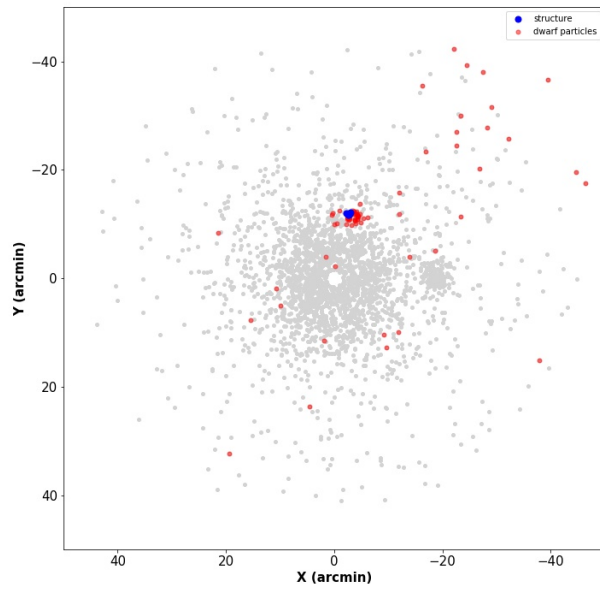
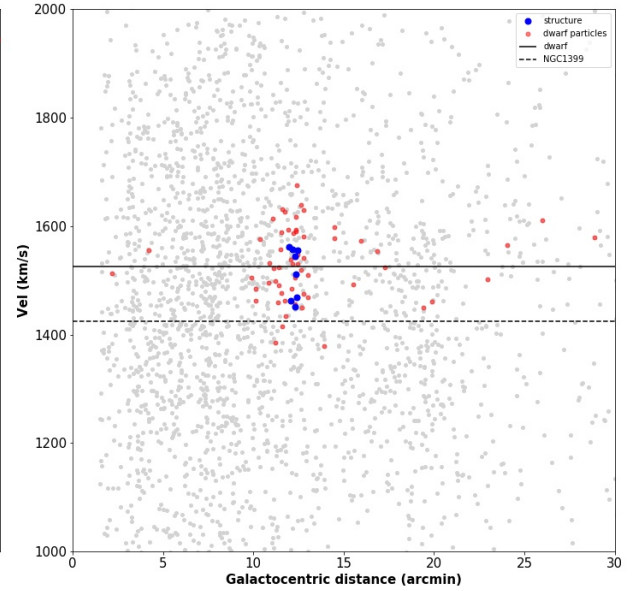
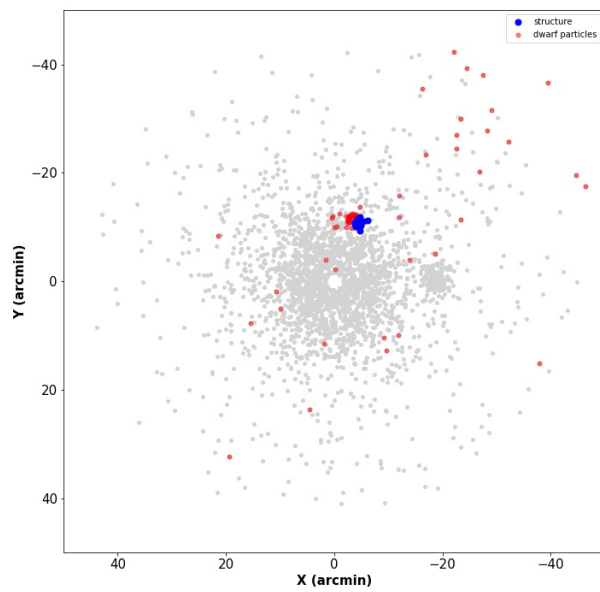
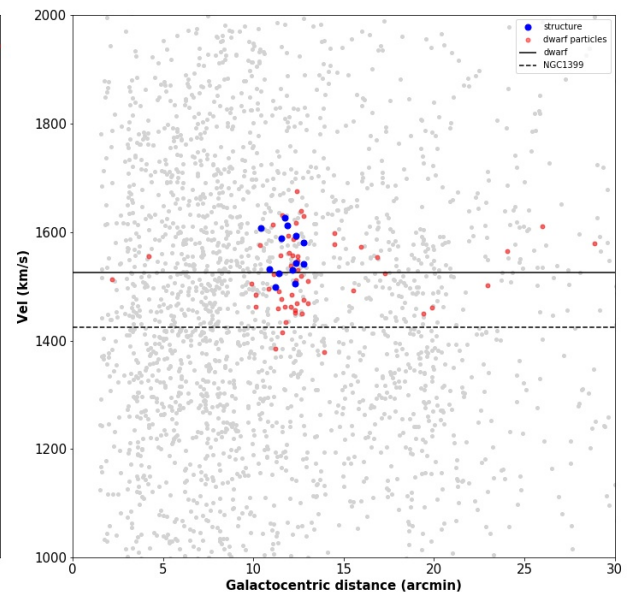
(a) Set of parameters $k=10$, $n=1.3$, $N_{\min}=6$ (b) Set of parameters $k=10$, $n=1.3$, $N_{\min}=6$ (c) Set of parameters $k=10$, $n=2$, $N_{\min}=8$ (d) Set of parameters $k=10$, $n=2$, $N_{\min}=8$

Figure 4.14: Structures of the galmer dwarf using a snapshot of 1600 Myr, the blue points represent the structures detected while the red points are the particles extracted from the dwarf. The dashed and the solid line in the phase-space represent the velocity of the simulated cD and of the dwarf, respectively.

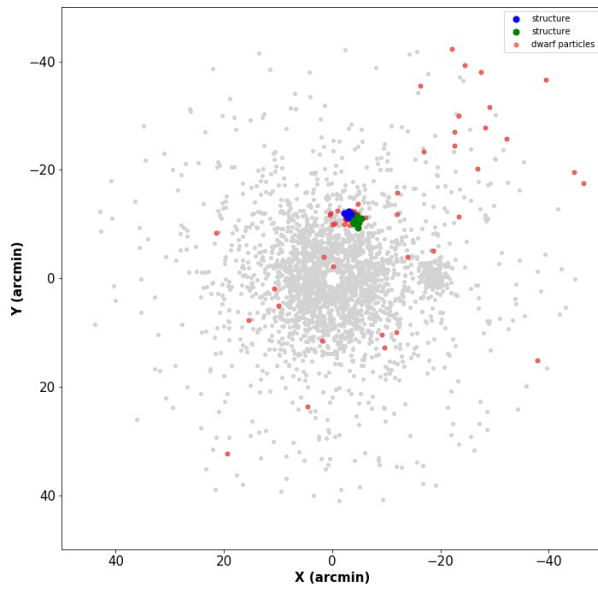
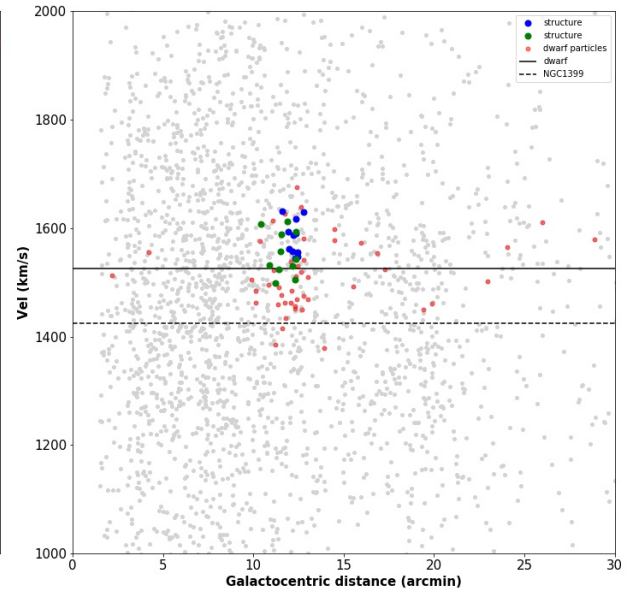
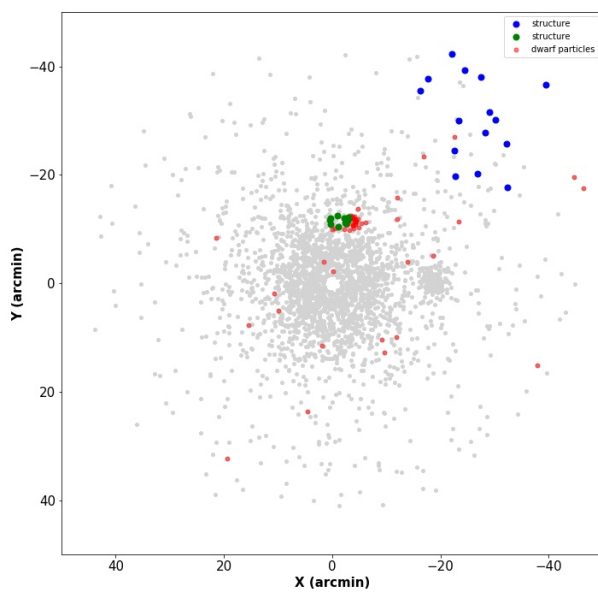
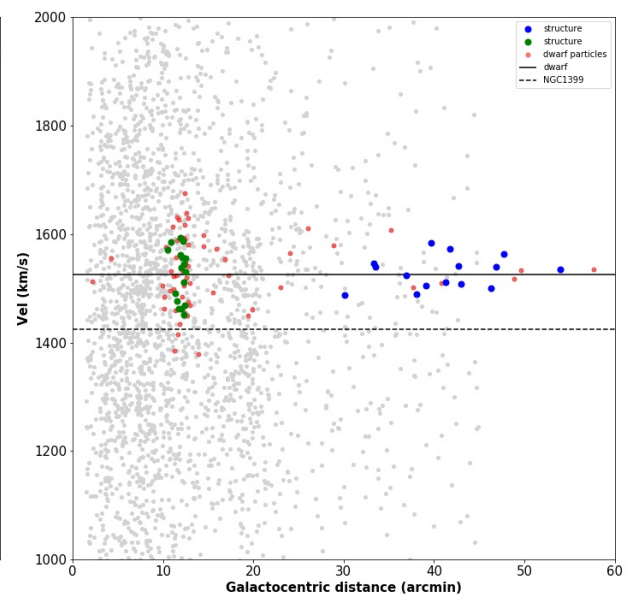
(a) Set of parameters $k=15$, $n=1.5$, $N_{\min}=9$ (b) Set of parameters $k=15$, $n=1.5$, $N_{\min}=9$ (c) Set of parameters $k=30$, $n=1.8$, $N_{\min}=13$ (d) Set of parameters $k=30$, $n=1.8$, $N_{\min}=13$

Figure 4.15: Structures of the galmer dwarf using a snapshot of 1600 Myr, the blue and the green points represent the structures detected while the red points are the particles extracted from the dwarf. The dashed and the solid line in the phase-space represent the velocity of the simulated cD and of the dwarf, respectively.

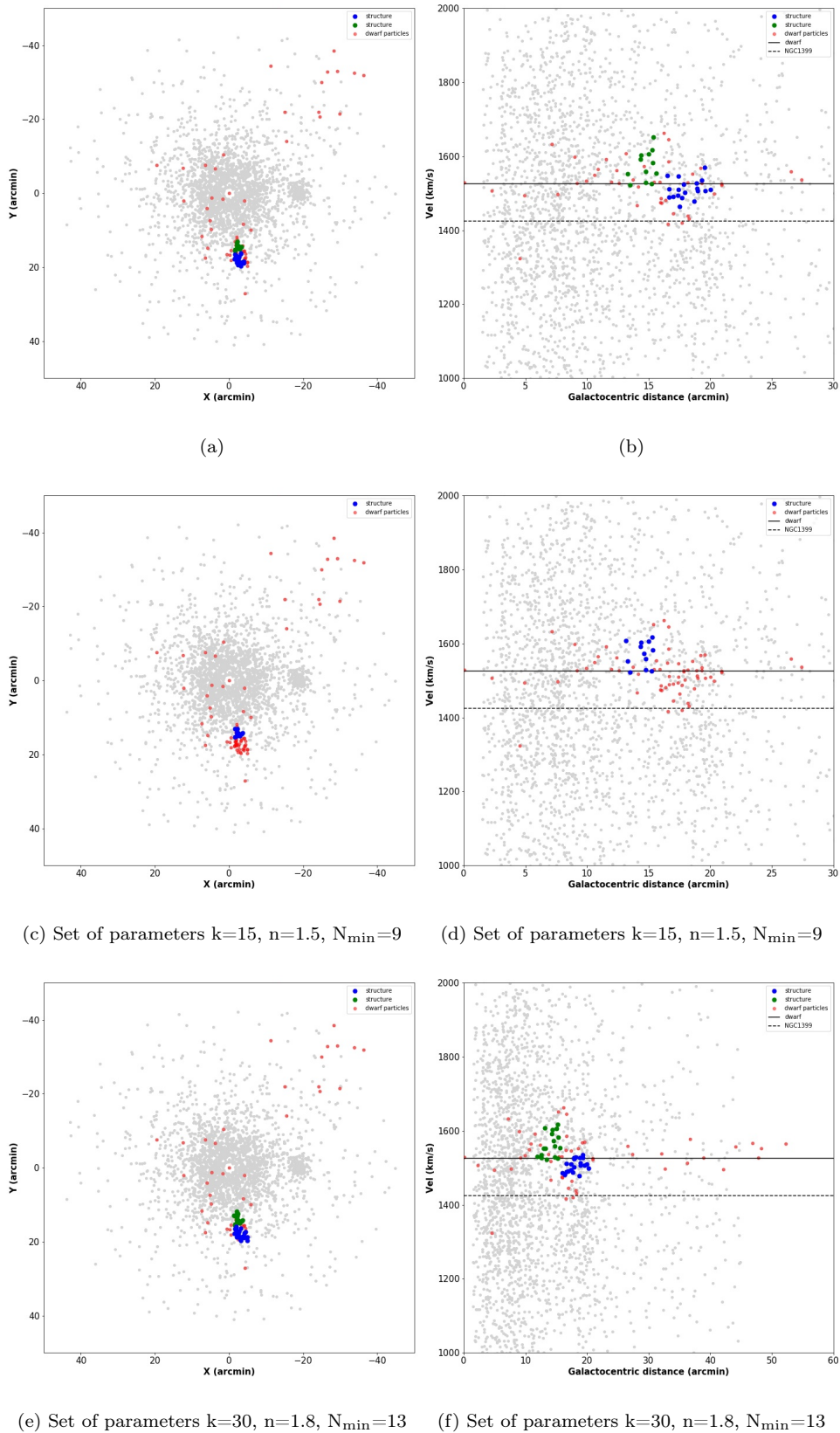


Figure 4.16: Structures of the galmer dwarf using a snapshot of 2100 Myr, the blue and the green points represent the structures detected while the red points are the particles extracted from the dwarf. The dashed and the solid line in the phase-space represent the velocity of the simulated cD and of the dwarf, respectively.

show a particular pattern, and have an average velocity similar or slightly different to that of the dwarf (the solid line in the images).

To conclude, this very preliminary test on simulations shows that our algorithm is able to detect real streams, and due to a combination of density of points and kinematics, it can generally see particles that are in the close vicinity of a disrupting galaxies (i.e. of the kind of S2 and S3) and in some case it can also detect the longer debris of the dwarf left behind long before the current position of the dwarf (i.e. like S5). We expect to explore more these comparison with simulations in the future development of this work, possibly using more dedicate ad hoc simulations for the Fornax cluster.

Conclusions and perspectives

In this work a new method to detect cold kinematical substructures in the intracluster regions of the Fornax cluster, one of the nearest and most massive cluster of galaxies, has been presented. In the first chapter I described the theory of the evolution of the galaxies, focusing on the evolution of the cD galaxies. In the chapter 2 I presented briefly the Fornax cluster, while in the chapter 3 I described the sample of GCs and PNe and the population of the dwarf galaxies in the core of Fornax. In the last chapter I described the finding streams method of cold kinematics substructures and their analysis. In this concluding section I summarize the main results contained in the last Chapter of the Thesis and draw some perspective for future applications. I have concentrated on substructures that could have their origin in a past or recent close encounter between the more massive galaxies inhabiting the cluster core like the cD galaxy, NGC 1399, or the early type galaxies NGC 1404 and NGC 1387 and dwarf galaxies.

Since the dynamical friction is lower for less massive galaxies and the dynamical time is longer in the intracluster regions of a cluster, the low velocity dispersion of a dwarf (of the order of 50 km s^{-1}) should be preserved for a long time in the tidal stripped particles expected to be distributed on elongated streams populating the extended halo of the cD, before these substructures mix-up and lose all memory of their original motion. This has been demonstrated in cosmological simulations (e.g. Amorisco 2018)^[2] and also recently found in studies looking into the deep photometry of the Fornax cluster (Iodice et al. 2016^[128], 2017^[127]) and into the spatial distribution of the globular cluster (D'Abrusco et al. 2016^[66]).

To test our new method we have also used cosmological simulations, in particular, a suite of publicly available simulations (Galmer, Chilingarian et al. 2010^[45]) and we have finally applied the method to the data of the FDS survey (Iodice et al. 2016^[128]) to produce a first list of stream candidates to be used for future follow-up observations to confirm them and, if real, to characterize their dynamics.

The stream finding algorithm has been designed to explore the space of the positions (RA and DEC) and a reduced phase space (radial velocity vs distance from the center of the cD) in order to find objects correlated both in position and in velocity. This algorithm it is based on a nearest-neighbors approach, taking also kinematic informations in order to unveil structures having an overall velocity dispersion which is smaller than the local velocity dispersion generally dominated by the cluster potential in the intracluster regions.

Here, I have used GCs and PNe as test particles, because they are easily observable up to the Fornax cluster distance and their radial velocity comfortably easy to measure with a good precision also at large distance from the galaxy centers of the order of several effective radii. Hence, they can trace the kinematics of the intracluster regions where the stellar light has a too low surface brightness and so it is really hard to perform spectroscopy in order to measure the radial velocity of the regular stellar population.

Generally GCs and PNe have intrinsically a slightly different kinematics within the galaxy potential they originally belong to, however in the intracluster regions although generally consistent within the errors (see Spiniello et al. 2018^[211]). In low-mass galaxies, like dwarfs, we do not have much information of the PN and GC populations, however we do not have reason to exclude that they should reflect more or less the same similarity of more massive galaxies. If the intracluster population of PNe and GCe has originated by the disruption of such a small galaxies, we can reasonably expect that in an encounter PN and GC kinematical differences are kept within velocity uncertainties and so we can not distinguish the two subpopulations from their radial velocity.

To test this hypothesis I have performed a Kolmogorov-Smirnov test, which has confirmed that PNe and GCs follow the same kinematic distribution in the intracluster regions, hence we can use both population as the same test particles in the algorithm increasing the statistics, hence enhanced our probability to find cold kinematic structures.

Before we applied the algorithm to real data, we have performed extensive tests based on Montecarlo simulations of the Fornax core in order to find the best set-up for the parameter of our algorithm. In this phase, in particular I have ran the algorithm 100 simulations with only relaxed particle and no artificial stream added. As a result of this test, we have seen that the probability to extract spurious substructures was larger than 50% (reliability lower than 50%) in only few parameter combinations, if we retained only final substructures with overall velocity dispersion of the order of 40 kms^{-1} and some more configurations if we used a cut-off velocity dispersion of the order of 50 kms^{-1} . We finally collected all parameter combinations which

instead returned reliability larger than 70% and we decided to test all these on the real data to look for stream candidates.

Before doing this we have also tested whether the algorithm was capable of detecting stream particles that in real circumstances might be mixed to relaxed particles with a different phase space structure (e.g. an elongated spatial distribution with narrow gaussian velocity distribution). To do that we have added to our simulations two simulated streams located randomly across the simulated cluster and asked the algorithm to go finding them in the 100 simulations of the Fornax cluster.

With the exception of a single value of one parameter set-up, the streams have been detected in more of 80% of the simulations and most of the parameter set-ups caught the streams in more of 90% of the Montecarlo simulations. This was surprisingly good and encouraging that the algorithm can effectively return real streams in real data.

I finally applied the algorithm to the real data, and found a list of substructures, some of which turned out to be recurrent almost independently of the particular set-up. This was a first indication that the process of the extraction in real data was not random, but there were some stable features in the data. Some of these features were found with parameter set-up corresponding to very high reliability factors (see Table 4.7).

In particular, two of them (S1 and S2) have a reliability above the 90%, while warmer substructures have generally 70% or lower reliability and only one qualifies as “bona fide” with reliability lower than 70% (e.g. we have looked into a structure, S6 see Section 4.3.5, with lower reliability but the check on the images showed indeed that this it could be a spurious structures).

As a first immediate check of the plausibility of the selected candidates we have compared the spatial positions of the substructures with that of the dwarf galaxies in the core of Fornax listed in recent literature (i.e. Munoz et al. 2015^[167] and Venhola et al. 2018^[230]) and interestingly found that three out of six substructures (S2, S3 and S5) are very close to at least one dwarf galaxy. As mentioned before, we have specifically designed our method to automatically look into substructures generated by debris of close encounters between dwarf galaxies and larger target, in particular the large cD of the cluster, NGC 1399.

In particular, two of them (S2 and S5) are near to a *low surface brightness* galaxy (LSB), a diffuse galaxy with a very low surface brightness level and hence very hard to detect. Unfortunately we do not have the systemic velocity of this galaxy to check whether this is compatible with the mean velocity of these streams (1325 km/s for S2 and 1440 km/s for S5). Indeed, if the streams and the galaxy have the same systemic velocity, this would be the first hint that the

particles belonging to the stream might be originated by the LSB galaxy and that our candidate is a previously undetected stream. This is definitely a very promising step for follow-up studies (see below).

The other three substructure that qualified as “bona fide” candidates are not clearly associated to listed dwarf galaxies. We had a visual inspection to the deep images of the FDS survey to see whether these could be associated to some missed dwarf galaxy or some very small low surface brightness stream, but we could not find anything conclusive. However two out these three substructures are very close to the cD and if they are part of a tail of a dwarf galaxy entering the cD halo, there is a good chance that the progenitor system could have been accreted and either dissolved or difficult to be seen in the bright galaxy halo. Here a possible future development of this work could be an accurate 2D modeling of the cD galaxy to subtract to the FDS images to check for faint compact systems in the residual images (see below). For the third substructure with no clear close association, a possible explanation is that this is part of a long tail, originated by some dwarf orbiting around the cD, which is only partially detected by the algorithm.

Since all these evidences are still speculative and need further analysis and observations to be confirmed, we decided to perform an additional test on simulations to substantiate the reliability of our stream candidates. For this purpose we have used the publicly available hydrodynamical simulations Galmer, which provide a list of merging events, including the one between giant galaxies and dwarf systems. The advantage of these simulations was that we could separate the particles belonging to the dwarf galaxy from the ones of the companion target system and characterize their phase-space, including the one of the particles belonging to the long streams produced in the fly-by of the dwarf galaxy through the central galaxy halo. Being these Galmer simulations general in their purpose and limited in the parameter space, we could not find a configuration which closely resembled the case of the Fornax core. However we picked a simulation which showed reasonable parameters, in particular, the central velocity dispersion of the dwarf galaxy was of the order of 70 km s^{-1} . We have also inspected different snapshots of different epochs of the encounter and measured randomly the velocity dispersion of the long tails produced in the simulation due to the interaction of the dwarf galaxy and the large early-type companion and found that typically the velocity dispersion of random groups of particles was of the order of 60 km s^{-1} or below. Our test consisted to extract randomly a number of particles of the Galmer dwarf galaxy consistent with the original GC+PN population of a dwarf galaxy (of the order of 100) and add these particles to our simulation to ask the algorithm to find this new, more realistic substructure. In this random extraction most of the particles were picked from

the part of the tidal tail close to the bulk of the galaxy, but there were also particles belonging to the long plume emerged from the dwarf at the beginning of its interaction (see Fig. 4.14 and 4.15). To check closely our results, we have located the Galmer dwarf center (in a late stage of disruption) in positions which were compatible with the ones of the real dwarf galaxies from Munoz et al. 2015^[167] Even in this case the algorithm succeeded to recover the simulated substructure. Depending on the parameter set-up, it mainly recognized the particles close to the dwarf center (hence stripped recently) as part of the stream (like the case of S2, S3 and S5 we have found in the real phase-space of the Fornax core), but in some cases also the particles of the far part of the stream which are not closely associated to the progenitor dwarf and that live tens of kiloparsec apart from the current position of the dwarf system. This latter result shows that, in principle, the algorithm has the ability to detect also isolated substructures left behind by the dwarf systems even Gyrs before the current epoch of observations.

In synthesis we are confident that most of the cold kinematic substructures found with this method have a physical origin, likely they are remnants of a past or recent encounter between a dwarf and the cD. This method is thus very useful to detect candidate debris of merger events, further observations in the regions identified by these cold substructures should be performed in order to better investigate and analyze these remnants and hence obtain important informations on the mechanism that lead the evolution of the galaxies. This method can also be useful to research, close the positions of the cold substructures, the low-surface brightness galaxies that might be hard to detect even with deep photometry.

As anticipated, we foresee interesting developments of this work, especially in the perspective of confirmation of the new finding. First, we do not think that the search of stream candidate is over in the area. For lack of time we tried to lift up the threshold of the dispersion substructures to 60 kms^{-1} and found no new candidates, but we did not try to get to 70 kms^{-1} (which according to some preliminary test can still give a reasonably small amount of spurious structures and possibly look for more energetic streams). Second, and more important, the spectroscopy of the dwarf galaxies likely associated to the streams S2, S3 and S5. By comparing their systemic velocity and the kinematics of the particles I have associated to the stream, it will be possible 1) to confirm that the latter is dynamically connected to the close galaxies and 2) try to infer the orbits of the stream and the dynamics of the impact. Furthermore we can refine the selection of GCs and PNe in the area to see whether there are more particles tracing the stream and the dynamics of the dwarfs, which will be very useful for the comparison with simulations (see below). A third line of development in the Fornax core is to investigate deeper the low surface

brightness features in the galaxy halo and the presence of missed LSB systems or compact object closer to the galaxy center. This can be done by performing an accurate 2D model of the cD and subtract this from the deep FDS images in order to have a clean residual image where such faint populations can be seen with higher contrast. This will make the association of our orphan stream candidates with some unseen satellite possible and finally demonstrate the effectiveness of the machinery we have put together. A fourth and very promising development can be to make more detailed comparison with hydrodynamical simulations, possibly more updated and better calibrated to the Fornax core than Galmer. This will give insight on the possible association of the detected streams (if confirmed) with their progenitor galaxies and possibly reconstruct the recent accretion processes of the cluster core.

With this thesis we have moved the first steps to develop a tool for stream hunting in phase-space of discrete kinematical tracers, to be used for next observational campaign. Stellar streams, indeed, are expected to become a useful and popular tool to constraint the models of the galaxy evolution in dense environments such galaxy clusters, in particular to help to understand the recent mass assembly history of the large central dominant systems.

Appendix A

Theory of the merger

In this section I present the theory laying behind the encounters of galaxies and some of their observable consequences; a detailed analytic description of this theory is discussed in the "Galactic dynamics" by Binney and Tremaine, thus I refer to this book throughout the whole section.

Sometimes can occur that two or multiple galaxies falling towards one another; this event has remarkable consequences on these systems. Encounters can change the morphology of the galaxies, their kinematics, the star formation rate, leaving a system completely different from the original ones. The final effects of this interaction depends on many parameters, as the relative orientation of the velocity of the galaxies involved, their morphology, their mass ratio and many others. Sometimes if the relative velocity of the two galaxies is small enough, the collision ends with a **merger**, at the end of which there is a single stellar system. These events are the most violent interactions between galaxies, changing permanently properties of the systems involved. Therefore the mergers are a critical ingredients to understand the theory of the galaxy evolution. The dynamic of the mergers is very complicated, and it is an area still under investigation. We can divide mergers into two main types:

- **Major merger:** This is a collision between two galaxies with a comparable mass. The final product is a single stellar system very different from the original.
- **Minor merger:** This event occurs when a galaxy is much more massive than the other one. Usually, in this case, the smallest galaxy is completely destroyed, whereas the massive one is almost unchanged.

During a major merger the gravitational potential change very quickly, influencing strongly the

orbits of the stars, that completely lose memory of their previous motion. This process is called *violent relaxation*., during which energy of the ordered motion is transferred to the random motions of the single constituent of the galaxies. This conversion is so rapid that the whole process has a duration of about few crossing times, thus studying them analytically is very difficult and it need numerical simulations.

Arp produced in the 1966 a catalogue of *peculiar* objects made of 338 galaxies that have very unusual structures. Although it wasn't know the real nature of these galaxies, now it's clear that most of them are colliding systems; hence observing these galaxies may be useful to understand some of the observable signatures of merger events. In the figureA.1 there is an example of galaxies belong to the Arp's catalogue, a system called "Antennae" due to the pattern of these colliding galaxies. The tails very evident in the figure are one of the most important signature of a major merger event, they extend for over 100 Kpc. In 1972 Toomre & Toomre showed that tails are the results of a merger between two disks galaxies of comparable size, long tidal tails are narrow because baryons come from stellar system with a low velocity dispersion, those belong to the disk. Tails are also present in minor mergers, when a satellite collide with a larger galaxy. The physical process that play the dominant role when two systems of unequal mass collide, is the **dynamical friction**, that is a frictional force on a moving body opposite to the velocity, due to gravitational interactions with other systems (Chandrasekhar 1943). This process leads orbits to decay and to shrink progressively, while at the same time tidal effects rise. As the strength of the tidal forces increase, as many stars and globular clusters are stripped from the satellite, enriching the intra-cluster medium or the stellar population of the massive galaxy (this explains the higher specific frequency S_N observed in some galaxies). Usually at the end of this process there is the total destruction of the lighter galaxy, a process known as *galactic cannibalism*; sometime its core survives and continue to orbit around the massive galaxy. It is possible that some of the greatest globular clusters or some of the ultra compact galaxies are the remains of a galaxy in a merger event. Some examples of minor merger are satellites of the Milky Way. The dynamical friction formula was derived from the first time by Chandrasekhar in 1943, here I report the formula derived in the approximation of a test body of mass M , moving through a cloud of smaller stellar systems of individual mass m_a ($m_a \ll M$), that are members of a huge systems of mass $M' \gg M$. In this case:

$$\frac{d\mathbf{v}_M}{dt} = -4\pi G^2 M m_a n \ln \Lambda \frac{\mathbf{v}_M}{v_M^3} \quad (\text{A.1})$$

where n is the density of the stellar field, G is the gravitational constant and Λ is the *Coulomb*

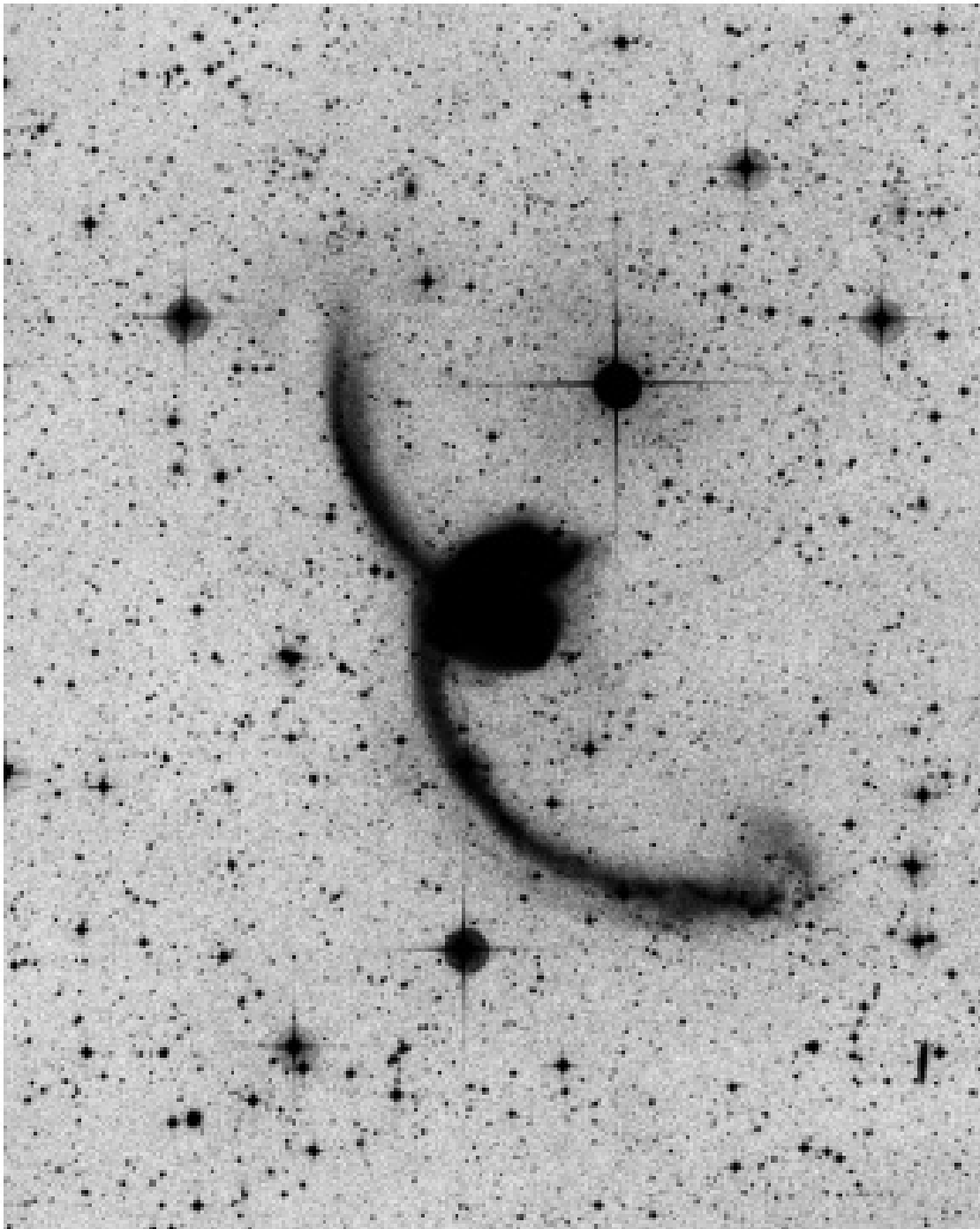


Figure A.1: The interacting galaxies NGC 4038 and NGC 4039, the *Antennae*. This is an overexposed image to emphasize the low surface-brightness tidal tails. The distance from the overlapping blobs at the center to the bright star above and to the right of them is 40 kpc. Image taken from the Binney & Tremaine

term. From this formula we can see some interesting features about the dynamical friction:

- The frictional force is inversely proportional to the factor v_M^2 , so diminishes quickly with increasing of the relative velocity. This is in contrast to the drag of a body moving through a fluid whose friction is proportional to the velocity.
- The frictional drag is proportional to the density n of the surrounding medium.
- The frictional force is proportional to the mass M of the body; thus lighter satellites feel a lower drag. Since dynamical friction has a small effect in minor mergers, especially when the mass ratio between the two galaxies is $M_{\text{sat}}/M_{\text{host}} \leq 1/50$, the material stripped from the satellite preserve much of its initial angular momentum and kinetic energy.

The most important effect of the dynamical friction is the decay of the orbit of the satellite galaxy, as I mentioned before. As the orbit decay tidal forces become strongest and as many as stars and globular clusters are stripped from the outskirts of the galaxy, leading to filaments or sheets or tidal streamers. As time passes these substructures will disperse and the stars could spread and give rise to shells like structures. All these structures are the most important signatures of minor merger events, so their research is very important to probe dynamical effects of an encounter.

Bibliography

- [1] J. A. L. Aguerri, J. Iglesias-Paramo, J. M. Vilchez, and C. Muoz-Tun.
Environmental effects in the structural parameters of galaxies in the coma cluster.
The Astronomical Journal, 127, 03 2004.
- [2] N. C. Amorisco.
Globular cluster populations and the kinematical fingerprints of minor mergers.
ArXiv e-prints, Feb. 2018.
- [3] M. Arnaboldi, J. A. L. Aguerri, N. R. Napolitano, O. Gerhard, K. C. Freeman, J. Feldmeier,
M. Capaccioli, R. P. Kudritzki, and R. H. Méndez.
Intracluster Planetary Nebulae in Virgo: Photometric Selection, Spectroscopic Validation,
and Cluster Depth.
Astronomical Journal, 123:760–771, Feb. 2002.
- [4] M. Arnaboldi, K. C. Freeman, R. H. Mendez, M. Capaccioli, R. Ciardullo, H. Ford, O. Ger-
hard, X. Hui, G. H. Jacoby, R. P. Kudritzki, and P. J. Quinn.
The Kinematics of the Planetary Nebulae in the Outer Regions of NGC 4406.
The astrophysical journal, 472:145, Nov. 1996.
- [5] M. Arnaboldi and O. Gerhard.
JD2 - Diffuse Light in Galaxy Clusters.
Highlights of Astronomy, 15:97–110, Nov. 2010.
- [6] M. Arnaboldi, O. Gerhard, J. A. L. Aguerri, K. C. Freeman, N. R. Napolitano, S. Okamura,
and N. Yasuda.
The Line-of-Sight Velocity Distributions of Intracluster Planetary Nebulae in the Virgo
Cluster Core.
The astrophysical journal, Letters, 614:L33–L36, Oct. 2004.
- [7] M. Arnaboldi, G. Ventimiglia, E. Iodice, O. Gerhard, and L. Coccato.
A tale of two tails and an off-centered envelope: diffuse light around the cD galaxy NGC
3311 in the Hydra I cluster.
Astronomy and Astrophysics, 545:A37, Sept. 2012.
- [8] J. A. Arnold, A. J. Romanowsky, J. P. Brodie, L. Chomiuk, L. R. Spitler, J. Strader, A. J.
Benson, and D. A. Forbes.
The fossil record of two-phase galaxy assembly: Kinematics and metallicities in the nearest
s0 galaxy.
The Astrophysical Journal, 736, 08 2011.
- [9] B. Ascaso, J. A. L. Aguerri, J. Varela, A. Cava, D. Bettoni, M. Moles, and M. D’Onofrio.

- Evolution of brightest cluster galaxy structural parameters in the last ~ 6 gyr: Feedback processes versus merger events.
The Astrophysical Journal, 726, 01 2011.
- [10] K. M. Ashman and S. E. Zepf.
The formation of globular clusters in merging and interacting galaxies.
The astrophysical journal, 384:50–61, Jan. 1992.
- [11] K. M. Ashman and S. E. Zepf.
Globular Cluster Systems.
May 1998.
- [12] N. A. Bahcall.
Clusters and Groups of Galaxies, page 613.
2000.
- [13] G. J. B. J. E. Barnes.
The line-of-sight velocity distributions of simulated merger remnants.
Monthly Notices of the Royal Astronomical Society, 316, 2000.
- [14] J. Barnes.
Experimental studies of mergers.
In T. Thuan, C. Balkowski, and J. Tran Thanh Van, editors, *Physics of Nearby Galaxies: Nature or Nurture?*, page 301, 1992.
- [15] J. Barnes and L. Hernquist.
Fueling starburst galaxies with gas-rich mergers.
The astrophysical journal, 370:L65–L68, apr 1991.
- [16] L. P. Bassino, F. R. Faifer, J. C. Forte, B. Dirsch, T. Richtler, D. Geisler, and Y. Schuberth.
Large-scale study of the NGC 1399 globular cluster system in Fornax.
Astronomy and Astrophysics, 451:789–796, June 2006.
- [17] N. F. Bate, A. R. Conn, B. McMonigal, G. F. Lewis, N. F. Martin, A. W. McConnachie, J. Veljanoski, A. D. Mackey, A. M. N. Ferguson, R. A. Ibata, M. J. Irwin, M. Fardal, A. P. Huxor, and A. Babul.
Major substructure in the m31 outer halo: the south-west cloud.
Monthly Notices of the Royal Astronomical Society, 437, 02 2014.
- [18] K. Bekki, D. A. Forbes, M. A. Beasley, and W. J. Couch.
Globular cluster formation from gravitational tidal effects of merging and interacting galaxies.
Monthly Notices of the Royal Astronomical Society, 335, 2002.
- [19] K. Bekki, D. A. Forbes, M. A. Beasley, and W. J. Couch.
Dynamical evolution of globular cluster systems in clusters of galaxies - I. The case of NGC 1404 in the Fornax cluster.
Monthly Notices of the RAS, 344:1334–1344, Oct. 2003.
- [20] E. F. Bell, S. Phleps, R. S. Somerville, C. Wolf, A. Borch, and K. Meisenheimer.
The merger rate of massive galaxies.
The Astrophysical Journal, 652, 11 2006.
- [21] V. Belokurov, N. W. Evans, M. J. Irwin, P. C. Hewett, and M. I. Wilkinson.
The discovery of tidal tails around the globular cluster ngc 5466.
The Astrophysical Journal, 637, 01 2006.

- [22] R. Bender, J. Kormendy, M. E. Cornell, and D. B. Fisher.
Structure and Formation of cD Galaxies: NGC 6166 in ABELL 2199.
The astrophysical journal, 807:56, July 2015.
- [23] G. Bergond, E. Athanassoula, S. Leon, C. Balkowski, V. Cayatte, L. Chemin, R. Guzmán, G. Meylan, and P. Prugniel.
Globular clusters and dwarf galaxies in Fornax. I. Kinematics in the cluster core from multi-object spectroscopy.
Astronomy and Astrophysics, 464:L21–L24, Mar. 2007.
- [24] M. Bernardi.
The σ - l correlation in nearby early-type galaxies.
The Astronomical Journal, 133, 05 2007.
- [25] M. Bernardi.
Evolution in the structural properties of early-type brightest cluster galaxies at small look-back time and dependence on the environment.
Monthly Notices of the Royal Astronomical Society, 395, 2009.
- [26] R. Bezanson, P. van Dokkum, T. Tal, D. Marchesini, M. Kriek, M. Franx, and P. Coppi.
The Relation Between Compact, Quiescent High-redshift Galaxies and Massive Nearby Elliptical Galaxies: Evidence for Hierarchical, Inside-Out Growth.
The astrophysical journal, 697:1290–1298, June 2009.
- [27] J. P. Blakeslee, M. Cantiello, and E. W. Peng.
The mass-metallicity relation of globular clusters in the context of nonlinear color-metallicity relations.
The Astrophysical Journal, 710, 02 2010.
- [28] J. P. Blakeslee, A. Jordán, S. Mei, P. Côté, L. Ferrarese, L. Infante, E. W. Peng, J. L. Tonry, and M. J. West.
The ACS Fornax Cluster Survey. V. Measurement and Recalibration of Surface Brightness Fluctuations and a Precise Value of the Fornax-Virgo Relative Distance.
The astrophysical journal, 694:556–572, Mar. 2009.
- [29] J. P. Blakeslee, G. R. Meurer, H. C. Ford, N. Benitez, R. L. White, K. C. Zekser, and M. Sirianni.
Extreme Globular Cluster Systems.
In *IAU Joint Discussion*, volume 6 of *IAU Joint Discussion*, 2003.
- [30] A. Bluck, C. Conselice, F. Buitrago, R. Grützbauch, C. Hoyos, A. Mortlock, and A. Bauer.
The structures and total (minor + major) merger histories of massive galaxies up to $z \sim 3$ in the hst goods nicmos survey: A possible solution to the size evolution problem.
The astrophysical journal, 747:34, mar 2012.
- [31] M. Bois, F. Bournaud, E. Emsellem, K. Alatalo, L. Blitz, M. Bureau, M. Cappellari, R. L. Davies, T. A. Davis, P. T. de Zeeuw, J. Falcon-Barroso, S. Khochfar, D. Krajnovic, H. Kuntschner, P.-Y. Lablanche, R. M. McDermid, R. Morganti, T. Naab, M. Sarzi, N. Scott, P. Serra, R. C. E. van den Bosch, G. van de Ven, A. Weijmans, L. M. Young, V. P. Debattista, and C. C. Popescu.
Aip conference proceedings [aip hunting for the dark: The hidden side of galaxy formation - malta (19–23 october 2009)] - formation of slowly rotating elliptical galaxies in major mergers. a resolution study.
2010.
- [32] F. Bournaud, C. J. Jog, and F. Combes.

- Galaxy mergers with various mass ratios: Properties of remnants.
Astronomy and Astrophysics, 437:69–85, July 2005.
- [33] M. Boylan-Kolchin, C.-P. Ma, and E. Quataert.
Red mergers and the assembly of massive elliptical galaxies: the fundamental plane and its projections.
Monthly Notices of the Royal Astronomical Society, 369, 2006.
- [34] T. J. Bridges, D. A. Hanes, and W. E. Harris.
The globular cluster system of NGC 1399.
Astronomical journal, 101:469–482, Feb. 1991.
- [35] J. P. Brodie and J. Strader.
Extragalactic globular clusters and galaxy formation.
Annual Review of Astronomy and Astrophysics, 44, 09 2006.
- [36] S. Brough, C. A. Collins, D. J. Burke, P. D. Lynam, and R. G. Mann.
Environmental dependence of the structure of brightest cluster galaxies.
Monthly Notices of the Royal Astronomical Society, 364, 2005.
- [37] F. Buitrago, I. Trujillo, C. J. Conselice, R. J. Bouwens, M. Dickinson, and H. Yan.
Size evolution of the most massive galaxies at $1.7 < z < 3$ from goods nicmos survey imaging.
The Astrophysical Journal, 687, 11 2008.
- [38] J. S. Bullock and K. V. Johnston.
Tracing Galaxy Formation with Stellar Halos. I. Methods.
The astrophysical journal, 635:931–949, Dec. 2005.
- [39] M. Cantiello and J. P. Blakeslee.
On the bimodal color distribution of Globular Cluster systems .
Memorie della Societa Astronomica Italiana Supplementi, 19:184, 2012.
- [40] M. Cantiello, R. D’Abrusco, M. Spavone, M. Paolillo, M. Capaccioli, L. Limatola, A. Grado, E. Iodice, G. Raimondo, N. Napolitano, J. P. Blakeslee, E. Brocato, D. A. Forbes, M. Hilker, S. Mieske, R. Peletier, G. van de Ven, and P. Schipani.
VizieR Online Data Catalog: NGC3115 & NGC1399 VEGAS-SSS globular clusters (Cantiello+, 2018).
VizieR Online Data Catalog, 361, Nov. 2017.
- [41] N. Caon, M. Capaccioli, and M. D’Onofrio.
‘Global mapping’ B-band photometry of a complete sample of Fornax and Virgo early-type galaxies.
Astronomy and Astrophysics, Supplement, 106:199–242, Aug. 1994.
- [42] P. Cassata, M. Giavalisco, Y. Guo, A. Renzini, H. Ferguson, A. M. Koekemoer, S. Salimbeni, C. Scarlata, C. J. Grogin, N. A. and Conselice, T. Dahlen, J. M. Lotz, M. Dickinson, and L. Lin.
The relative abundance of compact and normal massive early-type galaxies and its evolution from redshift $z \sim 2$ to the present.
The Astrophysical Journal, 743, 12 2011.
- [43] P. Cassata, M. Giavalisco, C. C. Williams, Y. Guo, B. Lee, A. Renzini, S. F. Ferguson, H. and Faber, G. Barro, D. H. McIntosh, Y. Lu, E. F. Bell, D. C. Koo, C. J. Papovich, R. E. Ryan, C. J. Conselice, N. Grogin, A. Koekemoer, and N. P. Hathi.
Constraining the assembly of normal and compact passively evolving galaxies from redshift $z = 3$ to the present with candels.
The Astrophysical Journal, 775, 10 2013.

- [44] A. L. Chies-Santos, S. S. Larsen, H. Kuntschner, P. Anders, E. M. Wehner, J. Strader, J. P. Brodie, and J. F. C. Santos.
Ages of Globular Cluster Systems and the Relation to Galaxy Morphology.
In C. Carignan, F. Combes, and K. C. Freeman, editors, *Tracing the Ancestry of Galaxies*, volume 277 of *IAU Symposium*, pages 321–324, Dec. 2011.
- [45] I. V. Chilingarian, P. Di Matteo, F. Combes, A.-L. Melchior, and B. Semelin.
The GalMer database: galaxy mergers in the virtual observatory.
Astronomy and Astrophysics, 518:A61, July 2010.
- [46] J. Choi, C. Conroy, J. Moustakas, G. J. Graves, B. P. Holden, M. Brodwin, M. J. I. Brown, and P. G. van Dokkum.
The Assembly Histories of Quiescent Galaxies since $z = 0.7$ from Absorption Line Spectroscopy.
The astrophysical journal, 792:95, Sept. 2014.
- [47] A. Cimatti, P. Cassata, L. Pozzetti, J. Kurk, M. Mignoli, A. Renzini, E. Daddi, M. Bolzonella, M. Brusa, G. Rodighiero, M. Dickinson, A. Franceschini, G. Zamorani, S. Berta, P. Rosati, and C. Halliday.
GMASS ultradeep spectroscopy of galaxies at $z \sim 2$. II. Superdense passive galaxies: how did they form and evolve?
Astronomy and Astrophysics, 482:21–42, Apr. 2008.
- [48] T. S. Ciotti, Luca; van Albada.
The $m_{\text{BH}} - \sigma_c$ relation as a constraint on the formation of elliptical galaxies.
The Astrophysical Journal, 552, 5 2001.
- [49] L. Coccato, O. Gerhard, M. Arnaboldi, P. Das, N. G. Douglas, K. Kuijken, M. R. Merrifield, N. R. Napolitano, E. Noordermeer, A. J. Romanowsky, M. Capaccioli, A. Cortesi, F. De Lorenzi, and K. C. Freeman.
Kinematic properties of early-type galaxy haloes using planetary nebulae*.
Monthly Notices of the RAS, 394:1249–1283, Apr. 2009.
- [50] M. G. O. Coccato, L.; Arnaboldi.
Signatures of accretion events in the haloes of early-type galaxies from comparing pne and gcs kinematics.
Monthly Notices of the Royal Astronomical Society, 436, 12 2013.
- [51] M. Colless and A. M. Dunn.
Structure and Dynamics of the Coma Cluster.
The astrophysical journal, 458:435, Feb. 1996.
- [52] C. A. Collins, J. P. Stott, M. Hilton, S. T. Kay, S. A. Stanford, M. Davidson, M. Hosmer, B. Hoyle, A. Liddle, and E. Lloyd-Davies.
Early assembly of the most massive galaxies.
Nature, 458, 2009.
- [53] C. Conselice, A. F. L. Bluck, F. Buitrago, A. E. Bauer, R. Grützbauch, R. J. Bouwens, S. B. A. Mortlock, M. D. E. Daddi, H. Yan, D. Scott, S. C. Chapman, R.-R. Chary, H. C. Ferguson, M. Giavalisco, N. Grogin, G. Illingworth, S. Jogee, A. M. Koekemoer, R. A. Lucas, B. Mobasher, L. Moustakas, C. Papovich, S. Ravindranath, B. Siana, H. Teplitz, I. Trujillo, M. Urry, and T. Weinzierl.
The hubble space telescope goods nicmos survey: overview and the evolution of massive galaxies at $1.5 < z < 3$.
Monthly Notices of the Royal Astronomical Society, 413, 2011.

- [54] G. V. A. B. S. Contini, E.; De Lucia.
On the formation and physical properties of the intracluster light in hierarchical galaxy formation models.
Monthly Notices of the Royal Astronomical Society, 437, 02 2014.
- [55] A. P. Cooper, D. Martínez-Delgado, J. Helly, C. Frenk, S. Cole, K. Crawford, S. Zibetti, J. A. Carballo-Bello, and R. Jay GaBany.
The formation of shell galaxies similar to ngc 7600 in the cold dark matter cosmogony.
The Astrophysical Journal, 743, 12 2011.
- [56] A. Cortesi, M. R. Merrifield, M. Arnaboldi, O. Gerhard, I. Martinez-Valpuesta, K. Saha, L. Coccato, S. Bamford, N. R. Napolitano, P. Das, N. G. Douglas, A. J. Romanowsky, K. Kuijken, M. Capaccioli, and K. C. Freeman.
Unravelling the origins of S0 galaxies using maximum likelihood analysis of planetary nebulae kinematics.
Monthly Notices of the Royal Astronomical Society, 414:642–651, June 2011.
- [57] A. Cortesi, M. R. Merrifield, L. Coccato, M. Arnaboldi, O. Gerhard, S. Bamford, N. R. Napolitano, A. J. Romanowsky, N. G. Douglas, K. Kuijken, M. Capaccioli, K. C. Freeman, K. Saha, and A. L. Chies-Santos.
Planetary Nebula Spectrograph survey of S0 galaxy kinematics - II. Clues to the origins of S0 galaxies.
Monthly Notices of the RAS, 432:1010–1020, June 2013.
- [58] H. G. Corwin, A. de Vaucouleurs, and G. de Vaucouleurs.
Southern galaxy catalogue. A catalogue of 5481 galaxies south of declination -17 grad. found on 1.2m UK Schmidt IIIa J plates.
1985.
- [59] P. Côté.
Kinematics of the Galactic Globular Cluster System: New Radial Velocities for Clusters in the Direction of the Inner Galaxy.
Astronomical journal, 118:406–420, July 1999.
- [60] P. Côté, R. O. Marzke, and M. J. West.
The Formation of Giant Elliptical Galaxies and Their Globular Cluster Systems.
The astrophysical journal, 501:554–570, July 1998.
- [61] P. Côté, D. E. McLaughlin, J. G. Cohen, and J. P. Blakeslee.
Dynamics of the Globular Cluster System Associated with M49 (NGC 4472): Cluster Orbital Properties and the Distribution of Dark Matter.
The astrophysical journal, 591:850–877, July 2003.
- [62] P. Côté, D. E. McLaughlin, D. A. Hanes, T. J. Bridges, D. Geisler, D. Merritt, J. E. Hesser, G. L. H. Harris, and M. G. Lee.
Dynamics of the Globular Cluster System Associated with M87 (NGC 4486). II. Analysis.
The astrophysical journal, 559:828–850, Oct. 2001.
- [63] L. Cowie and J. Binney.
Radiative regulation of gas flow within clusters of galaxies - A model for cluster X-ray sources.
The astrophysical journal, 215:723–732, Aug. 1977.
- [64] N. Cretton, T. Naab, H.-W. Rix, and A. Burkert.
The Kinematics of 3:1 Merger Remnants and the Formation of Low-Luminosity Elliptical Galaxies.

- The astrophysical journal*, 554:291–297, June 2001.
- [65] W. Cui, G. Murante, P. Monaco, S. Borgani, G. L. Granato, M. Killevar, G. De Lucia, V. Presotto, and K. Dolag.
Characterizing diffused stellar light in simulated galaxy clusters.
Monthly Notices of the RAS, 437:816–830, Jan. 2014.
- [66] R. D’Abrusco, M. Cantiello, M. Paolillo, V. Pota, N. R. Napolitano, L. Limatola, M. Spavone, A. Grado, E. Iodice, M. Capaccioli, R. Peletier, G. Longo, M. Hilker, S. Mieske, E. K. Grebel, T. Lisker, C. Wittmann, G. van de Ven, P. Schipani, and G. Fabbiano.
The Extended Spatial Distribution of Globular Clusters in the Core of the Fornax Cluster.
Astrophysical Journal, Letters, 819:L31, Mar. 2016.
- [67] E. Daddi, A. Renzini, N. Pirzkal, A. Cimatti, S. Malhotra, M. Stiavelli, A. Xu, C. and Pasquali, J. E. Rhoads, M. Brusa, S. di Serego Alighieri, H. C. Ferguson, A. M. Koekemoer, L. A. Moustakas, N. Panagia, and R. A. Windhorst.
Passively evolving early-type galaxies at $1.4 \leq z \leq 2.5$ in the hubble ultra deep field.
The Astrophysical Journal, 626, 06 2005.
- [68] I. Damjanov, P. J. McCarthy, R. G. Abraham, K. Glazebrook, H. Yan, E. Mentuch, D. Le Borgne, S. Savaglio, D. Crampton, R. Murowinski, S. Juneau, R. G. Carlberg, I. Jorgensen, K. Roth, H.-W. Chen, and R. O. Marzke.
Red nuggets at $z \sim 1.5$: Compact passive galaxies and the formation of the kormendy relation.
The Astrophysical Journal, 695, 04 2009.
- [69] F. de Lorenzi, O. Gerhard, L. Coccato, M. Arnaboldi, M. Capaccioli, N. G. Douglas, K. C. Freeman, K. Kuijken, M. R. Merrifield, N. R. Napolitano, E. Noordermeer, A. J. Romanowsky, and V. P. Debattista.
Dearth of dark matter or massive dark halo? Mass-shape-anisotropy degeneracies revealed by NMAGIC dynamical models of the elliptical galaxy NGC 3379.
Monthly Notices of the RAS, 395:76–96, May 2009.
- [70] J. De Lucia, G.; Blaizot.
The hierarchical formation of the brightest cluster galaxies.
Monthly Notices of the Royal Astronomical Society, 375, 2007.
- [71] G. de Vaucouleurs.
Book-Review - Third Reference Catalogue of Bright Galaxies.
Science, 254:1667, Dec. 1991.
- [72] A. J. Deason, V. Belokurov, N. W. Evans, and I. G. McCarthy.
Elliptical Galaxy Masses Out to Five Effective Radii: The Realm of Dark Matter.
The astrophysical journal, 748:2, Mar. 2012.
- [73] A. Dekel, F. Stoehr, G. A. Mamon, T. J. Cox, G. S. Novak, and J. R. Primack.
Lost and found dark matter in elliptical galaxies.
Nature, 437:707–710, Sept. 2005.
- [74] E. P. V. S. D. S. K. Dolag.
Intracluster stars in simulations with active galactic nucleus feedback.
Monthly Notices of the Royal Astronomical Society, 406, 2010.
- [75] G. M. M. G. O. G. M. A. S. B. K. Dolag.
The importance of mergers for the origin of intracluster stars in cosmological simulations of galaxy clusters.

- Monthly Notices of the Royal Astronomical Society*, 377, 2007.
- [76] R. Dominguez-Tenreiro, J. Onorbe, A. Saiz, H. Artal, and A. Serna.
The lack of structural and dynamical evolution of elliptical galaxies since $z \sim 1.5$: Clues from self-consistent hydrodynamic simulations.
The Astrophysical Journal, 636, 01 2006.
- [77] M. A. Dopita, G. H. Jacoby, and E. Vassiliadis.
A theoretical calibration of the planetary nebular cosmic distance scale.
The astrophysical journal, 389:27–38, Apr. 1992.
- [78] N. G. Douglas, N. R. Napolitano, A. J. Romanowsky, L. Coccato, K. Kuijken, M. R. Merrifield, M. Arnaboldi, O. Gerhard, K. C. Freeman, H. R. Merrett, E. Noordermeer, and M. Capaccioli.
The PN.S Elliptical Galaxy Survey: Data Reduction, Planetary Nebula Catalog, and Basic Dynamics for NGC 3379.
The astrophysical journal, 664:257–276, July 2007.
- [79] A. Dressler.
Galaxy morphology in rich clusters - implications for the formation and evolution of galaxies.
The astrophysical journal, 236:351–365, mar 1980.
- [80] M. Drinkwater, M. Gregg, B. Holman, and M. Brown.
The evolution and star formation of dwarf galaxies in the fornax cluster.
Monthly Notices of the Royal Astronomical Society, 326, 2001.
- [81] M. J. Drinkwater, S. Phillipps, J. B. Jones, M. D. Gregg, J. H. Deady, J. I. Davies, Q. A. Parker, E. M. Sadler, and R. M. Smith.
The Fornax spectroscopic survey. I. Survey strategy and preliminary results on the redshift distribution of a complete sample of stars and galaxies.
Astronomy and Astrophysics, 355:900–914, Mar. 2000.
- [82] P. R. Durrell, J. C. Mihos, J. J. Feldmeier, G. H. Jacoby, and R. Ciardullo.
Kinematics of Planetary Nebulae in M51's Tidal Debris.
The astrophysical journal, 582:170–183, Jan. 2003.
- [83] L. O. V. Edwards and D. R. Patton.
Close companions to brightest cluster galaxies: support for minor mergers and downsizing.
Monthly Notices of the Royal Astronomical Society, 425, 2012.
- [84] B. G. Elmegreen.
The Specific Frequency of Globular Clusters in Galaxies.
Astrophysics and Space Science, 269:469–484, Dec. 1999.
- [85] A. Fabian.
The effect of cooling flows on the global X-ray properties of clusters.
In H. Böhringer and S. Schindler, editors, *Studying the Universe with Clusters of Galaxies*, pages 169–171, June 1994.
- [86] H. C. Ferguson.
Galaxy populations in the Fornax and Virgo clusters.
Astrophysics and Space Science, 157:227–233, July 1989.
- [87] H. C. Ferguson and B. Binggeli.
Dwarf elliptical galaxies.
Astronomy and Astrophysics Reviews, 6:67–122, Nov. 1994.

- [88] B. Flaugher, H. T. Diehl, K. Honscheid, T. M. C. Abbott, O. Alvarez, R. Angstadt, J. T. Annis, M. Antonik, O. Ballester, L. Beaufore, G. M. Bernstein, R. A. Bernstein, B. Bigelow, M. Bonati, D. Boprie, D. Brooks, E. J. Buckley-Geer, J. Campa, L. Cardiel-Sas, F. J. Castander, J. Castilla, H. Cease, J. M. Cela-Ruiz, S. Chappa, E. Chi, C. Cooper, L. N. da Costa, E. Dede, G. Derylo, D. L. DePoy, J. de Vicente, P. Doel, A. Drlica-Wagner, J. Eiting, A. E. Elliott, J. Emes, J. Estrada, A. Fausti Neto, D. A. Finley, R. Flores, J. Frieman, D. Gerdes, M. D. Gladders, B. Gregory, G. R. Gutierrez, J. Hao, S. E. Holland, S. Holm, D. Huffman, C. Jackson, D. J. James, M. Jonas, A. Karcher, I. Karliner, S. Kent, R. Kessler, M. Kozlovsky, R. G. Kron, D. Kubik, K. Kuehn, S. Kuhlmann, K. Kuk, O. Lahav, A. Lathrop, J. Lee, M. E. Levi, P. Lewis, T. S. Li, I. Mandrichenko, J. L. Marshall, G. Martinez, K. W. Merritt, R. Miquel, F. Muñoz, E. H. Neilsen, R. C. Nichol, B. Nord, R. Ogando, J. Olsen, N. Palaio, K. Patton, J. Peoples, A. A. Plazas, J. Rauch, K. Reil, J.-P. Rheault, N. A. Roe, H. Rogers, A. Roodman, E. Sanchez, V. Scarpine, R. H. Schindler, R. Schmidt, R. Schmitt, M. Schubnell, K. Schultz, P. Schurter, L. Scott, S. Serrano, T. M. Shaw, R. C. Smith, M. Soares-Santos, A. Stefanik, W. Stuermer, E. Suchyta, A. Sypniewski, G. Tarle, J. Thaler, R. Tighe, C. Tran, D. Tucker, A. R. Walker, G. Wang, M. Watson, C. Weaverdyck, W. Wester, R. Woods, B. Yanny, and DES Collaboration.
The Dark Energy Camera.
Astronomical journal, 150:150, Nov. 2015.
- [89] A. Fontana, S. Salimbeni, A. Grazian, E. Giallongo, L. Pentericci, M. Nonino, F. Fontanot, N. Menci, P. Monaco, S. Cristiani, E. Vanzella, C. de Santis, and S. Gallozzi.
The Galaxy mass function up to $z = 4$ in the GOODS-MUSIC sample: into the epoch of formation of massive galaxies.
Astronomy and Astrophysics, 459:745–757, Dec. 2006.
- [90] D. Forbes.
Globular Clusters in Elliptical Galaxies: Constraints on Mergers.
ArXiv Astrophysics e-prints, Nov. 1997.
- [91] D. A. Forbes, L. R. Spitler, J. Strader, A. J. Romanowsky, J. P. Brodie, and C. Foster.
Evidence for two phases of galaxy formation from radial trends in the globular cluster system of NGC 1407.
Monthly Notices of the RAS, 413:2943–2949, June 2011.
- [92] J. C. Forte, R. E. Martinez, and J. C. Muzzio.
On the origin of the globular cluster system of M87.
Astronomical Journal, 87:1465–1469, Nov. 1982.
- [93] C. Foster, H. Lux, A. J. Romanowsky, D. Martínez-Delgado, S. Zibetti, J. A. Arnold, J. P. Brodie, R. Ciardullo, R. J. GaBany, M. R. Merrifield, N. Singh, and J. Strader.
Kinematics and simulations of the stellar stream in the halo of the Umbrella Galaxy.
Monthly Notices of the RAS, 442:3544–3564, Aug. 2014.
- [94] M. Franx, P. G. van Dokkum, N. M. Förster Schreiber, S. Wuyts, I. Labbé, and S. Toft.
Structure and Star Formation in Galaxies out to $z = 3$: Evidence for Surface Density Dependent Evolution and Upsizing.
The astrophysical journal, 688:770–788, Dec. 2008.
- [95] J. Gallagher, III and J. Ostriker.
A note on mass loss during collisions between galaxies and the formation of giant systems.
The astrophysical journal, 77:288, may 1972.
- [96] A. M. Gilbert and W. D. Vacca.

- The formation and evolution of massive stellar clusters in IC4662.
Astrophysics and Space Science, 324:147–154, Dec. 2009.
- [97] O. Y. Gnedin.
Dynamical Evolution of Galaxies in Clusters.
The astrophysical journal, 589:752–769, June 2003.
- [98] P. L. Gomez, R. C. Nichol, C. J. Miller, M. L. Balogh, T. Goto, A. I. Zabludoff, A. K. Romer, M. Bernardi, A. M. Sheth, R. van Dokkum, F. J. Castander, D. P. B. J. Connolly, Andrew J. and Schneider, D. Q. Lamb, M. SubbaRao, and D. G. York.
Galaxy star formation as a function of environment in the early data release of the sloan digital sky survey.
The Astrophysical Journal, 584, 02 2003.
- [99] A. H. Gonzalez, D. Zaritsky, and A. I. Zabludoff.
A Census of Baryons in Galaxy Clusters and Groups.
The astrophysical journal, 666:147–155, Sept. 2007.
- [100] A. Graham, T. R. Lauer, M. Colless, and M. Postman.
Brightest Cluster Galaxy Profile Shapes.
The astrophysical journal, 465:534, July 1996.
- [101] A. W. Graham and R. Guzmán.
Hst photometry of dwarf elliptical galaxies in coma, and an explanation for the alleged structural dichotomy between dwarf and bright elliptical galaxies.
The Astronomical Journal, 125, 06 2003.
- [102] G. L. Granato, G. De Zotti, L. Silva, A. Bressan, and L. Danese.
A physical model for the coevolution of quasars and their spheroidal hosts.
The Astrophysical Journal, 600, 01 2004.
- [103] M. J. Gregg, Michael D.; West.
Nature, 396, 12 1998.
- [104] J. Gunn and J. Oke.
Spectrophotometry of faint cluster galaxies and the Hubble diagram - an approach to cosmology.
The astrophysical journal, 195:255–268, Jan. 1975.
- [105] J. R. I. Gunn, James E.; Gott.
On the infall of matter into clusters of galaxies and some effects on their evolution.
The Astrophysical Journal, 176, 08 1972.
- [106] L. Hagen, E. Hoversten, C. Gronwall, C. Wolf, M. Siegel, M. Page, and A. Hagen.
The evolution of the far-uv luminosity function and star formation rate density of the chandra deep field south from $z = 0.2$ to 1.2 with swift/uvot.
The astrophysical journal, 808:178, aug 2015.
- [107] W. E. Harris, C. J. Pritchet, and R. D. McClure.
Globular cluster systems in three cD galaxies within rich Abell clusters.
The astrophysical journal, 441:120–128, Mar. 1995.
- [108] W. E. Harris and S. van den Bergh.
Globular clusters in galaxies beyond the local group. I - New cluster systems in selected northern ellipticals.
Astronomical Journal, 86:1627–1642, Nov. 1981.

- [109] J. Hartke, M. Arnaboldi, A. Longobardi, O. Gerhard, K. Freeman, and S. Okamura.
The halo of M49 and its environment as traced by planetary nebulae.
In X. Liu, L. Stanghellini, and A. Karakas, editors, *Planetary Nebulae: Multi-Wavelength Probes of Stellar and Galactic Evolution*, volume 323 of *IAU Symposium*, pages 293–297, Oct. 2017.
- [110] A. Helmi, J. F. Navarro, A. Meza, M. Steinmetz, and V. R. Eke.
The Nature of the Ring-Like Structure in the Outer Galactic Disk.
In F. Prada, D. Martinez Delgado, and T. J. Mahoney, editors, *Satellites and Tidal Streams*, volume 327 of *Astronomical Society of the Pacific Conference Series*, page 87, Dec. 2004.
- [111] A. Helmi, S. D. M. White, P. T. de Zeeuw, and H. Zhao.
Nature, 402, 11 1999.
- [112] L. Hernquist.
An analytical model for spherical galaxies and bulges.
The astrophysical journal, 356:359–364, June 1990.
- [113] L. Hernquist and P. J. Quinn.
Formation of shell galaxies. I - Spherical potentials.
The astrophysical journal, 331:682–698, Aug. 1988.
- [114] L. Hernquist and P. J. Quinn.
Formation of shell galaxies. II - Nonspherical potentials.
The astrophysical journal, 342:1–16, July 1989.
- [115] K. A. Herrmann and R. Ciardullo.
Planetary Nebulae in Face-On Spiral Galaxies. III. Planetary Nebula Kinematics and Disk Mass.
The astrophysical journal, 705:1686–1703, Nov. 2009.
- [116] M. Hilker.
Stellar population properties of the most massive globular clusters and ultra-compact dwarf galaxies of the Fornax cluster.
IAU General Assembly, 22:2215721, Aug. 2015.
- [117] M. Hilker, L. Infante, and T. Richtler.
The central region of the Fornax cluster. III. Dwarf galaxies, globular clusters, and cD halo - are there interrelations?
Astrophysics and Space Science, 138:55–70, July 1999.
- [118] J. Hoessel and D. Schneider.
CCD observations of Abell clusters. IV - Surface photometry of 175 brightest cluster galaxies.
Astronomical Journal, 90:1648–1664, Sept. 1985.
- [119] D. W. Hogg, M. R. Blanton, J. Brinchmann, D. J. Eisenstein, D. J. Schlegel, J. E. Gunn, T. A. McKay, H.-W. Rix, N. A. Bahcall, J. Brinkmann, and A. Meiksin.
The dependence on environment of the color-magnitude relation of galaxies.
The Astrophysical Journal, 601, 01 2004.
- [120] A. M. Hopkins, N. M. McClure-Griffiths, and B. M. Gaensler.
Linked Evolution of Gas and Star Formation in Galaxies Over Cosmic History.
Astrophysical Journal, Letters, 682:L13, July 2008.
- [121] P. F. Hopkins, R. S. Somerville, T. J. Cox, L. Hernquist, S. Jogee, D. Keres, C.-P. Ma, B. Robertson, and K. Stewart.
The effects of gas on morphological transformation in mergers: implications for bulge and disc demographics.

- Monthly Notices of the Royal Astronomical Society*, 397, 2009.
- [122] X. Hui, H. C. Ford, K. C. Freeman, and M. A. Dopita.
The Planetary Nebula System and Dynamics of NGC 5128. III. Kinematics and Halo Mass Distributions.
The astrophysical journal, 449:592, Aug. 1995.
- [123] R. Ibata, M. Irwin, G. F. Lewis, and A. Stolte.
Galactic Halo Substructure in the Sloan Digital Sky Survey: The Ancient Tidal Stream from the Sagittarius Dwarf Galaxy.
Astrophysical Journal, Letters, 547:L133–L136, Feb. 2001.
- [124] R. Ibata, G. F. Lewis, M. Irwin, E. Totten, and T. Quinn.
Great Circle Tidal Streams: Evidence for a Nearly Spherical Massive Dark Halo around the Milky Way.
The astrophysical journal, 551:294–311, Apr. 2001.
- [125] R. A. Ibata, R. F. G. Wyse, G. Gilmore, M. J. Irwin, and N. B. Suntzeff.
The Kinematics, Orbit, and Survival of the Sagittarius Dwarf Spheroidal Galaxy.
Astronomical Journal, 113:634–655, Feb. 1997.
- [126] O. Ilbert, M. Salvato, E. Le Floch, H. Aussel, P. Capak, H. McCracken, B. Mobasher, J. Kartaltepe, N. Scoville, and D. Sanders.
Galaxy stellar mass assembly between $0.2 \leq z \leq 2$ from the S-COSMOS survey.
In S. Boissier, M. Heydari-Malayeri, R. Samadi, and D. Valls-Gabaud, editors, *SF2A-2010: Proceedings of the Annual meeting of the French Society of Astronomy and Astrophysics*, page 355, Dec. 2010.
- [127] E. Iodice, M. Spavone, M. Cantiello, R. D’Abrusco, M. Capaccioli, M. Hilker, S. Mieske, N. R. Napolitano, R. F. Peletier, L. Limatola, A. Grado, A. Venhola, M. Paolillo, G. V. d. Ven, and P. Schipani.
Intracluster patches of baryons in the core of the fornax cluster.
The Astrophysical Journal, 851, 12 2017.
- [128] M. Iodice, E.; Capaccioli, A. Grado, L. Limatola, M. Spavone, N. R. Napolitano, M. Paolillo, R. F. Peletier, M. Cantiello, T. Lisker, C. Wittmann, A. Venhola, M. Hilker, R. D’Abrusco, V. Pota, and P. Schipani.
The fornax deep survey with vst. i. the extended and diffuse stellar halo of ngc 1399 out to 192 kpc.
The Astrophysical Journal, 820, 03 2016.
- [129] R. Jimenez, M. Bernardi, Z. Haiman, B. Panter, and A. F. Heavens.
The ages, metallicities, and star formation histories of early-type galaxies in the sdss.
The Astrophysical Journal, 669, 11 2007.
- [130] K. V. Johnston, J. S. Bullock, S. Sharma, A. Font, B. E. Robertson, and S. N. Leitner.
Tracing Galaxy Formation with Stellar Halos. II. Relating Substructure in Phase and Abundance Space to Accretion Histories.
The astrophysical journal, 689:936–957, Dec. 2008.
- [131] K. V. Johnston, H. S. Zhao, D. N. Spergel, and L. Hernquist.
Tidal Streams as Probes of the Galactic Potential.
In *American Astronomical Society Meeting Abstracts*, volume 30 of *Bulletin of the American Astronomical Society*, page 1378, Dec. 1998.
- [132] J. Khochfar, Sadegh; Silk.
A simple model for the size evolution of elliptical galaxies.

- The Astrophysical Journal*, 648, 09 2006.
- [133] S. Khochfar and A. Burkert.
The Importance of Spheroidal and Mixed Mergers for Early-Type Galaxy Formation.
Astrophysical Journal, Letters, 597:L117–L120, Nov. 2003.
- [134] S. Khochfar and J. Silk.
A Simple Model for the Size Evolution of Elliptical Galaxies.
The astrophysical journal, 648:L21–L24, Sept. 2006.
- [135] A. Koch, R. M. Rich, D. B. Reitzel, N. F. Martin, R. A. Ibata, S. C. Chapman, S. R. Majewski, M. Mori, Y.-S. Loh, J. C. Ostheimer, and M. Tanaka.
Kinematic and Chemical Constraints on the Formation of M31’s Inner and Outer Halo.
The astrophysical journal, 689:958–982, Dec. 2008.
- [136] J. Koda, M. Yagi, H. Yamanoi, and Y. Komiyama.
Approximately a Thousand Ultra-diffuse Galaxies in the Coma Cluster.
The astrophysical journal, Letters, 807:L2, July 2015.
- [137] J. Kormendy, D. B. Fisher, M. E. Cornell, and R. Bender.
Structure and formation of elliptical and spheroidal galaxies.
The Astrophysical Journal Supplement Series, 182, 05 2009.
- [138] E. Kourkchi, H. G. Khosroshahi, D. Carter, K. Chiboucas, and A. M. Karick.
Dynamical and Photometric Properties of Dwarf Galaxies in Coma Cluster.
In M. Koleva, P. Prugniel, and I. Vauglin, editors, *EAS Publications Series*, volume 48 of *EAS Publications Series*, pages 307–308, July 2011.
- [139] K. Kuijken.
OmegaCAM: ESO’s Newest Imager.
The Messenger, 146:8–11, Dec. 2011.
- [140] C. F. P. Laporte, S. D. M. White, T. Naab, and L. Gao.
The growth in size and mass of cluster galaxies since $z = 2$.
Monthly Notices of the Royal Astronomical Society, 435, 10 2013.
- [141] T. Lauer, S. Tremaine, D. Richstone, and S. Faber.
Selection Bias in Observing the Cosmological Evolution of the M- σ and M-L Relationships.
The astrophysical journal, 670:249–260, Nov. 2007.
- [142] O. Le Fèvre, S. J. Abraham, O.; Lilly, R. S. Ellis, J. Brinchmann, D. Schade, L. Tresse, M. Colless, D. Crampton, K. Glazebrook, F. Hammer, and T. Broadhurst.
Hubble space telescope imaging of the cfrs and ldss redshift surveys – iv. influence of mergers in the evolution of faint field galaxies from $z \sim 1$.
Monthly Notices of the Royal Astronomical Society, 311, 2000.
- [143] M. G. Lee and D. Geisler.
Metal abundances for a large sample of globular clusters in M87.
Astronomical journal, 106:493–506, Aug. 1993.
- [144] C. Lidman, A. Suherli, J. and Muzzin, G. Wilson, R. Demarco, S. Brough, A. Rettura, A. Cox, J. and DeGroot, H. K. C. Yee, D. Gilbank, H. Hoekstra, M. Balogh, E. Ellingson, A. Hicks, J. Nantais, A. Noble, M. Lacy, J. Surace, and T. Webb.
Evidence for significant growth in the stellar mass of brightest cluster galaxies over the past 10 billion years.
Monthly Notices of the Royal Astronomical Society, 427, 11 2012.

- [145] Y.-T. Lin and J. Mohr.
K-band Properties of Galaxy Clusters and Groups: Brightest Cluster Galaxies and Intra-cluster Light.
The astrophysical journal, 617:879–895, Dec. 2004.
- [146] P. J. E. Loeb, Abraham; Peebles.
Cosmological origin of the stellar velocity dispersions in massive early-type galaxies.
The Astrophysical Journal, 589, 05 2003.
- [147] A. Longobardi, M. Arnaboldi, and O. Gerhard.
The Ongoing Growth of the M87 Halo through Accretion Events.
Galaxies, 3:212–219, Dec. 2015.
- [148] A. Longobardi, E. W. Peng, P. Côté, J. C. Mihos, L. Ferrarese, T. H. Puzia, A. Lançon, H.-X. Zhang, R. P. Muñoz, J. P. Blakeslee, P. Guhathakurta, P. R. Durrell, R. Sánchez-Janssen, E. Toloba, A. Jordán, S. Eyheramendy, J.-C. Cuillandre, S. D. J. Gwyn, A. Boselli, P.-A. Duc, C. Liu, K. Alamo-Martínez, M. Powalka, and S. Lim.
The Next Generation Virgo Cluster Survey (NGVS). XXXI. The Kinematics of Intracluster Globular Clusters in the Core of the Virgo Cluster.
The astrophysical journal, 864:36, Sept. 2018.
- [149] S. R. Majewski, M. F. Skrutskie, M. D. Weinberg, and J. C. Ostheimer.
A Two Micron All Sky Survey View of the Sagittarius Dwarf Galaxy. I. Morphology of the Sagittarius Core and Tidal Arms.
The astrophysical journal, 599:1082–1115, Dec. 2003.
- [150] E. Malumuth and D. Richstone.
The evolution of clusters of galaxies. ii - tidal stripping versus mergers as a function of richness.
The astrophysical journal, 276:413–422, jan 1984.
- [151] D. Marchesini, P. G. van Dokkum, N. M. Förster Schreiber, M. Franx, I. Labbé, and S. Wuyts.
The evolution of the stellar mass function of galaxies from $z = 4.0$ and the first comprehensive analysis of its uncertainties: Evidence for mass-dependent evolution.
The Astrophysical Journal, 701, 08 2009.
- [152] D. Martínez-Delgado, R. J. Gabany, K. Crawford, S. Zibetti, S. R. Majewski, H.-W. Rix, J. Fliri, J. A. Carballo-Bello, D. C. Bardalez-Gagliuffi, J. Peñarrubia, T. S. Chonis, B. Madore, I. Trujillo, M. Schirmer, and D. A. McDavid.
Stellar tidal streams in spiral galaxies of the local volume: A pilot survey with modest aperture telescopes.
The Astronomical Journal, 140, 10 2010.
- [153] K. L. Masters, A. Jordán, P. Côté, L. Ferrarese, J. P. Blakeslee, L. Infante, E. W. Peng, S. Mei, and M. J. West.
The Advanced Camera for Surveys Fornax Cluster Survey. VII. Half-light Radii of Globular Clusters in Early-type Galaxies.
The astrophysical journal, 715:1419–1437, June 2010.
- [154] A. W. McConnachie, M. J. Irwin, R. A. Ibata, J. Dubinski, L. M. Widrow, N. F. Martin, P. Côté, A. L. Dotter, J. F. Navarro, A. M. N. Ferguson, T. H. Puzia, G. F. Lewis, A. Babul, P. Barmby, O. Bienaymé, S. C. Chapman, R. Cockcroft, M. L. M. Collins, M. A. Fardal, W. E. Harris, A. Huxor, A. D. Mackey, J. Peñarrubia, R. M. Rich, H. B. Richer, A. Siebert, N. Tanvir, D. Valls-Gabaud, and K. A. Venn.

- The remnants of galaxy formation from a panoramic survey of the region around M31.
Nature, 461:66–69, Sept. 2009.
- [155] T. McGlynn and J. P. Ostriker.
Galactic cannibalism. IV - The evidence-correlations between dynamical time scales and Bautz-Morgan type.
The astrophysical journal, 241:915–924, Nov. 1980.
- [156] R. J. McLure, J. S. Pearce, H. J. and Dunlop, M. Cirasuolo, E. Curtis-Lake, V. A. Bruce, K. I. Caputi, O. Almaini, D. G. Bonfield, E. J. Bradshaw, F. Buitrago, R. Chuter, S. Foucaud, W. G. Hartley, and M. J. Jarvis.
The sizes, masses and specific star formation rates of massive galaxies at $1.3 < z < 1.5$: strong evidence in favour of evolution via minor mergers.
Monthly Notices of the Royal Astronomical Society, 428, 01 2013.
- [157] E. McNeil, M. Arnaboldi, O. Gerhard, K. Freeman, P. Das, and L. Coccato.
JD1-The Planetary Nebulae and the Dynamics of NGC 1399.
Highlights of Astronomy, 15:66–66, Nov. 2010.
- [158] N. Menci, A. Fontana, E. Giallongo, A. Grazian, and S. Salimbeni.
The abundance of distant and extremely red galaxies: The role of agn feedback in hierarchical models.
The Astrophysical Journal, 647, 08 2006.
- [159] R. H. Méndez, A. Riffeser, R.-P. Kudritzki, M. Matthias, K. C. Freeman, M. Arnaboldi, M. Capaccioli, and O. E. Gerhard.
Detection, Photometry, and Slitless Radial Velocities of 535 Planetary Nebulae in the Flattened Elliptical Galaxy NGC 4697.
The astrophysical journal, 563:135–150, Dec. 2001.
- [160] H. R. Merrett, K. Kuijken, M. R. Merrifield, A. J. Romanowsky, N. G. Douglas, N. R. Napolitano, M. Arnaboldi, M. Capaccioli, K. C. Freeman, O. Gerhard, N. W. Evans, M. I. Wilkinson, C. Halliday, T. J. Bridges, and D. Carter.
Tracing the star stream through M31 using planetary nebula kinematics.
Monthly Notices of the RAS, 346:L62–L66, Dec. 2003.
- [161] D. Merritt.
Relaxation and tidal stripping in rich clusters of galaxies. iii - growth of a massive central galaxy.
The astrophysical journal, 289:18–32, feb 1985.
- [162] S. Mieske.
The Early-Type Dwarf Galaxy Population of the Fornax Cluster.
In F. Combes and J. Palouš, editors, *Galaxy Evolution across the Hubble Time*, volume 235 of *IAU Symposium*, pages 226–226, May 2007.
- [163] S. Mieske, A. Jordán, P. Côté, E. W. Peng, L. Ferrarese, J. P. Blakeslee, S. Mei, H. Baumgardt, J. L. Tonry, L. Infante, and M. J. West.
The ACS Fornax Cluster Survey. IX. The Color-Magnitude Relation of Globular Cluster Systems.
The astrophysical journal, 710:1672–1682, Feb. 2010.
- [164] C. Mihos.
Intragroup and Intracluster Light.
IAU General Assembly, 22:2247903, Aug. 2015.

- [165] B. Moore, N. Katz, G. Lake, A. Dressler, and A. Oemler.
Galaxy harassment and the evolution of clusters of galaxies.
Nature, 379, 1996.
- [166] M. Mouhcine, R. Ibata, and M. Rejkuba.
Are small-scale substructures a universal property of galaxy haloes? The case of the giant elliptical NGC 5128.
Monthly Notices of the RAS, 415:993–1001, Aug. 2011.
- [167] R. P. Muñoz, P. Eigenthaler, T. H. Puzia, M. A. Taylor, Y. Ordenes-Briceño, K. Alamo-Martínez, K. X. Ribbeck, S. Ángel, M. Capaccioli, P. Côté, L. Ferrarese, G. Galaz, M. Hempel, M. Hilker, A. Jordán, A. Lançon, S. Mieske, M. Paolillo, T. Richtler, R. Sánchez-Janssen, and H. Zhang.
Unveiling a Rich System of Faint Dwarf Galaxies in the Next Generation Fornax Survey.
The astrophysical journal, Letters, 813:L15, Nov. 2015.
- [168] J. C. Muzzio, V. H. Dessaunet, and M. M. Vergne.
Tidal stripping and accretion in clusters of galaxies with smoothly distributed missing mass.
The astrophysical journal, 313:112–120, Feb. 1987.
- [169] A. Naab, Thorsten; Burkert.
Statistical properties of collisionless equal- and unequal-mass merger remnants of disk galaxies.
The Astrophysical Journal, 597, 11 2003.
- [170] T. Naab, P. H. Johansson, and J. P. Ostriker.
Minor mergers and the size evolution of elliptical galaxies.
The Astrophysical Journal, 699, 07 2009.
- [171] T. Naab, P. H. Johansson, J. P. Ostriker, and G. Efstathiou.
Formation of early-type galaxies from cosmological initial conditions.
The Astrophysical Journal, 658, 04 2007.
- [172] N. R. Napolitano, M. Arnaboldi, and M. Capaccioli.
NGC 1399: A complex dynamical case.
Astronomy and Astrophysics, 383:791–800, Mar. 2002.
- [173] N. R. Napolitano, M. Arnaboldi, K. C. Freeman, and M. Capaccioli.
Planetary nebulae as mass tracers of their parent galaxies: Biases in the estimate of the kinematical quantities.
Astronomy and Astrophysics, 377:784–800, Oct. 2001.
- [174] N. R. Napolitano, M. Pannella, M. Arnaboldi, O. Gerhard, J. A. L. Aguerri, K. C. Freeman, M. Capaccioli, S. Ghigna, F. Governato, T. Quinn, and J. Stadel.
Intracluster stellar population properties from n -body cosmological simulations. i. constraints at $z = 0$.
The Astrophysical Journal, 594, 09 2003.
- [175] N. R. Napolitano, V. Pota, A. J. Romanowsky, D. A. Forbes, J. P. Brodie, and C. Foster.
The SLUGGS survey: breaking degeneracies between dark matter, anisotropy and the IMF using globular cluster subpopulations in the giant elliptical NGC 5846.
Monthly Notices of the RAS, 439:659–672, Mar. 2014.
- [176] N. R. Napolitano, A. J. Romanowsky, M. Capaccioli, N. G. Douglas, M. Arnaboldi, L. Coccato, O. Gerhard, K. Kuijken, M. R. Merrifield, S. P. Bamford, A. Cortesi, P. Das, and K. C. Freeman.
The P.N.S Elliptical Galaxy Survey: a standard Λ CDM halo around NGC 4374?

- Monthly Notices of the RAS*, 411:2035–2053, Mar. 2011.
- [177] N. R. Napolitano, A. J. Romanowsky, L. Coccato, M. Capaccioli, N. G. Douglas, E. Noordermeer, O. Gerhard, M. Arnaboldi, F. de Lorenzi, K. Kuijken, M. R. Merrifield, E. O’Sullivan, A. Cortesi, P. Das, and K. C. Freeman.
The Planetary Nebula Spectrograph elliptical galaxy survey: the dark matter in NGC 4494.
Monthly Notices of the RAS, 393:329–353, Feb. 2009.
- [178] J. Ostriker.
Elliptical Galaxies are not Made by Merging Spiral Galaxies.
Comments on Astrophysics, 8:177, 1980.
- [179] J. Ostriker and S. Tremaine.
Another evolutionary correction to the luminosity of giant galaxies.
The astrophysical journal, 202:L113–L117, dec 1975.
- [180] P. Ostrov, D. Geisler, and J. C. Forte.
The metallicity gradient and distribution function of globular clusters around NGC 1399.
Astronomical Journal, 105:1762–1778, May 1993.
- [181] M. Paolillo, G. Fabbiano, G. Peres, and D.-W. Kim.
Deep ROSAT HRI Observations of the NGC 1399/NGC 1404 Region: Morphology and Structure of the X-Ray Halo.
The astrophysical journal, 565:883–907, Feb. 2002.
- [182] S. Parsa, J. S. Dunlop, R. J. McLure, and A. Mortlock.
The galaxy uv luminosity function at $z \sim 2-4$; new results on faint-end slope and the evolution of luminosity density.
Monthly Notices of the Royal Astronomical Society, 456, 03 2016.
- [183] E. Peng, M. Takamiya, P. Cote, M. J. West, J. P. Blakeslee, L. Ferrarese, A. Jordan, and S. Mei.
The Spatial Distributions of Globular Cluster Systems.
In *American Astronomical Society Meeting Abstracts*, volume 38 of *Bulletin of the American Astronomical Society*, page 1062, Dec. 2006.
- [184] M. Postman and T. R. Lauer.
Brightest cluster galaxies as standard candles.
The astrophysical journal, 440:28–47, Feb. 1995.
- [185] M. Postman, M.; Geller.
The morphology-density relation - the group connection.
The astrophysical journal, 281:95–99, jun 1984.
- [186] V. Pota, D. A. Forbes, A. J. Romanowsky, J. P. Brodie, L. R. Spitler, J. Strader, C. Foster, J. A. Arnold, A. Benson, C. Blom, K. L. Hargis, J. R. and Rhode, and C. Usher.
The slugs survey: kinematics for over 2500 globular clusters in 12 early-type galaxies.
Monthly Notices of the Royal Astronomical Society, 428, 01 2013.
- [187] V. Pota, N. R. Napolitano, M. Hilker, M. Spavone, C. Schulz, M. Cantiello, C. Tortora, E. Iodice, M. Paolillo, R. D’Abrusco, M. Capaccioli, T. Puzia, R. F. Peletier, A. J. Romanowsky, G. van de Ven, C. Spiniello, M. Norris, T. Lisker, R. Munoz, P. Schipani, P. Eigenthaler, M. A. Taylor, R. Sánchez-Janssen, and Y. Ordenes-Briceño.
The Fornax Cluster VLT Spectroscopic Survey - I. VIMOS spectroscopy of compact stellar systems in the Fornax core region.
Monthly Notices of the RAS, 481:1744–1756, Dec. 2018.

- [188] C. Ragone-Figueroa, G. L. Granato, M. E. Ferraro, G. Murante, V. Biffi, S. Borgani, S. Planelles, and E. Rasia.
Bcg mass evolution in cosmological hydro-simulations.
Monthly Notices of the Royal Astronomical Society, 06 2018.
- [189] J. I. Read, M. I. Wilkinson, N. W. Evans, G. Gilmore, and J. T. Kleyana.
The tidal stripping of satellites.
Monthly Notices of the Royal Astronomical Society, 366, 2006.
- [190] T. Richtler, R. Salinas, I. Misgeld, M. Hilker, G. K. T. Hau, A. J. Romanowsky, Y. Schuberth, and M. Spolaor.
The dark halo of the Hydra I galaxy cluster: core, cusp, cosmological? Dynamics of NGC 3311 and its globular cluster system.
Astronomy and Astrophysics, 531:A119, July 2011.
- [191] B. Robertson, J. S. Bullock, T. J. Cox, T. Di Matteo, L. Hernquist, V. Springel, and N. Yoshida.
A merger-driven scenario for cosmological disk galaxy formation.
The Astrophysical Journal, 645, 07 2006.
- [192] A. J. Romanowsky, J. P. Brodie, J. S. Bullock, R. Ciardullo, P. Guhathakurta, L. Hoffman, K. A. G. Olsen, J. R. Primack, and G. van de Ven.
Structure and Substructure of Galactic Spheroids.
In *astro2010: The Astronomy and Astrophysics Decadal Survey*, volume 2010 of *ArXiv Astrophysics e-prints*, 2009.
- [193] A. J. Romanowsky, N. G. Douglas, M. Arnaboldi, K. Kuijken, M. R. Merrifield, N. R. Napolitano, M. Capaccioli, and K. C. Freeman.
A Dearth of Dark Matter in Ordinary Elliptical Galaxies.
Science, 301:1696–1698, Sept. 2003.
- [194] A. J. Romanowsky, J. Strader, J. P. Brodie, J. C. Mihos, L. R. Spitler, D. A. Forbes, C. Foster, and J. A. Arnold.
The Ongoing Assembly of a Central Cluster Galaxy: Phase-space Substructures in the Halo of M87.
The astrophysical journal, 748:29, Mar. 2012.
- [195] N. Roy, N. Napolitano, F. La Barbera, C. Tortora, F. Getman, M. Radovich, M. Capaccioli, M. Brescia, S. Caviuoti, G. Longo, M. Raj, E. Puddu, G. Covone, V. Amaro, C. Vellucci, A. Grado, K. Kuijken, G. Verdoes Kleijn, and E. Valentijn.
Evolution of galaxy size-stellar mass relation from the kilo-degree survey.
Monthly Notices of the Royal Astronomical Society, 480:1057–1080, 10 2018.
- [196] C. S. Rudick, J. C. Mihos, L. H. Frey, and C. K. McBride.
Tidal Streams of Intracluster Light.
The astrophysical journal, 699:1518–1529, July 2009.
- [197] V. Ruzkowski, M.; Springel.
The role of dry mergers for the formation and evolution of brightest cluster galaxies.
The Astrophysical Journal, 696, 05 2009.
- [198] R. P. Saglia, A. Kronawitter, O. Gerhard, and R. Bender.
The Orbital Structure and Potential of NGC 1399.
Astronomical journal, 119:153–161, Jan. 2000.
- [199] A. Sandage.

- The Redshift-Distance Relation. I. Angular Diameter of First Ranked Cluster Galaxies as a Function of Redshift: the Aperture Correction to Magnitudes.
The astrophysical journal, 173:485, May 1972.
- [200] P. Schipani, J. Argomedo, L. Marty, N. M. Radziwill, and G. Chiozzi.
Spie proceedings [spie spie astronomical telescopes + instrumentation - amsterdam, netherlands (sunday 1 july 2012)] software and cyberinfrastructure for astronomy ii - commissioning the vst telescope control software.
volume 8451, 2012.
- [201] D. Schönberner, R. Jacob, C. Sandin, and M. Steffen.
The evolution of planetary nebulae. VII. Modelling planetary nebulae of distant stellar systems.
Astronomy and Astrophysics, 523:A86, Nov. 2010.
- [202] Y. Schuberth, T. Richtler, M. Hilker, B. Dirsch, L. P. Bassino, A. J. Romanowsky, and L. Infante.
The globular cluster system of NGC 1399. V. dynamics of the cluster system out to 80 kpc.
Astronomy and Astrophysics, 513:A52, Apr. 2010.
- [203] Y. Schuberth, T. Richtler, M. Hilker, R. Salinas, B. Dirsch, and S. S. Larsen.
Dynamics of the NGC 4636 globular cluster system. II. Improved constraints from a large sample of globular cluster velocities.
Astronomy and Astrophysics, 544:A115, Aug. 2012.
- [204] C. Schulz, M. Hilker, P. Kroupa, and J. Pflamm-Altenburg.
Distribution of star formation rates during the rapid assembly of NGC 1399 as deduced from its globular cluster system.
Astronomy and Astrophysics, 594:A119, Oct. 2016.
- [205] F. Shankar, F. Marulli, M. Bernardi, M. Boylan-Kolchin, X. Dai, and S. Khochfar.
Further constraining galaxy evolution models through the size function of SDSS early-type galaxies.
Monthly Notices of the Royal Astronomical Society, 405:948–960, June 2010.
- [206] A. Sheardown, E. Roediger, Y. Su, R. P. Kraft, T. Fish, J. A. ZuHone, W. R. Forman, C. Jones, E. Churazov, and P. E. J. Nulsen.
The Recent Growth History of the Fornax Cluster Derived from Simultaneous Sloshing and Gas Stripping: Simulating the Infall of NGC 1404.
The astrophysical journal, 865:118, Oct. 2018.
- [207] H.-Y. Shih and R. H. Méndez.
Possible Stellar Streams in the Edge-on Spiral NGC 891 Discovered from Kinematics of Planetary Nebulae.
The astrophysical journal, Letters, 725:L97–L100, Dec. 2010.
- [208] J. Silk.
Accretion by galaxy clusters and the relationship between X-ray luminosity and velocity dispersion.
The astrophysical journal, 208:646–649, Sept. 1976.
- [209] R. S. Somerville, P. F. Hopkins, T. J. Cox, B. E. Robertson, and L. Hernquist.
A semi-analytic model for the co-evolution of galaxies, black holes and active galactic nuclei.
Monthly Notices of the Royal Astronomical Society, 391:481–506, Dec. 2008.
- [210] M. Spavone, M. Capaccioli, N. R. Napolitano, E. Iodice, A. Grado, L. Limatola, A. P. Cooper, M. Cantiello, D. A. Forbes, M. Paolillo, and P. Schipani.

- Unveiling the Nature of Giant Ellipticals and their Stellar Halos with the VST.
The Messenger, 170:34–39, Dec. 2017.
- [211] C. Spiniello, N. R. Napolitano, M. Arnaboldi, C. Tortora, L. Coccato, M. Capaccioli, O. Gerhard, E. Iodice, M. Spavone, M. Cantiello, R. Peletier, M. Paolillo, and P. Schipani.
The Fornax Cluster VLT Spectroscopic Survey II - Planetary Nebulae kinematics within 200 kpc of the cluster core.
Monthly Notices of the RAS, 477:1880–1892, June 2018.
- [212] E. Starckenburg, A. Helmi, H. L. Morrison, P. Harding, H. van Woerden, M. Mateo, E. W. Olszewski, T. Sivarani, J. E. Norris, K. C. Freeman, S. A. Shectman, R. C. Dohm-Palmer, L. Frey, and D. Oravetz.
Mapping the Galactic Halo. VIII. Quantifying Substructure.
The astrophysical journal, 698:567–579, June 2009.
- [213] J. P. Stott, C. A. Collins, C. Burke, V. Hamilton-Morris, and G. P. Smith.
Little change in the sizes of the most massive galaxies since $z = 1$.
Monthly Notices of the Royal Astronomical Society, 414, 2011.
- [214] T. Tal, P. G. van Dokkum, J. Nelan, and R. Bezanson.
The frequency of tidal features associated with nearby luminous elliptical galaxies from a statistically complete sample.
The Astronomical Journal, 138, 11 2009.
- [215] A. M. Teodorescu, R. H. Méndez, F. Bernardi, A. Riffeser, and R. P. Kudritzki.
Planetary Nebulae in the Elliptical Galaxy NGC 821: Kinematics and Distance Determination.
The astrophysical journal, 721:369–382, Sept. 2010.
- [216] J. Thomas, R. P. Saglia, R. Bender, D. Thomas, K. Gebhardt, J. Magorrian, E. M. Corsini, and G. Wegner.
Regularized orbit models unveiling the stellar structure and dark matter halo of the coma elliptical ngc 4807.
Monthly Notices of the Royal Astronomical Society, 360, 2005.
- [217] S. Toft, P. van Dokkum, M. Franx, I. Labbe, N. M. Forster Schreiber, S. Wuyts, T. Webb, G. Rudnick, A. Zirm, M. Kriek, P. van der Werf, J. P. Blakeslee, G. Illingworth, H. Rix, C. Papovich, and A. Moorwood.
Hubble space telescope and spitzer imaging of red and blue galaxies at $z \sim 2.5$: A correlation between size and star formation activity from compact quiescent galaxies to extended star-forming galaxies.
The Astrophysical Journal, 671, 12 2007.
- [218] A. Toomre.
Theories of spiral structure.
Annual Review of Astronomy and Astrophysics, 15, 09 1977.
- [219] T. Treu, R. S. Ellis, T. X. Liao, P. G. van Dokkum, P. Tozzi, A. Coil, J. Newman, M. C. Cooper, and M. Davis.
The Assembly History of Field Spheroidals: Evolution of Mass-to-Light Ratios and Signatures of Recent Star Formation.
The astrophysical journal, 633:174–197, Nov. 2005.
- [220] I. Trujillo, C. J. Conselice, K. Bundy, M. Cooper, P. Eisenhardt, and R. Ellis.
Strong size evolution of the most massive galaxies since $z \sim 2$.
Monthly Notices of the RAS, 382:109–120, Nov. 2007.

- [221] I. Trujillo, A. W. Graham, and N. Caon.
On the estimation of galaxy structural parameters: the Sérsic model.
Monthly Notices of the RAS, 326:869–876, Sept. 2001.
- [222] A. V. Tutukov and A. V. Fedorova.
The origin of intergalactic stars in galaxy clusters.
Astronomy Reports, 55:383–391, May 2011.
- [223] T. Valentinuzzi, J. Fritz, B. M. Poggianti, A. Cava, D. Bettoni, G. Fasano, M. D’Onofrio, W. J. Couch, A. Dressler, M. Moles, A. Moretti, A. Omizzolo, P. Kjærgaard, E. Vanzella, and J. Varela.
Superdense massive galaxies in wings local clusters.
The Astrophysical Journal, 712, 03 2010.
- [224] A. van der Wel, E. F. Bell, F. van den Bosch, A. Gallazzi, and H.-W. Rix.
On the Size and Comoving Mass Density Evolution of Early-Type Galaxies.
The astrophysical journal, 698:1232–1243, June 2009.
- [225] A. van der Wel, B. P. Holden, A. Zirm, M. Franx, A. Rettura, G. Illingworth, and H. Ford.
Recent Structural Evolution of Early-Type Galaxies: Size Growth from $z = 1$ to $z = 0$.
The astrophysical journal, 688:48–58, Nov. 2008.
- [226] P. G. van Dokkum, M. Franx, M. Kriek, B. Holden, D. Illingworth, Garth D. and Magee, R. Bouwens, D. Marchesini, R. Quadri, G. Rudnick, E. N. Taylor, and S. Toft.
Confirmation of the remarkable compactness of massive quiescent galaxies at $z \sim 2.3$: Early-type galaxies did not form in a simple monolithic collapse.
The Astrophysical Journal, 677, 04 2008.
- [227] P. G. van Dokkum, E. J. Nelson, M. Franx, P. Oesch, I. Momcheva, G. Brammer, N. M. Förster Schreiber, R. E. Skelton, K. E. Whitaker, A. van der Wel, R. Bezanson, M. Fumagalli, G. D. Illingworth, M. Kriek, J. Leja, and S. Wuyts.
Forming Compact Massive Galaxies.
The astrophysical journal, 813:23, Nov. 2015.
- [228] P. G. van Dokkum, K. E. Whitaker, G. Brammer, M. Franx, M. Kriek, I. Labbé, D. Marchesini, R. Quadri, R. Bezanson, G. D. Illingworth, A. Muzzin, G. Rudnick, T. Tal, and D. Wake.
The growth of massive galaxies since $z = 2$.
The Astrophysical Journal, 709, 02 2010.
- [229] J. Veljanoski and A. Helmi.
The kinematics of globular clusters systems in the outer halos of the Aquarius simulations.
Astronomy and Astrophysics, 592:A55, July 2016.
- [230] A. Venhola, R. Peletier, E. Laurikainen, H. Salo, T. Lisker, E. Iodice, M. Capaccioli, G. V. Kleijn, E. Valentijn, S. Mieske, M. Hilker, C. Wittmann, G. van de Ven, A. Grado, M. Spavone, M. Cantiello, N. Napolitano, M. Paolillo, and J. Falcon-Barroso.
VizieR Online Data Catalog: Fornax Deep Survey with VST. III. LSB galaxies (Venhola+, 2017).
VizieR Online Data Catalog, 360, Feb. 2018.
- [231] A. Venhola, R. Peletier, E. Laurikainen, H. Salo, T. Lisker, E. Iodice, M. Capaccioli, G. Verdois Kleijn, E. Valentijn, S. Mieske, M. Hilker, C. Wittmann, G. van de Ven, A. Grado, M. Spavone, M. Cantiello, N. Napolitano, M. Paolillo, and J. Falcón-Barroso.
The Fornax Deep Survey with VST. III. Low surface brightness dwarfs and ultra diffuse galaxies in the center of the Fornax cluster.

- Astronomy and Astrophysics*, 608:A142, Dec. 2017.
- [232] D. Villegas, A. Jordán, E. W. Peng, J. P. Blakeslee, P. Côté, L. Ferrarese, M. Kissler-Patig, S. Mei, L. Infante, J. L. Tonry, and M. J. West.
The ACS Fornax Cluster Survey. VIII. The Luminosity Function of Globular Clusters in Virgo and Fornax Early-type Galaxies and Its Use as a Distance Indicator.
The astrophysical journal, 717:603–616, July 2010.
- [233] A. Von Der Linden, P. N. Best, G. Kauffmann, and S. D. M. White.
How special are brightest group and cluster galaxies?
Monthly Notices of the Royal Astronomical Society, 379, 2007.
- [234] M. G. Walker and J. Peñarrubia.
A Method for Measuring (Slopes of) the Mass Profiles of Dwarf Spheroidal Galaxies.
The astrophysical journal, 742:20, Nov. 2011.
- [235] T. M. A. Webb, A. Muzzin, A. Noble, N. Bonaventura, J. Geach, Y. Hezevah, C. Lidman, G. Wilson, H. K. C. Yee, J. Surace, and D. Shupe.
The star formation history of bcgs to $z = 1.8$ from the sparcS/swire survey: Evidence for significant in situ star formation at high redshift.
The Astrophysical Journal, 814, 11 2015.
- [236] M. J. West, P. Cote, C. Jones, W. Forman, and R. O. Marzke.
Intracluster Globular Clusters.
The astrophysical journal, Letters, 453:L77, Nov. 1995.
- [237] M. J. West, P. Côté, R. O. Marzke, and A. Jordán.
Reconstructing galaxy histories from globular clusters.
Nature, 427:31–35, Jan. 2004.
- [238] I. M. Whaley, A. Aragón-Salamanca, G. De Lucia, A. von der Linden, S. P. Bamford, P. Best, M. N. Bremer, P. Jablonka, O. Johnson, B. Milvang-Jensen, S. Noll, B. M. Poggianti, G. Rudnick, R. Saglia, S. White, and D. Zaritsky.
The evolution of the brightest cluster galaxies since $z \sim 1$ from the ESO Distant Cluster Survey (EDisCS).
Monthly Notices of the RAS, 387:1253–1263, July 2008.
- [239] M. J. White, S. D. M.; Rees.
Core condensation in heavy halos: a two-stage theory for galaxy formation and clustering.
Monthly Notices of the Royal Astronomical Society, 183, 07 1978.
- [240] R. E. White.
Globular clusters belonging to galaxy clusters.
Monthly Notices of the Royal Astronomical Society, 227, 07 1987.
- [241] S. D. M. White.
The dynamics of rich clusters of galaxies.
Monthly Notices of the Royal Astronomical Society, 177, 12 1976.
- [242] D. J. C. Whitmore, B.C.; Gilmore.
What determines the morphological fractions in clusters of galaxies.
The astrophysical journal, 407:489–509, apr 1993.
- [243] B. Willman, F. Governato, J. Wadsley, and T. Quinn.
The origin and properties of intracluster stars in a rich cluster.
Monthly Notices of the Royal Astronomical Society, 355, 2004.

- [244] K. A. Woodley and W. E. Harris.
Possible Subgroups of Globular Clusters and Planetary Nebulae in NGC 5128.
Astronomical journal, 141:27, Jan. 2011.
- [245] X.-X. Xue, H.-W. Rix, B. Yanny, T. C. Beers, E. F. Bell, G. Zhao, J. S. Bullock, K. V. Johnston, H. Morrison, C. Rockosi, S. E. Koposov, X. Kang, C. Liu, A. Luo, Y. S. Lee, and B. A. Weaver.
Quantifying kinematic substructure in the milky way's stellar halo.
The Astrophysical Journal, 738, 09 2011.
- [246] S.-J. Yoon, S.-Y. Lee, J. P. Blakeslee, E. W. Peng, S. T. Sohn, J. Cho, H.-S. Kim, C. Chung, S. Kim, and Y.-W. Lee.
Nonlinear color-metallicity relations of globular clusters. iii. on the discrepancy in metallicity between globular cluster systems and their parent elliptical galaxies.
The Astrophysical Journal, 743, 12 2011.
- [247] S.-J. Yoon, S.-Y. Lee, S. Yi, and Y.-W. Lee.
On the Origin of Bimodal Color Distribution of Globular Clusters in Early-type Galaxies.
In *American Astronomical Society Meeting Abstracts #207*, volume 207 of *American Astronomical Society Meeting Abstracts*, page 128.22, June 2006.
- [248] S. Zibetti, S. D. M. White, D. P. Schneider, and J. Brinkmann.
Intergalactic stars in $z \sim 0.25$ galaxy clusters: systematic properties from stacking of sloan digital sky survey imaging data.
Monthly Notices of the Royal Astronomical Society, 358, 2005.
- [249] A. W. Zirm, A. van der Wel, M. Franx, I. Labbe, I. Trujillo, P. van Dokkum, S. Toft, E. Daddi, G. Rudnick, H. Rix, H. J. A. Rottgering, and P. van der Werf.
Nicmos imaging of drgs in the hdf-s: A relation between star formation and size at $z \sim 2.5$.
The Astrophysical Journal, 656, 02 2007.